UNIVERSITY OF CALIFORNIA, SAN DIEGO

Conformational Dynamics of the Acetylcholine Binding Protein, a Nicotinic Receptor Surrogate

A dissertation submitted in partial satisfaction of the requirements for the degree

Doctor of Philosophy

in

Biomedical Sciences

by

Ryan E. Hibbs

Committee in charge:

Professor Palmer W. Taylor, Chair
Professor Darwin K. Berg
Professor David A. Johnson
Professor J. Andrew McCammon
Professor Alexandra C. Newton
Professor Stanley J. Opella

2006

The dissertation of Ryan E. Hibbs is approved, and it is acceptable

in quality and form for publication on microfilm:

Chair

University of California, San Diego

2006

TABLE OF CONTENTS

LIST OF ABBREVIATIONS

AChE	acetylcholinesterase
AChBP	acetylcholine binding protein
Bgt	α-bungarotoxin
Carb	carbamylcholine
Cbt	α-cobratoxin
CMV	cytomegalovirus
DMEM	Dulbecco's modified Eagles medium
DTT	dithiothreitol
d-Tubo	*d*-tubocurarine
MTS-EDANS	N-(methanethiosulfonylethylcarboxamidoethyl)-5-naphthylamine-1-sulfonic acid
Epi	epibatidine
FITC	fluorescein isothiocyanate
Fl	fluorescein
FRET	fluorescence resonance energy transfer
HEK	human embryonic kidney
LGIC	ligand-gated ion channel
MLA	methyllycaconitine
MTS	methanethiosulfonate
4-OH,2-MeO-BA	4-hydroxy, 2-methoxy-benzylidene anabaseine
nAChR	nicotinic acetylcholine receptor
Nic	nicotine

PCR	polymerase chain reaction
SDS-PAGE	sodium dodecyl sulfate-polyacrylamide gel electrophoresis
TCEP	tris(2-carboxyethyl)phosphine
TMR	tetramethylrhodamine

Amino Acid Residues

Ala or A	alanine
Arg or R	arginine
Asn or N	asparagine
Asp or D	aspartate
Cys or C	cysteine
Glu or E	glutamate
Gln or Q	glutamine
Gly or G	glycine
His or H	histidine
Ile or I	isoleucine
Lys or K	lysine
Leu or L	leucine
Met or M	methionine
Phe or F	phenylalanine
Pro or P	proline
Ser or S	serine

Thr or T	threonine
Trp or W	tryptophan
Tyr or Y	tyrosine
Val or V	valine

LIST OF FIGURES

LIST OF TABLES

ACKNOWLEDGMENTS

Foremost, I thank my mentor and dissertation advisor Dr. Palmer Taylor for his intellectual guidance, patience, and wisdom in my development as a scientist. Dr. Taylor is to me a superior scientific role model: brilliant, curious, objective, hard-working, and generous. He has provided me with many opportunities to present my work at scientific meetings worldwide and opened professional doors for me that I am only beginning to appreciate. I am grateful to Dr. David Johnson, Professor at UC Riverside, for his time and expertise relating to fluorescence spectroscopy techniques. He taught me much about protein dynamics, and I value highly the time I spent working with him. I also thank Dr. Larry Brunton, Professor at UCSD, for professional guidance before and during graduate school.

Many people in the Taylor laboratory, past and present, contributed to this work in some manner. Specifically, Dr. Zoran Radić made himself consistently available to teach me about binding kinetics and topics in fluorescence when I found myself in a quandary; he is an excellent teacher, and I am lucky to have had the opportunity to work with him. I thank Shelley Camp for her unending efforts to maintain a functional level of organization in the laboratory, as well as for her personal encouragement in my scientific development. Dr. Todd Talley, a post-doctoral fellow, helped me through my first protein purifications and radioligand binding assays. I am grateful to him not only for his help at the bench but also for fruitful scientific discussion and keeping the atmosphere light when some of the inevitable frustrations of being a graduate student set in. I thank Dr. Scott Hansen, who for several years was a graduate student with me also studying the nicotinic receptor, for synthesizing the initial AChBP cDNAs, for engaging scientific and

social discussions, and for being a great travel partner on numerous domestic and international adventures as we traveled to scientific meetings. I also thank Dr. Hansen for guiding me through protein crystallization and crystallographic structure refinement. I thank Dr. Jian Shi for teaching me about fluorescence anisotropy decay analysis and for providing mass spectrometry data and Davide Comoletti for help with analytical ultracentrifugation experiments and for very useful professional criticism. I was fortunate to work with Christine Gould and Alfred Chappell, graduate rotation students, and Samar Yalda, Diana Nguyen, and Jennifer Fu, undergraduate research students, who assisted me in mutagenesis and protein purification efforts and allowed me the opportunity to try my hand at teaching. Others in the Taylor lab who contributed to my successful experience at UCSD were Pam Tetu, Akos Nemecz, Meghan Miller, Anne Valle, Wenru Yu, Dr. Warren Lewis, Dr. Lori Jennings, Sventja von Daake, Robyn Flynn, and Helen Newlin.

I am grateful to my family for their support up to and through my graduate studies. I thank my parents for emphasizing the importance of education and providing the means to attend the undergraduate institution of my choosing. I thank my mother for teaching me my times tables, for her constant encouragement, and for her insight into professional and personal relationships. I thank my father for instilling in me a curiosity in the natural world and physical sciences, and, as a Professor of Forestry at Oregon State University, for providing me with the opportunity to work in a research laboratory as a high school student. I sincerely thank my girlfriend and partner of five years, Colleen Noviello, also a graduate student, for her continuing support and encouragement.

Chapter IV, in full, is a reprint of the material as it appears in the *Journal of Biological Chemistry* 2004, Hibbs RE, Talley TT, Taylor, P, American Society for Biochemistry and Molecular Biology, 2004. Chapter V, in full, is a reprint of the material as it appears in *Biochemistry* 2005, Hibbs RE, Johnson DA, Shi J, Hansen SB, Taylor P, American Chemical Society 2005. Chapter VI, in full, has been accepted for publication of the material as it appears to the *Journal of Biological Chemistry*, Hibbs RE, Radić Z, Taylor P, Johnson DA, American Society for Biochemistry and Molecular Biology, 2006. The dissertation author was the primary investigator and author of these articles and submitted manuscripts.

VITA

2000	B.A., Whitman College
2001-2006	Research Associate, University of California, San Diego
2004-2006	Dissertation Research Fellow, Pharmaceutical Research and Manufacturers of America Foundation
2006	Ph.D., University of California, San Diego

FIELD OF STUDY

Major Field: Biomedical Sciences

Studies in Protein Structure-Function Relationships
Professor Palmer W. Taylor

PUBLICATIONS

Hibbs R.E., Radić Z., Taylor P., and Johnson D.A. "Influence of agonists and antagonists on the segmental motion of residues near the agonist binding pocket of the acetylcholine binding protein" *Journal of Biological Chemistry*, in press 2006.

Hibbs R.E., Johnson D.A., Shi J., Hansen S.B., and Taylor P. (2005) "Structural dynamics of the α-neurotoxin-acetylcholine binding protein complex: hydrodynamic and fluorescence anisotropy decay analyses" *Biochemistry* 44:16602-11.

Hibbs R.E., Talley T.T., and Taylor P. (2004) "Acrylodan conjugated cysteine side chains reveal conformational state and ligand site locations of the acetylcholine binding protein" *Journal of Biological Chemistry* 279:28483-91.

Taylor P., Hansen S.B., Talley T.T., Hibbs R.E., and Radić Z. (2004) "Contemporary paradigms for cholinergic ligand design guided by biological structure" *Bioorganic and Medicinal Chemistry Letters* 14:1875-1877.

ABSTRACTS

Hibbs, R.E., Johnson, D.A., Taylor, P. "Agonists increase and antagonists decrease F-loop mobility suggesting its involvement in the nicotinic receptor activation network." International Union of Pharmacology, Beijing, China, July 2006.

Hibbs, R.E., Johnson, D.A., Taylor, P. "Structural dynamics of the acetylcholine binding protein analyzed by time-resolved fluorescence anisotropy decay." American Society for Pharmacology and Experimental Therapeutics at Experimental Biology, San Francisco, CA, April 2006

Talley, T.T., Kem, W.R., Soti, F.S., Tsigelny, I., Hibbs, R.E., Taylor, P. "Structure-activity relationships and determinants of selectivity for congeners of the selective alpha7 partial agonist 3-(2,4-dimethoxybenzylidene)-anabaseine (DMXBA or GTS-21) with the ACh binding proteins." American Society for Pharmacology and Experimental Therapeutics at Experimental Biology, San Francisco, CA, April 2006

Johnson, D.A., Hibbs, R.E., Taylor, P. "Agonists increase and antagonists decrease the mobility of the lower part of the acetylcholine binding protein F-loop: a time-resolved fluorescence anisotropy study." Biophysical Society, Salt Lake City, UT, February 2006

Talley T.T., Kem W.R., Soti, F.S., Tsigelny I., Hibbs R.E., Taylor P. "Molecular determinants of specificity and binding for the selective α7 partial agonist 3-(2,4-dimethoxybenzylidene)-anabaseine (DMXBA or GTS-21) and a series of related compounds to ACh binding proteins." Society for Neurosciences, Washington DC, November 2005

Hibbs R.E., Johnson D.A., Taylor P. "Solution behavior of the acetylcholine binding protein monitored by diffusion analysis and decay of fluorescence anisotropy." Society for Neurosciences, Washington DC, November 2005

Hibbs R.E., Johnson, D.A., Shi, J., Taylor, P. "Structural dynamics of the acetylcholine binding protein: hydrodynamic and fluorescence anisotropy decay analyses." XIIth International Symposium on Cholinergic Mechanisms, Alicante, Spain, October 2005

Hibbs R.E., Johnson D.A., Taylor P. "Fluorophore-conjugated cysteine side chains reveal ligand binding site locations and conformational fluctuations of the acetylcholine binding protein." American Society for Pharmacology and Experimental Therapeutics at Experimental Biology, San Diego, CA, April 2005

Johnson D.A., Hibbs R.E., Taylor P. "Nanosecond Dynamics of the Acetylcholine Binding Protein: A Time-Resolved Fluorescence Anisotropy Approach." Biophysical Society 49th annual meeting, Long Beach, CA, February 2005

Hibbs R.E., Johnson D.A., Taylor P. "Fluorophore-conjugated cysteine side chains reveal conformational state and ligand binding site locations of the acetylcholine binding protein." Society for Neurosciences, San Diego, CA, October 2004

Talley T.T., Hibbs R.E., Hansen S.B., Taylor, P., Radić, Z. "Molecular interactions between the acetylcholine binding protein and allosterically potentiating ligands of nicotinic acetylcholine receptors." American Society for Pharmacology and Experimental Therapeutics at Experimental Biology, Washington DC, April 2004

Hibbs R.E., Johnson D.A., Taylor P. "Ligand-induced conformational changes in the acetylcholine binding protein, a nicotinic receptor surrogate." American Society for Pharmacology and Experimental Therapeutics at Experimental Biology, Washington DC, April 2004

Hibbs R.E., Johnson D.A., Taylor P. "Characterization of ligand binding sites and backbone flexibility in the acetylcholine binding protein, a nicotinic receptor surrogate." Western Pharmacology Society, Honolulu, HI, February 2004

Talley T.T., Hansen S.B., Radić Z., Hibbs R.E., Molles B.E., Tsigelny I., Taylor P. "Characterization and production of two acetylcholine binding proteins." American Society for Pharmacology and Experimental Therapeutics at Experimental Biology, San Diego, CA, April 2003

Hibbs R.E., Taylor P. "Elucidation of ligand binding sites in the acetylcholine binding protein by cysteine labeling mutagenesis and fluorescence spectroscopy." American Society for Pharmacology and Experimental Therapeutics at Experimental Biology, San Diego, CA, April 2003

Hibbs R.E., Taylor P. “Elucidation of ligand binding sites in the acetylcholine binding protein by cysteine labeling mutagenesis and fluorescence spectroscopy.” Western Pharmacology Society, Lake Tahoe, NV, February 2003

ABSTRACT OF THE DISSERTATION

Conformational Dynamics of the Acetylcholine Binding Protein,

a Nicotinic Receptor Surrogate

by

Ryan E. Hibbs

Doctor of Philosophy in Biomedical Sciences

University of California, San Diego, 2006

Professor Palmer W. Taylor, Chair

Nicotinic acetylcholine receptors (nAChRs) are ligand-gated ion channels that mediate rapid neurotransmission in the central and peripheral nervous systems. The acetylcholine binding protein (AChBP) is a soluble structural and functional surrogate of the extracellular, ligand-binding domain of the nAChR that allows for studies not amenable to study of the nAChR as an integral membrane protein. In particular, AChBP provides a system in which to study solution dynamics and conformational changes related to ligand binding.

To deduce ligand binding sites and infer conformational changes, cysteine mutants of AChBP were generated and labeled with the solvent-sensitive fluorophore, acrylodan. The fluorescence emission spectra from acrylodan-labeled AChBP mutants were examined in the absence and presence of nicotinic ligands. Binding of small molecules and large peptide toxins caused acrylodan conjugated to Q178C to move into environments of opposite polarities. From this, I proposed a hinge position at Q178 that allows for flexibility of the C-loop, such that it can expand or contract as a rigid body to accommodate bound ligand. Distinctive changes in acrylodan emission were also observed in the F-loop, indicating that this region of the protein likely plays a role in ligand binding, a finding not evident from existing structures.

Complementary hydrodynamic and fluorescence anisotropy studies of AChBP free in solution and in complex with an 8 kD three-fingered α-neurotoxin indicated that the bound α-toxin has minimal effects on the translational and rotational diffusion properties of AChBP. Anisotropy experiments showed that, when bound, the α-toxin is highly dynamic. Its central finger, that contains β-sheet structure and interacts with the agonist binding site, is the most rigid portion.

The segmental flexibility of AChBP was studied by measuring decay of fluorescence anisotropy from fluorescein-labeled AChBP mutants. The results revealed that AChBP exhibits wide regional variation in α-carbon backbone flexibility, with the C-loop being overall most rigid in the picosecond-nanosecond time domain. In studying the effect of ligand binding on conformational flexibility, we found that the F-loop conformational change associated with ligand binding is pharmacologically correlated.

Solution-based structural studies of conformation related to ligand binding should facilitate structure-guided drug design and increase understanding of nAChR function.

Chapter I

Introduction to the Nicotinic Acetylcholine Receptor, the Acetylcholine Binding Protein, and Cysteine Substitution for Mutagenesis

This dissertation describes the application of cysteine substitution mutagenesis to the acetylcholine binding protein (AChBP), which this laboratory and several others are using as a structural and functional surrogate of the nicotinic acetylcholine receptor (nAChR) extracellular domain. As the first cell-surface receptor identified and characterized, the nAChR and its structure, function, and physiological roles have been the focus of many reviews and texts. Also, the potential of cysteine-substitution mutagenesis and fluorophore labeling to inform us about the solution dynamics of protein structure has been well documented. This introduction serves to familiarize the reader with aspects of these fields relevant to this dissertation.

A. Historical Perspective

In the mid to late 19th century, the French physiologist Claude Bernard investigated the paralytic properties of the natural product curare, which had been used by native South Americans to poison the tips of arrows. Bernard noted that curare does not block contraction of muscle itself, but rather affects the action of the motor nerve on the muscle. In the early 20th century working with preparations of denervated frog muscle, the English physiologist John Langley noted that nicotine also blocked muscle contraction when applied at the same site as curare, however in a different manner such that first the muscle would contract and then produce a block of function. The actions of nicotine and curare would later be defined as agonist and antagonist, respectively, as the

agonist activates and the response desensitizes, whereas the antagonist antagonizes the action of the agonist. In 1906, Langley described the mediator of the action of these two compounds, nicotine and curare, as a "receptive substance," and this event marked the beginning of receptor theory (1). In 1914, Sir Henry Dale described a single neurotransmitter, acetylcholine, that would stimulate two components of the cholinergic nervous system; one was also activated specifically by muscarine, and was labeled muscarinic, while the other was activated specifically by nicotine, and was labeled nicotinic (2).

Since its identification via pharmacological methods, the nicotinic receptor has been studied extensively (for recent reviews of the field, see (3-5)). A rich source of nicotinic receptors in the electric organ of the *Torpedo* ray made much of this characterization possible in the era before molecular biological methods became commonplace (6). Advances in electrophysiological technology allowed for quantitative studies to be made of the ionic basis of a neuronal action potential and synaptic transmission (7), and details of receptor function began to emerge. In 1966 the discovery that a peptidic neurotoxin present in snake venom, α-bungarotoxin, binds specifically and with very high affinity to nicotinic receptors (8), provided a probe that identified the 250 kDa protein and its subunit composition of α, β, γ and δ, with two copies of the α subunit and two agonist binding sites per pentameric receptor molecule (Figure I.1). The specificity of this probe was so profound that it allowed, eventually, for purification of the nicotinic receptor in a physiologically relevant form competent for agonist binding (9). There have now been identified over 100 of these α-neurotoxins derived from snake venom that are specific for some nicotinic receptor subtypes but not others, which has

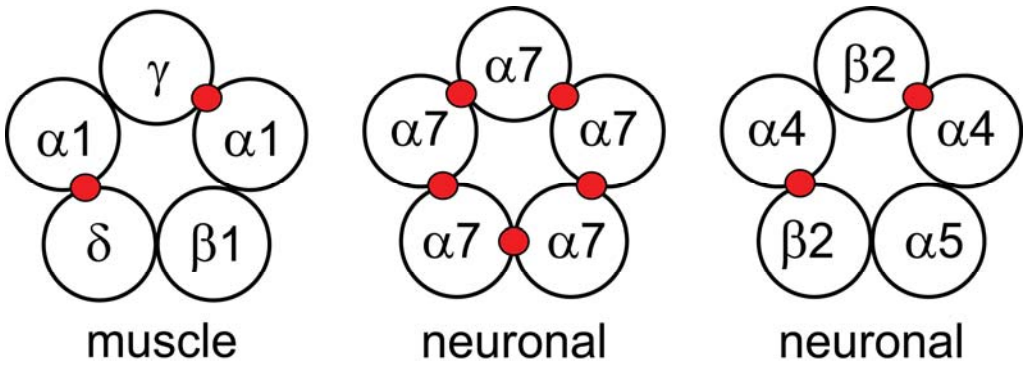

Figure I.1: nAChR Subunit Arrangement. Examples of subunit assembly and location of agonist binding sites (red circles) at α subunit-containing interfaces in nicotinic receptors. A total of 17 functional receptor isoforms have been observed *in vivo*, with different ligand specificity, relative Ca^{2+}/Na^{+} permeability, and physiological function as determined by their subunit composition. The only isoform found at the neuromuscular junction (and in the electric organ of *Torpedo*) is that shown here. The 16 neuronal receptor isoforms, found at autonomic ganglia and in the central nervous system, form homo- and heteropentameric nicotinic receptors composed of α2-α10 and β2-β4 subunits.

played a critical role in delineating the structure and physiological function of the different isoforms (10).

Over the last 30 years, much of the focus in nicotinic receptor study has been on determining the arrangement and composition of the agonist and competitive agonist binding site, the overall three-dimensional structure of the pentameric ligand-gated ion channel, and understanding the allosteric link between agonist binding in the extracellular domain and gating of ion flux through the membrane. Chemical and photo-affinity labeling and site-directed mutagenesis determined that the agonist binding site is formed at the interface of an α subunit and another subunit, and identified seven non-contiguous stretches of amino acids, or loops, that contribute to the agonist binding site, which were named the A, B and C loops on the α side of the subunit interface, and the D, E, F, and F' loops on the so-called complementary side of the subunit interface. Insight into the overall structure has been provided largely by two sources. First, the electron microscopy work of Nigel Unwin and coworkers, has progressed over many years from hazy images toward a very recent 4 angstrom structure of the receptor purified from *Torpedo* membranes (11). Second, X-ray crystallographic studies of the acetylcholine binding protein, a naturally-occurring soluble nicotinic receptor homolog (12), have provided high-resolution information about the atomic structure of the extracellular domain of the receptor. Many studies have sought to determine the allosteric mechanism leading to channel gating, employing techniques ranging from computer modeling, mutagenesis, electrophysiology, fluorescence spectroscopy, mass spectrometry, and structural biology; however, at best there remain significant gaps in our understanding of this concerted process.

B. Pharmacology and Physiology of Nicotinic Receptors

The nicotinic acetylcholine receptor (nAChR) is a member of a superfamily of pentameric ligand-gated ion channels (LGIC), the so-called Cys-loop receptors due to a conserved disulfide linkage in the extracellular domain of the receptor, that also includes that $GABA_A$, $GABA_C$, glycine and $5\text{-}HT_3$ receptors. The cation-selective nAChR is the primary post-synaptic LGIC responsible for fast neurotransmission at the neuromuscular junction and at the peripheral autonomic ganglia. The neuronal nAChR isoforms are largely pre-synaptic and serve to modulate the release of neurotransmitter from upstream terminals. Neuromuscular blocking agents acting at the nAChR, used commonly in pre-surgery anesthesia, are categorized as either competitive (*e.g.* curare), or depolarizing (*e.g.* succinylcholine). Agents acting at autonomic ganglia do so by activating or blocking nAChRs on the post-ganglionic neuron.

Pathological conditions of physiological consequence involving the nAChR include: Myasthenia gravis, an autoimmune disorder against the receptor; Alzheimer's disease, wherein symptoms are believed to arise from a deficit in cholinergic innervation of the cerebral cortex and deficiency of acetylcholine; and nicotine addiction (13). Spinal nAChRs are also believed to play a modulatory role in pain states. Central pre-synaptic receptors feed into several non-cholinergic signaling pathways, providing potential therapeutic targets for subtype-selective drugs in disorders not generally associated with the cholinergic nervous system, for example schizophrenia, Huntington's, and Parkinson's diseases.

The location and function of the different nAChR isoforms has been determined mainly through the use of subtype-selective ligands; those of particular significance and

relevance to this dissertation are shown in Figure I.2. While hundreds of natural and synthetic nAChR ligands have been characterized (14), and a large number of receptor isoforms with distinctive pharmacological properties has been documented, progress toward clinically-useful compounds with high subtype-selectivity has thus far been remarkably unsuccessful. The varied effects of the relatively non-selective agonist nicotine give insight into the potential benefits and negative side effects of drugs targeting the nAChR (Table I.1)

C. The Acetylcholine Binding Protein

Until 2001, all knowledge regarding the 3-dimensional structure of the nAChR was from biochemical inference or low-resolution electron microscopy studies (15,16). The stoichiometry of subunits and the handed-ness of the receptor had been determined and loops of the protein that must come together in space to form the agonist binding site had been predicted. In 2001, Titia Sixma and co-workers published the characterization and X-ray crystal structure at 2.7 angstroms resolution of the acetylcholine binding protein (AChBP) from *Lymnaea stagnalis*, which is homologous to the extracellular domain of the nAChR (12,17).

AChBP assembles as a soluble homopentamer (Figure I.3). Its structure confirmed nearly all of the hypotheses regarding the structure of the ligand-binding, extracellular domains of nAChRs and lent many new insights into determinants of ligand specificity, as well as suggested new hypotheses to be tested regarding an allosteric gating mechanism. AChBP most closely resembles the α7 neuronal nAChR in both amino acid sequence (25% identical) and ligand specificity. It binds α-bungarotoxin,

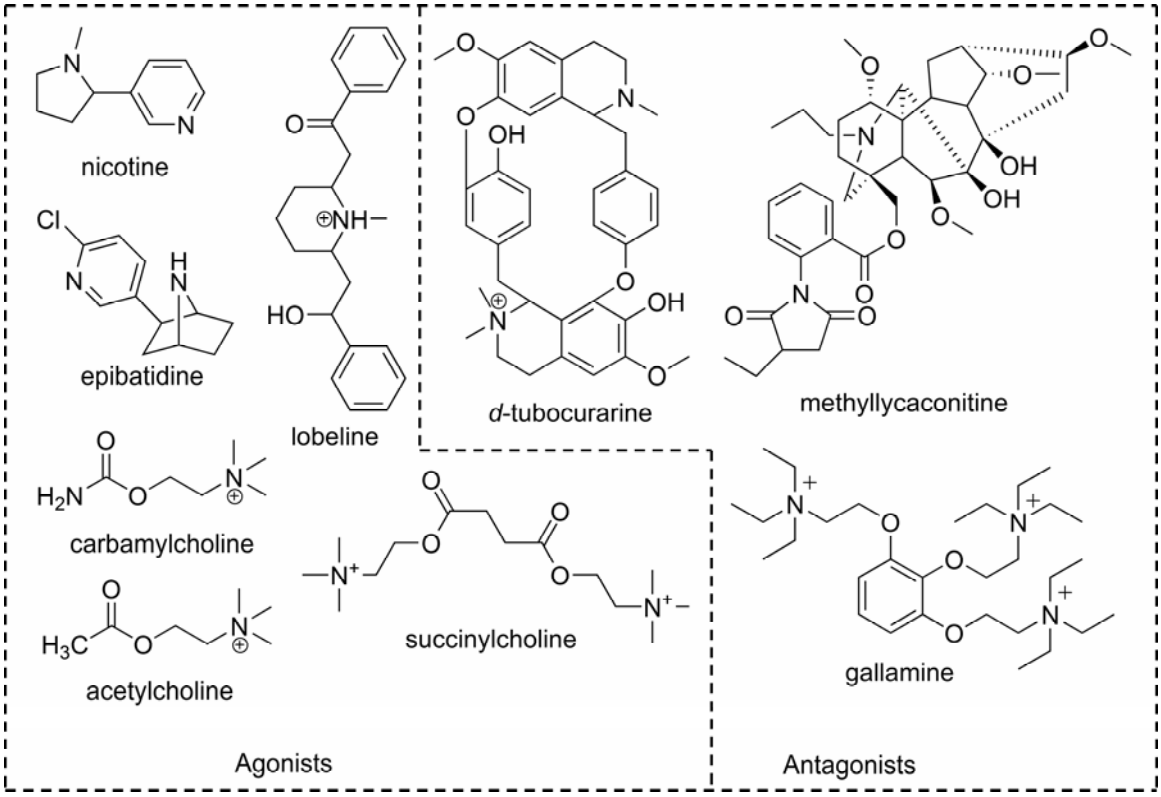

Figure I.2: Nicotinic Agonists and Antagonists

Table I.1

Major Pharmacological Effects of Nicotine (14)

Positive effects	Negative effects
Cognitive enhancement	Addiction
Analgesia	Seizures
Neuroprotection	Respiratory failure
Anxiolytic	Hypothermia
Antipsychotic	Hypertension
Cerebrovasodilation	Emetic

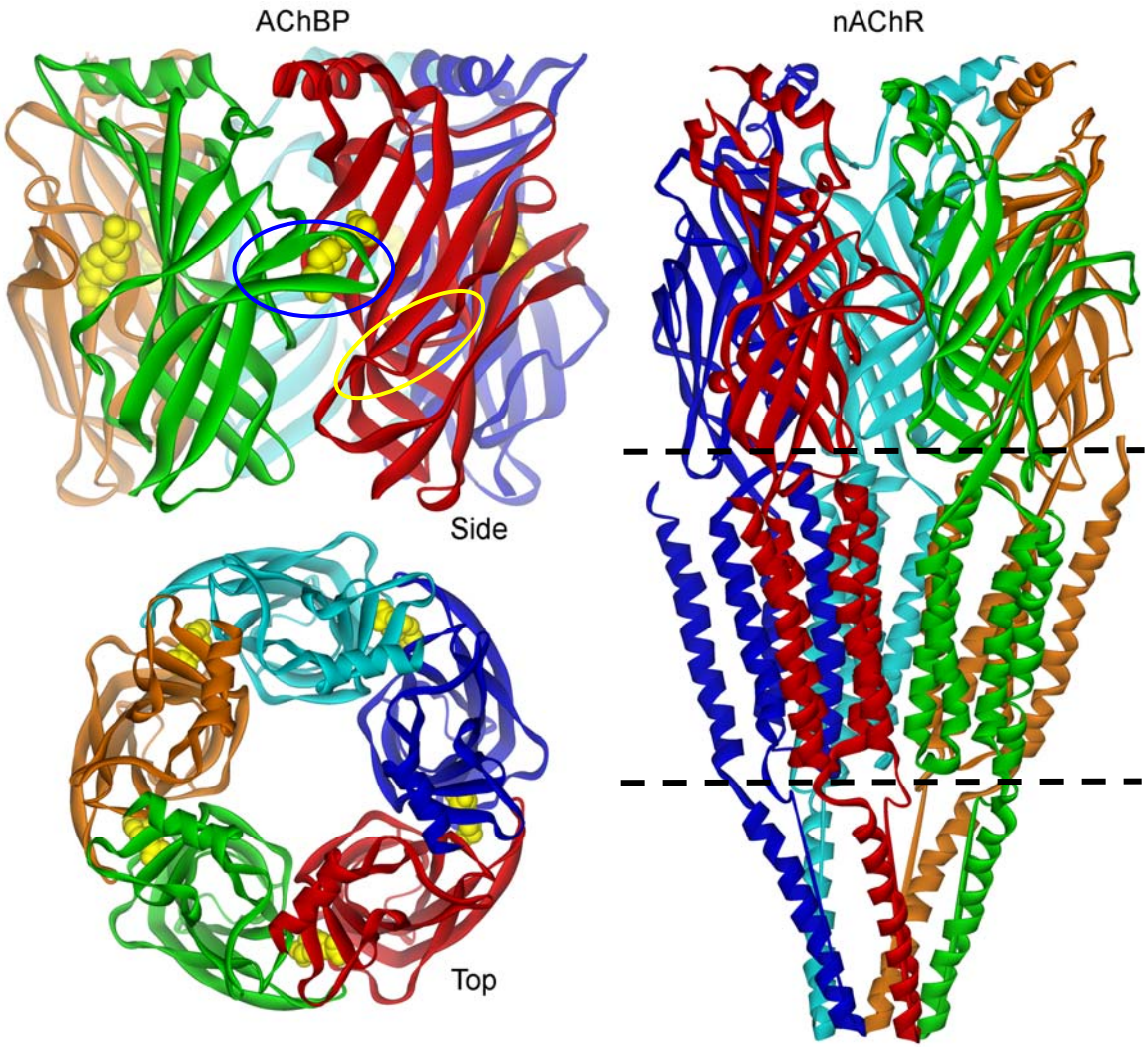

Figure I.3: Crystal Structures of AChBP (12) and the nAChR (11). AChBP is shown in the same orientation and adjacent to the homologous extracellular domain of the full-length nAChR; the central bundle of α-helices (indicated by dashed lines) constitutes the transmembrane portion of the receptor and ion gate. Agonist binding site is indicated by CPK model of HEPES buffer (yellow) in the subunit interfaces of AChBP. In AChBP, the principal subunit containing C-loop that folds over the binding pocket is shown in green, and the complementary subunit is shown in red. The C-loop structure is indicated with a blue ellipse and the F-loop with a yellow ellipse.

epibatidine and methyllycaconitine with high affinity (18). Its affinity for acetylcholine is quite high compared to that for the activatable nAChR (μM vs. mM), which led to the hypothesis that AChBP represents the desensitized (higher affinity for ACh) state of the receptor.

Since its original discovery and characterization in the freshwater snail *Lymnaea*, AChBPs from two other molluskan species have been crystallized: *Aplysia californica*, a saltwater "sea hare;" and *Bulinus truncatus*, another freshwater snail (19). No mammalian equivalent of AChBP has been discovered. AChBP from *Aplysia* has proved to be the most readily crystallizable of the three species, and a comprehensive comparison of agonist and antagonist-bound structures was recently completed in this laboratory (20). Each species of AChBP has its own ligand binding preferences (21), but the structures of the two more recent species offer little new insight into the structure-function relationships of the nAChR. AChBP from *Lymnaea* is capable of initiating gating when linked to the ion channel from the 5-HT3 receptor (22), indicating that not only is it a useful structural surrogate for receptor study, but that it is functional as well, at least when attached to a channel.

To date, AChBP has been used as a soluble model for study of the nAChR extracellular ligand binding domain, and that of other Cys-loop receptors, by a variety of techniques, including solution NMR (23), deuterium-hydrogen exchange (24), fluorescence (25,26), molecular modeling (27,28), and of course X-ray crystallography (29).

D. Cysteine Mutagenesis Labeling

The sulfhydryl side chain of the amino acid cysteine has been used extensively in biochemical studies of protein dynamics. As the strongest nucleophile among the amino acids, it can be reacted with high selectivity to various sulfhydryl-modifying agents, such as iodoacetamides, maleimides, and methanethiosulfonates (Figure I.4)(30).

To study a protein via cysteine labeling, one must have a single reactive cysteine in the protein in order to avoid ambiguity in the data analysis. As the extracellular milieu is oxidizing, most extracellular proteins have their cysteines in disulfide bonds as cystine, so all one must do is add an odd cysteine. Intracellular proteins often have multiple free cysteine residues, and removing them may or may not cause problems with folding or function of the protein. Generally, cysteine mutagenesis (removal or insertion) is well tolerated. Functional moieties that can be incorporated into the sulfhydryl-reactive compound to study protein dynamics include: hydrophobic, polar and charged groups to study the surface characteristics of a certain region of the protein; bulky groups to study the effect of addition of a large amino acid side chain, fluorescent groups to monitor the dielectric constant of their local environment or changes in protein backbone flexibility and global rotation rates; and spin labels, that possess an unpaired electron, and are popular for electron paramagnetic resonance spectroscopy studies examining protein secondary and tertiary structure as well as structural fluctuations in the picosecond-nanosecond time scale.

E. Objective of the Dissertation

At the start of my thesis research, the crystal structure of AChBP from *Lymnaea* had just been published and the nAChR field, at least the structural side of it, had taken a giant leap forward in its understanding of the receptor. Also, at long last the field had

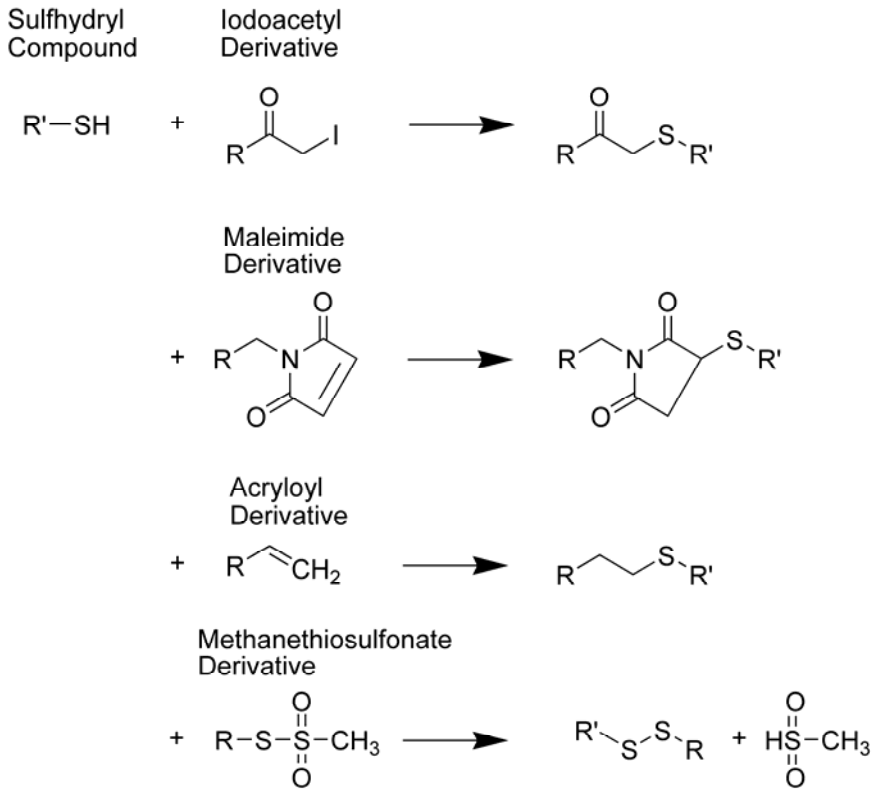

Figure I.4: Sulfhydryl Modifying Agents

possession of a soluble model to use to study the receptor extracellular domain with methods that had previously been prohibited due to the necessary evils of working with an integral membrane protein, such as the presence of detergent and low amounts of material. Some limitations inherent in the crystal structure were that the information was represented in a single rigid snapshot and was therefore not dynamic, and that the atomic interactions governing ligand binding had to be inferred from observed interactions with a molecule of bound HEPES buffer.

The objectives of my dissertation research were, then, to use AChBP as a soluble surrogate for the nAChR extracellular domain to study protein dynamics in solution. Specifically, using fluorescence and other biochemical and biophysical methods I sought to (1) determine ligand-induced changes in solvent exposure in regions of AChBP likely to be affected either directly or indirectly by ligand binding, (2) investigate the interaction of α-neurotoxins with AChBP from the perspectives of both translational and rotational diffusion to determine their relative flexibility when bound, and (3) to monitor ligand-induced changes in the α-carbon backbone flexibility of AChBP to determine which regions respond distinctively to agonists and antagonists of nAChRs.

F. References

1. Langley, J. N. (1906) in *Croonian Lecture, Proc. Roy. Soc. Ser. B.*

2. Dale, H. (1914) *J Pharmacol Exp Ther* **6**, 147-190

3. Karlin, A. (2002) *Nat Rev Neurosci* **3**, 102-114

4. Sine, S. M., and Engel, A. G. (2006) *Nature* **440**, 448-455

5. Changeux, J. P., and Edelstein, S. J. (2005) *Nicotinic Acetylcholine Receptors: From Molecular Biology to Cognition*, Editions Odile Jacob/Johns Hopkins University Press

6. Feldberg, W., Fessard, A., and Nachmansohn, D. (1940) *J Physiol* **97**, 3-4

7. Hodgkin, A. L., and Huxley, A. F. (1952) *J Physiol* **117**, 500-544

8. Lee, C. Y., and Chang, C. C. (1966) *Mem. Inst. Butantan Sao Paulo* **33**, 555-572

9. Changeux, J. P., Kasai, M., and Lee, C. Y. (1970) *Proc Natl Acad Sci U S A* **67**, 1241-1247

10. Nirthanan, S., and Gwee, M. C. (2004) *J Pharmacol Sci* **94**, 1-17

11. Unwin, N. (2005) *J Mol Biol* **346**, 967-989

12. Brejc, K., van Dijk, W. J., Klaassen, R. V., Schuurmans, M., van Der Oost, J., Smit, A. B., and Sixma, T. K. (2001) *Nature* **411**, 269-276

13. Brunton, L., Lazo, J., and Parker, K. (2006) *Goodman & Gilman's The Pharmacological Basis of Therapeutics*, 11 Ed., McGraw-Hill

14. Daly, J. W. (2005) *Cell Mol Neurobiol* **25**, 513-552

15. Miyazawa, A., Fujiyoshi, Y., Stowell, M., and Unwin, N. (1999) *J Mol Biol* **288**, 765-786

16. Unwin, N. (1993) *J Mol Biol* **229**, 1101-1124

17. Smit, A. B., Syed, N. I., Schaap, D., van Minnen, J., Klumperman, J., Kits, K. S., Lodder, H., van der Schors, R. C., van Elk, R., Sorgedrager, B., Brejc, K., Sixma, T. K., and Geraerts, W. P. (2001) *Nature* **411**, 261-268

18. Hansen, S. B., Radic, Z., Talley, T. T., Molles, B. E., Deerinck, T., Tsigelny, I., and Taylor, P. (2002) *J Biol Chem* **277**, 41299-41302

19. Celie, P. H., Klaassen, R. V., van Rossum-Fikkert, S. E., van Elk, R., van Nierop, P., Smit, A. B., and Sixma, T. K. (2005) *J Biol Chem* **280**, 26457-26466

20. Hansen, S. B., Sulzenbacher, G., Huxford, T., Marchot, P., Taylor, P., and Bourne, Y. (2005) *Embo J* **24**, 3635-3646

21. Hansen, S. B., Talley, T. T., Radic, Z., and Taylor, P. (2004) *J Biol Chem* **279**, 24197-24202

22. Bouzat, C., Gumilar, F., Spitzmaul, G., Wang, H. L., Rayes, D., Hansen, S. B., Taylor, P., and Sine, S. M. (2004) *Nature* **430**, 896-900

23. Gao, F., Mer, G., Tonelli, M., Hansen, S. B., Burghardt, T. P., Taylor, P., and Sine, S. M. (2006) *Mol Pharmacol*

24. Shi, J., Koeppe, J. R., Komives, E. A., and Taylor, P. (2006) *J Biol Chem* **281**, 12170-12177

25. Hibbs, R. E., Johnson, D. A., Shi, J., Hansen, S. B., and Taylor, P. (2005) *Biochemistry* **44**, 16602-16611

26. Hibbs, R. E., Talley, T. T., and Taylor, P. (2004) *J Biol Chem* **279**, 28483-28491

27. Reeves, D. C., Sayed, M. F., Chau, P. L., Price, K. L., and Lummis, S. C. (2003) *Biophys J* **84**, 2338-2344

28. Henchman, R. H., Wang, H. L., Sine, S. M., Taylor, P., and McCammon, J. A. (2005) *Biophys J* **88**, 2564-2576

29. Bourne, Y., Talley, T. T., Hansen, S. B., Taylor, P., and Marchot, P. (2005) *Embo J* **24**, 1512-1522

30. Hermanson, G. T. (1996) *Bioconjugate Techniques*, Academic Press/Elsevier Science, San Diego

Chapter II

Fluorescence Spectroscopy

In 1845 Sir John Frederick William Herschel described "an extremely vivid and beautiful celestial blue colour" emanating from a clear solution of quinine he had illuminated with sunlight, and thus the study of fluorescence began (1). During World War II, the Department of Defense was interested in therapies for malaria, for which quinine was one; this resulted in the development of the first practical spectrofluorometer in the 1950s at the newly-formed National Institutes of Health. Since then fluorescence has been used extensively in biochemical and biophysical research, and over the last 20 years its use has become mainstream in techniques such as DNA sequencing, microscopy, enzyme activity assays, and cell sorting by flow cytometry. Much of the background information for this chapter was gleaned from the excellent fluorescence text by J. R. Lakowicz (2).

A. Principles of Fluorescence

Luminescence is the emission of light from any substance and results from relaxation of electronically-excited states. Fluorescence, one form of luminescence, occurs when an electron in the excited singlet state returns to its paired electron in the ground state, and in process emits a photon. The process of fluorescence is very rapid (on the order of nanoseconds) because the return to the ground state is allowed due to proper spin coupling with the paired electron. Phosphorescence, the other form of luminescence, results from the emission of a photon from an electron in an excited triplet

state wherein its paired electron in the ground state has the same spin orientation; this emission is much slower as the return to the ground state is a disallowed transition. The lifetime of phosphorescence emission is on the order of milliseconds or slower, as demonstrated by the glow-in-the-dark toys.

The fundamental principles of fluorescence and phosphorescence are illustrated in the Jabloński diagram (Figure II.1). The singlet ground state is depicted as S_0, the first and second excited singlet states are S_1 and S_2, and the excited triplet state is T_1. The Franck-Condon principle dictates that the timescale of the absorption of a photon occurs on the order of 10^{-15} seconds, too fast for displacement of nuclei by factors such as energy transfer or solvent interactions that are able to affect the slower process of fluorescence emission (discussed later). Excitation to the excited singlet state usually occurs to a level above the lowest energy singlet state; relaxation back the lowest energy singlet state, the result of internal conversion, occurs in $\sim 10^{-12}$ seconds, much faster than fluorescence emission. Hence, fluorescence emission generally results from a thermally-equilibrated and lowest-energy excited state. An electron in its excited singlet state can also undergo intersystem crossing to the triplet state, which is generally of lower energy and hence the emitted photon is of longer wavelength than that from the singlet state.

B. Solvent Effects and Stokes' Shift

In 1852, Sir George G. Stokes observed that fluorescence emission occurs at a longer wavelength, and hence lower energy, than that of absorption (3). This shift in wavelength is called the Stokes' shift, and occurs universally for fluorophores in solution. Factors that commonly contribute to the Stokes' shift include rapid relaxation of the excited electron to the lowest vibrational state of S_1, decay upon emission to a higher

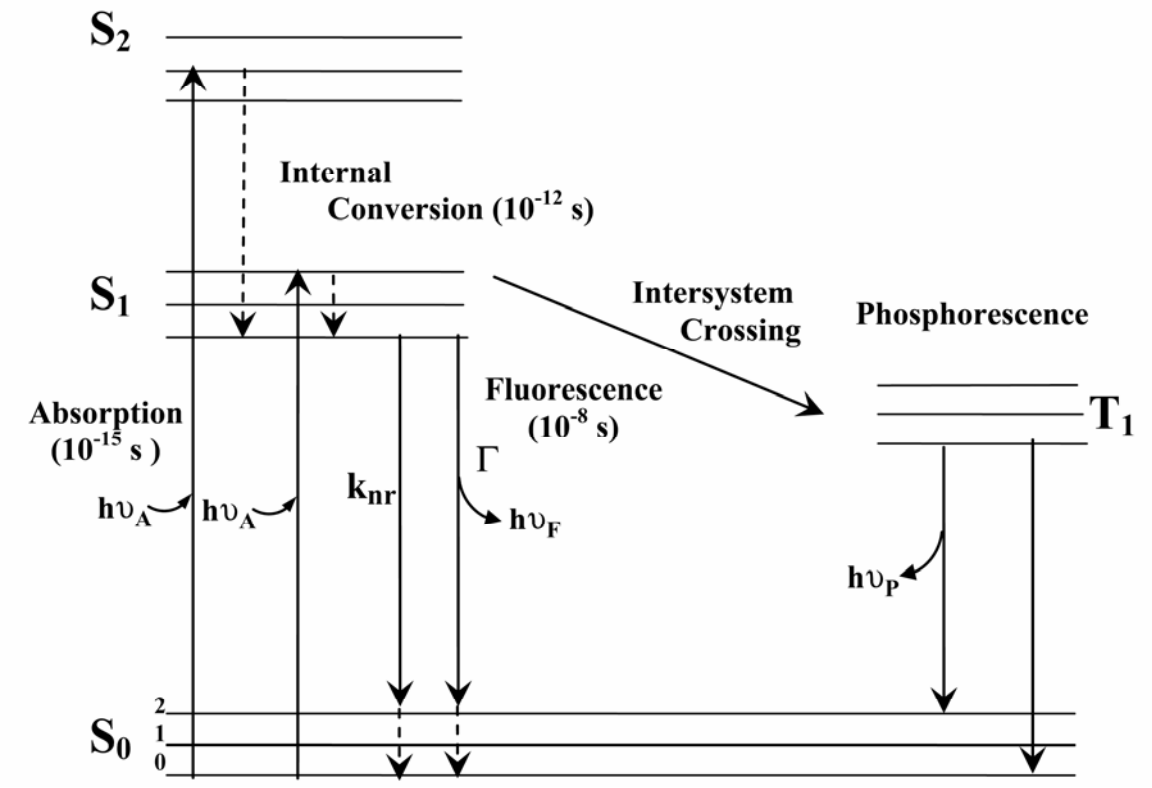

Figure II.1: Jabloński Diagram

vibrational level of S_0, energy transfer, and effects from the surrounding solvent molecules.

Solvent polarity and the local environment of a fluorophore in solution can have significant effects on its emission spectrum. An increase in solvent polarity, particularly in the case of a polar fluorophore, results in an S_1 excited state of lower energy and hence a shift to longer wavelength. Solvent affects the emission energy via stabilization of the excited state by polar solvent molecules. Typically, the fluorophore has a larger dipole moment in the excited state than in the ground state. After excitation, the solvent dipoles reorient around the new dipole moment of the fluorophore, which stabilizes the excited state, subsequently lowering the energy of emission. The timescale of absorption is much faster than solvent relaxation can occur, so absorption spectra are not affected by solvent stabilization of the excited state. In practice, solvent effects on fluorescence emission can be used to quantitate ligand binding in proteins and monitor changes in the local environment of a fluorescent probe tethered to a protein. The emission spectrum of the fluorophore acrylodan (Figure II.2) is especially sensitive to the dielectric constant of its local environment, and when tethered to a protein has the capacity to report changes in solvent exposure upon ligand binding or a conformational change.

C. Quantum Yield and Fluorescence Lifetime

The quantum yield of a fluorophore is its efficiency of fluorescence, that is, the fraction of photons emitted per photon absorbed. Substances with the highest quantum yields, approaching 1, are the brightest; fluorescein and rhodamine are good examples. The quantum yield can be calculated simply as

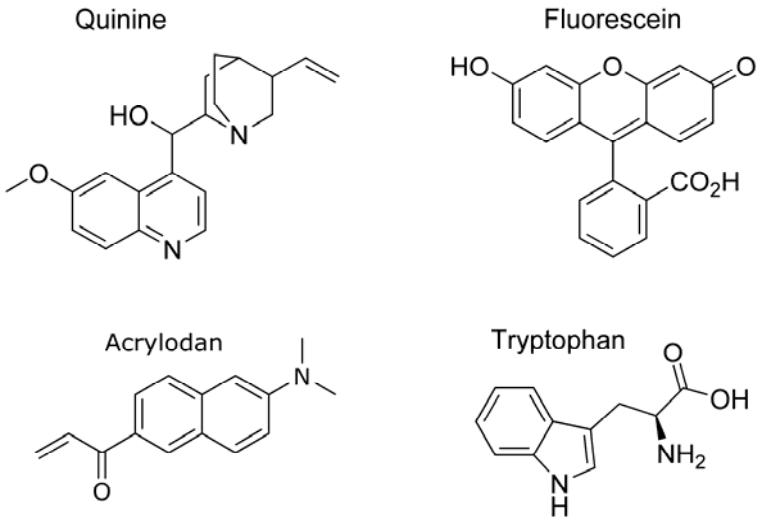

Figure II.2: Structures of Common Fluorophores

$$Q = \frac{\Gamma}{\Gamma + k_{nr}} \qquad \text{(Equation II.1)}$$

where Q is the quantum yield, Γ is the radiative decay rate, and k_{nr} is the non-radiative decay rate.

The fluorescence lifetime of a substance is the average time that a photon remains in the excited state, and the length of this lifetime, usually in the low nanoseconds, determines how much of an effect solvent interactions will have on the fluorescence emission spectrum. The excited state lifetime can be calculated as

$$\tau = \frac{1}{\Gamma + k_{nr}} \qquad \text{(Equation II.2)}$$

though calculated and experimental lifetimes often differ due to known or unknown factors, such as the presence of a quenching group near the fluorescent tryptophan residue in a protein. Fluorescein and acrylodan (Figure II.2) have lifetimes of approximately 4 nanoseconds; lanthanides are famous for their long lifetimes ranging from 0.3 to 3 microseconds.

D. Steady-State and Time-Resolved Fluorescence Anisotropy

Upon excitation with polarized light, fluorophores will emit partially-polarized light. The extent of polarization of the fluorescence emission is described in terms of its anisotropy (r). Intrinsic in each fluorophore are absorption and emission transition moments; these are usually oriented the same direction. Molecules in an isotropic population of fluorophores will be selectively excited by polarized light when their absorption transition moment is oriented along the electric vector of the incident light. This selective excitation results in an excited state population that is not randomly

oriented. The theoretical maximum anisotropy for a sample where the absorption and emission transition moments are parallel, and there are no factors resulting in depolarization of emission, is 0.4. This value is based on the probability of photon absorption as it relates to the fluorophore's orientation relative to the incident light, and is true for a randomly-oriented population of fluorophores in a rigid glass. If the excited state population is free to diffuse in solution, then some of those fluorophores excited by light polarized in a plane parallel to their absorption transition moment will reorient and emit light in the perpendicular plane. The degree of fluorescence anisotropy (r) is calculated as the difference between the emission intensity in the parallel plane and the perpendicular plane, divided by the total emission (Figure II.3):

$$r = \frac{I_{\parallel} - I_{\perp}}{I_{\parallel} + 2I_{\perp}}. \qquad \text{(Equation II.3)}$$

Depolarization of fluorescence emission most commonly depends upon rotational diffusion of the fluorophore. Biochemical assays that monitor emission polarization from a fluorophore conjugated to a macromolecule exploit this phenomenon to gain insight into protein size, conformation or shape, and flexibility. The Perrin equation describes the simplest case of emission depolarization from a rotating sphere:

$$\frac{r_0}{r} = 1 + \frac{\tau}{\theta} = 1 + 6D\tau \qquad \text{(Equation II.4)}$$

where r is the measured anisotropy, r_0 is the fundamental anisotropy, τ is the fluorescence lifetime, θ is the rotational correlation time, and D is the rotational diffusion coefficient. The fundamental anisotropy is unique to a given fluorophore, and is its maximal anisotropy in a rigid glass. For globular proteins without appreciable dimensional

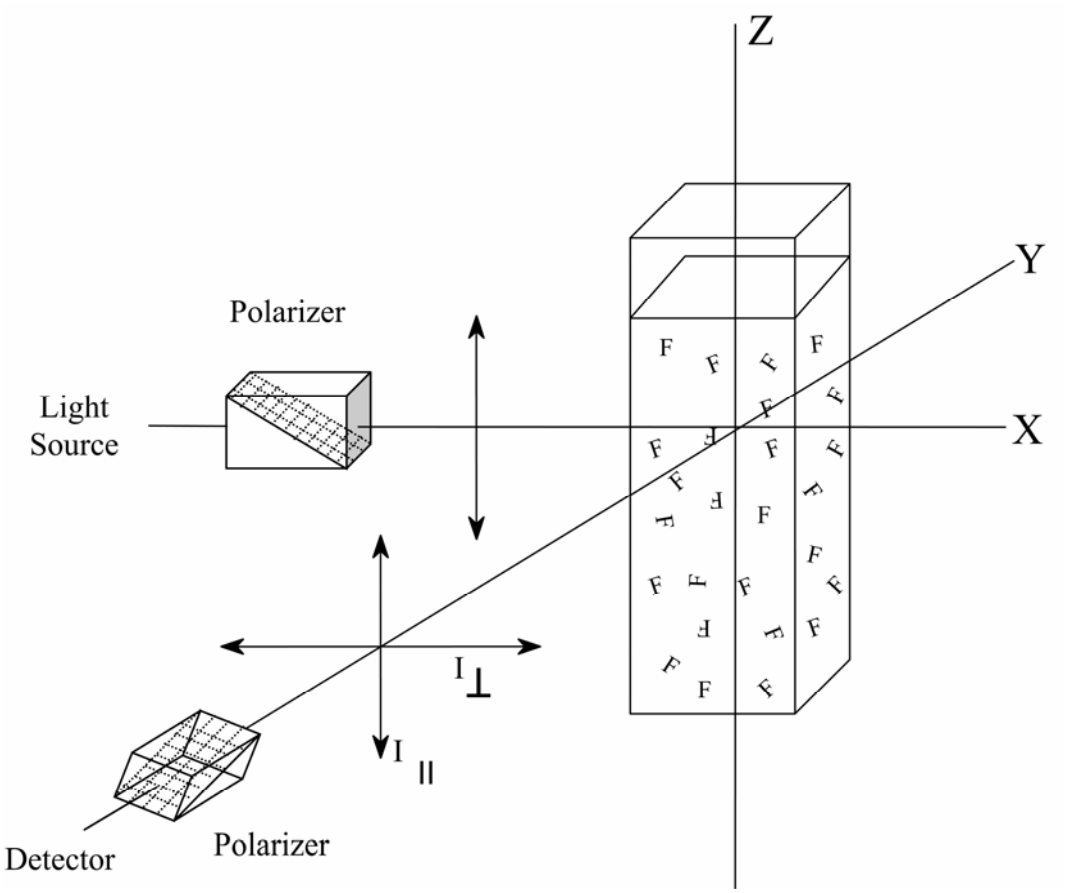

Figure II.3: Schematic for Measurement of Fluorescence Anisotropy

asymmetry, the rotational correlation time is ~related to the molecular weight. For many proteins, more than simple global rotation of the macromolecule contributes to a decrease in steady-state anisotropy, but what one measures is an average of all types of motion affecting to position of the fluorophore, and this observed anisotropy is heavily weighted by the rotational correlation time. Steady-state anisotropy is useful in describing the shape or size of a protein, or in monitoring association of two or more molecules that results in an increase in the hydrodynamic volume of the macromolecular complex, and subsequently the rotational correlation time.

Time-resolved anisotropy decay measurements allow for dissection of the different components of rotational diffusion that contribute to the observed anisotropy. For a simple sphere, anisotropy decay follows a single exponential, from which one can determine a single rotational correlation time. For a non-spherical fluorophore or a fluorophore as part of a protein, the global rotation is faster around one axis than another, which allows an estimate of shape from anisotropy decay measurements. Segmental motions of the protein α-carbon backbone also contribute to the re-orientation of a fluorophore during its emission lifetime, as does torsional motion of the fluorophore about its bond to the amino acid side chain to which it is tethered. Hence, in a protein with a conjugated fluorophore, one is frequently able to distinguish the three factors that contribute to its anisotropy decay: global rotation (slow), segmental motion (fast, 1-10 ns), and tether-arm motion (very fast, < 1 ns) (Figure II.4). We describe motion of a fluorophore conjugated to residues in the acetylcholine binding protein as a bi-exponential decay process

$$r(t) = \beta_1 \exp(-t/\phi_1) + \beta_2 \exp(-t/\phi_2) \qquad \text{(Equation II.5)}$$

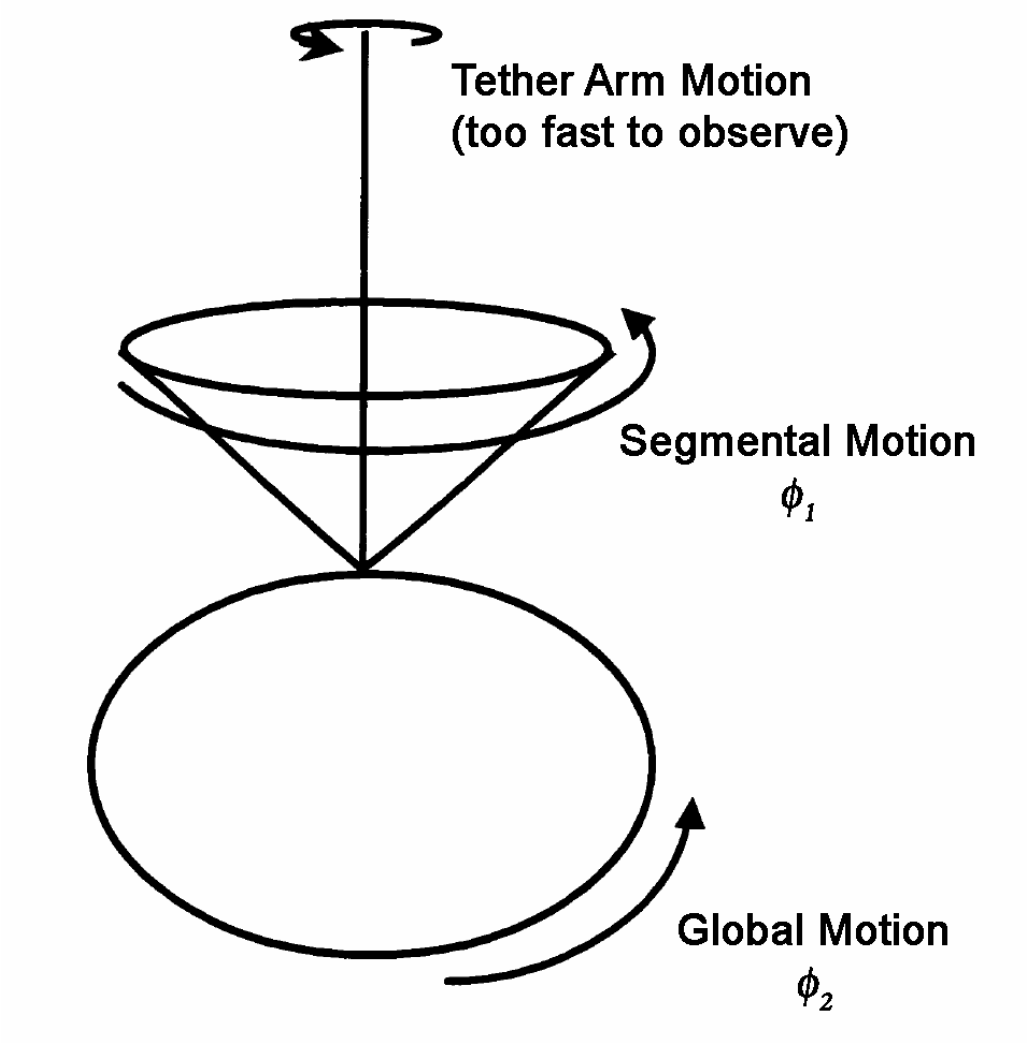

Figure II.4: Components of Rotational Motion of a Fluorophore Conjugated to a Macromolecule

where β_1 and β_2 are amplitudes of the fast and slow components, respectively, and ϕ_1 and ϕ_2 are the rotational correlation times of the components.

Segmental and tether arm motions can both be thought of as motion within a cone, as shown for segmental motion in Figure II.4, where one end of the fluorophore or protein backbone is a fulcrum and the rest of the fluorophore can diffuse a certain angle as limited by adjacent protein structure. The quantitative measurement of anisotropy decay over time allows one to determine an amplitude as well as a rate of decay for segmental or α-carbon backbone motion; here, the rate corresponds to how fast the backbone is moving within its "cone," and the amplitude relates to the physical excursion or cone angle through which the backbone can diffuse. Torsional or tether-arm motion is often too fast to allow accurate measurement of a rate, but one can calculate an amplitude as the difference between the observed total anisotropy ($\beta_1 + \beta_2$) and the fundamental anisotropy. More detailed methods for anisotropy data analysis are contained in Chapters V and VI.

E. Thiol-Reactive Fluorescent Probes

It is often necessary, or preferable, to use extrinsic fluorescent probes to study protein dynamics. The native fluorescent amino acids, tyrosine, phenylalanine and tryptophan are often present in multiplicity, which complicates analysis of their emission spectra. These aromatic amino acids also often play an important structural and/or functional role so they cannot be readily removed or substituted by another amino acid. The advantages of an extrinsic fluorophore are that it can be conjugated to a specific region in a protein, and that one can choose a fluorophore with properties well-suited to the experimental design.

A wide variety of small-molecule fluorescent probes are available with reactive specificity for the free positively charged lysine nitrogen or the free sulfhydryl of cysteine residues. For many of the studies presented in this dissertation, I chose to insert and fluorescently label cysteines, because there are many lysines in AChBP but only four cysteines (per subunit), all in disulfide bonds and generally not reactive to sulfhydryl-labeling reagents. The emission spectrum of the fluorophore acrylodan, described previously (Figure II.2), is exquisitely sensitive to solvent polarity, hence I used this fluorophore to monitor changes in solvent exposure upon ligand binding in an effort to map ligand binding sites and deduce conformation changes in the structure of AChBP. After much trial and error, I found that MTS-fluorescein, very bright, and MTS-EDANS (Figure II.5), a longer lifetime fluorophore (~20 ns), both worked well in decay of anisotropy studies. I settled on the methanethiosulfonate derivative of fluorescein because it reacted very quickly and specifically with most engineered cysteines in AChBP and gave a strong signal. MTS-EDANS was comparably dim, but provided a lifetime long enough to accurately measure global rotation rates. Fluorescein reported well on the faster segmental motion, so using the combination of fluorophores in parallel experiments worked well. For studies of α-neurotoxin dynamics (Chapter IV), I was fortunate to be provided with FITC-labeled α-cobratoxin by Dr. David Johnson from the University of California at Riverside. This fluorescein derivative was reacted with the native lysines in the toxin molecule, and individual, singly-labeled toxins were separated for study (4).

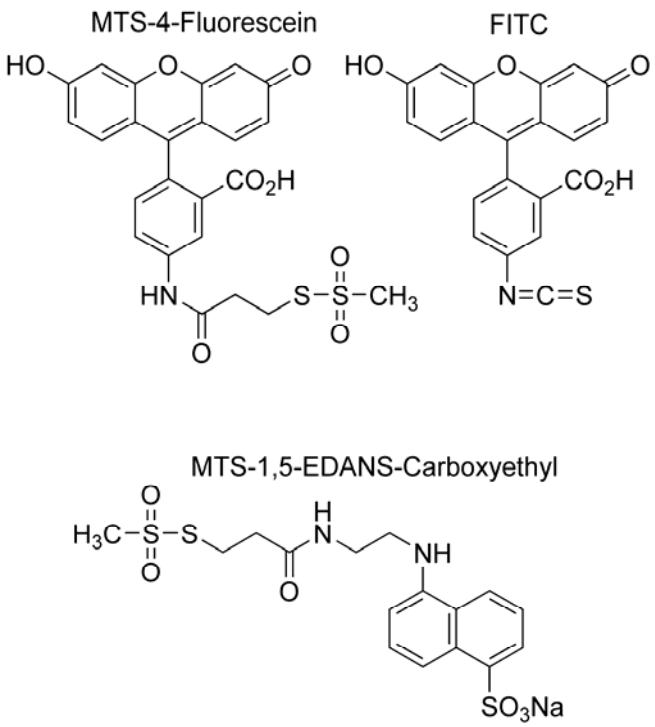

Figure II.5: Sulfhydryl-Reactive Fluorophores Used in Anisotropy Decay Experiments

F. References

1. Herschel, S. J. F. W. (1845) *Philos Trans R Soc Lond* **135**, 143-145

2. Lakowicz, J. R. (1999) *Principles of Fluorescence Spectroscopy*, 2nd Ed., Kluwer Academic Publishers and Plenum Publishing Corp., New York

3. Stokes, S. G. G. (1852) *Philos Trans R Soc Lond*, 463-562

4. Johnson, D. A., and Cushman, R. (1988) *J Biol Chem* **263**, 2802-2807

Chapter III

Production, Characterization, and Thiol Reactivity of Cysteine-Substituted Acetylcholine Binding Protein Mutants

Thirty four single cysteine mutants were attempted in AChBP from *Lymnaea*; of these, nine were useful in acrylodan-labeling studies of solvent exposure, and six were useful in MTS-fluorescein or MTS-EDANS labeling studies of anisotropy decay. Mutation positions were chosen based on their location in the AChBP X-ray crystal structure and their likelihood of conformational movement or being in proximity to a bound ligand. Mutant AChBPs were stably transfected into HEK-293 cells and protein was purified from the medium by affinity chromatography. Mutants were assays by FPLC and SDS-PAGE to monitor purity and assembly as a pentamer. Cysteine mutants were then assayed for their ability to bind reference ligands with high affinity, and subsequent labeling with various sulfhydryl-reactive fluorophores was attempted. Stoichiometry of labeling with fluorophores was assessed, as well as background fluorescence emission intensity. Clean mutant protein preparations that bound ligand with affinity comparable to wild-type protein and labeled specifically with a probe of interest were assayed further, as described in subsequent chapters.

A. Rationale for Selection of Mutation Sites

Points of cysteine mutagenesis in AChBP were chosen largely based on the crystal structure of AChBP (1). Thirty years of biochemical assays had determined regions of the protein important in ligand binding, and with this information and the three-dimensional template of the X-ray structure, choosing regions that might respond

either directly or indirectly to ligand binding was straightforward. An effort was made to choose sites that would not have deleterious effects of protein assembly, however in hindsight it was in most cases impossible to predict which mutants would or would not express and assemble properly. Table III.1 describes the mutations attempted and their respective outcomes; mutations in bold labeled successfully with one or more fluorophores.

B. Site-Directed Mutagenesis

The AChBP cDNA I used as a template for mutagenesis was synthesized from overlapping oligonucleotides by Scott Hansen shortly before I began my thesis research (2). The wild-type cDNA was inserted into the commercially-available p3×FLAG-CMV-9 expression vector (Sigma) that contains a preprotrypsin leader peptide followed by an amino-terminal 3×FLAG epitope, as well as vector DNA coding for ampicillin and neomycin resistance. A carboxy-terminus 6×Histidine tag was also inserted for radioligand binding assays. Site-directed mutagenesis PCR reactions were performed using standard molecular biology procedures, with a pair of anti-parallel 30-mer primers containing the 1-3 nucleotide mutation in the approximate center. PCR products were transformed into *E. coli* for expansion of DNA; the plasmid DNA was purified using the Qiagen miniprep kit and the sequence of the coding region of the AChBP gene was verified using an ABI DNA sequencer. Mutant cDNAs were subcloned into naïve vector and verified via restriction digest or re-sequencing before transfection.

Table III.1

Cysteine Mutants in AChBP from *Lymnaea*

Mutation	Location	Results
K34C	Membrane side of pocket, complementary face	No expression
W53C	**In pocket, complementary face**	**Expresses, labels w/ acrylodan**
N90C	Membrane side of pocket, complementary face	No expression
K94C	Membrane side of pocket, complementary face	Expresses but does not label
L112C	**Apical pocket, complementary face**	**Expresses, labels w/ acrylodan**
M114C	**Apical pocket, complementary face**	**Expresses, labels w/ acrylodan**
K139C	**Membrane side of pocket, principal face**	**Expresses, labels w/ acrylodan and MTS-Fl**
W143C	In binding pocket, principal face	Misfolded
T144C	Apical to binding pocket, principal face	No expression
E157C	**Outside pocket, complementary face**	**Expresses, labels with acrylodan**
N158C	**Outside pocket, complementary face**	**Expresses, labels w/ acrylodan and MTS-Fl**
Y164C	**Membrane side of pocket, complementary face**	**Expresses, labels w/ acrylodan and MTS-Fl**
L174C	Membrane side of C-loop, exposed	No expression
D175C	Membrane side of C-loop, exposed	No expression
V176C	Membrane side of C-loop, buried	No expression
T177C	**Membrane side of C-loop, exposed**	**Expresses, labels w/ MTS-Fl**
Q178C	**Membrane side of C-loop, buried**	**Expresses, labels w/ acrylodan**
K179C	Membrane side of C-loop, exposed	No expression
K180C	Membrane side of C-loop	No expression
N181C	Mid C-loop, oriented toward membrane	Misfolded
S182C	**Mid C-loop, solvent exposed**	**Expresses, labels w/ acrylodan**
V183C	**Mid C-loop, non-solvent exposed**	**Expresses, labels w/ acrylodan**
T184C	Mid C-loop, solvent exposed	No expression
Y185C	C-loop tip, points in	No expression
S186C	C-loop tip, solvent exposed	Misfolded
C187S	**C-loop tip**	**Expresses, labels w/ MTS-Fl**
C188S	C-loop tip	Expresses but does not label
P189C	Apical chain of C-loop	No expression
E190C	Apical chain of C-loop	No expression
A191C	Apical chain of C-loop	Expresses but does not label
Y192C	Apical chain of C-loop	No expression
E193C	Apical chain of C-loop	No expression
D194C	**Apical chain of C-loop**	**Expresses, labels w/ MTS-Fl**
E196C	Membrane side of pocket, complementary face	No expression

C. Protein Expression

HEK-293 cells were maintained in a standard medium containing DMEM + 10% FBS + L-glutamine. AChBP wild-type and mutant plasmids were transfected into HEK-293 cells using the method of calcium phosphate precipitation with approximately 20 μg of DNA per 10 cm tissue culture dish, and were assayed preliminarily for transient expression by radioligand binding and/or Western blot. The soluble radioligand binding assay was an adaptation of the Scintillation Proximity Assay (SPA, Amersham) using anti-HIS SPA beads and [^{3}H]-epibatidine. If the radioligand binding assay on tissue-culture medium from transiently-transfected cells did not show binding activity, an immuno-blot was used to test for presence of protein. In Western blots, the primary antibody was mouse anti-FLAG, and secondary was goat anti-mouse. If transient expression was positive, the tissue culture medium was supplemented with 800 μg/mL G418 antibiotic. Selection for stably-transfected cells usually required 2-4 weeks of passaging the transfected cell line. In some cases, single clones of transfected cells were grown up into clonal lines to optimize expression, however in the majority of cases clonal selection was not necessary. Once clonal selection was complete, cells were passaged in medium not containing G418.

D. Protein Purification

Stably-expressing cells from 4-5 nearly confluent 10 cm plates were used to seed 4 triple-layer flasks. Flasks were seeded with the standard tissue culture medium, allowed to approach confluency (2-5 days), and then FBS concentration was reduced to 2%. Media were then harvested ever 1-3 days as needed until cells sloughed off of the growing surface; flasks were generally maintained for 4-6 weeks. This amount of

medium usually provided enough protein for all of the fluorescence and radioligand binding assays.

AChBP protein was purified from the tissue-culture medium by adsorption onto an α-FLAG affinity column (Sigma), at 4°C. The average yield from the affinity resin was ~0.7 mg protein per mL resin, and the resin could be re-used with no detriment to the yield 4-5 times. In most cases, I poured a column of 4-5 mL of α-FLAG resin, and monitored the protein content of the flow-through by SPA. Upon saturation with protein, the column was washed with 0.5 L of Tris-buffered saline containing 0.02% NaN_3, and protein was eluted at room temperature with 1×FLAG peptide (Sigma) as per the manufacturer's instructions. Protein was then concentrated in Amicon Centricon YM-30 columns (Millipore) to ~2 mg/mL, stored at 4°C, and was generally stable in terms of ligand binding and lack of aggregation for six months to one year.

E. Characterization of Cysteine Mutants

Assembly as a pentamer was assessed by size-exclusion FPLC. Several mutant preparations contained some fraction of aggregation, however when separated as a species the aggregate ran at the appropriate monomer weight on a denaturing SDS-PAGE gel, bound ligand with an affinity identical to the "pentamer" FPLC peak, and had a pentameric molecular weight as determined by analytical ultracentrifugation. Mutants that did not have the predominant peak at the pentameric elution volume were not used in labeling experiments. Dissociation constants for two reference ligands, epibatidine and α-bungarotoxin, were determined by SPA using either direct saturation binding measurements with [^{3}H]-epibatidine or [^{125}I]-α-bungarotoxin, or competition against one of the radioligands. Detailed results from these experiments are listed in Chapters IV-VI.

For most mutant AChBPs, the affinity for either ligand was not affected by more than 5-fold. Also worth noting is that the C-loop was profoundly sensitive to mutagenesis relative to the rest of AChBP. Our conclusion was that as cysteines are inserted close to the loop tip, mixed disulfides are formed with the vicinal cysteines (C187, C188) that prevent protein expression. Removal of a single vicinal cysteine by replacement with a serine was informative. Since the protein expressed nearly as well as wild-type, bound ligands were found to have only moderately decreased affinities.

F. Fluorophore Labeling of Engineered Cysteines

Several sulfhydryl probes were investigated in efforts to label the engineered cysteine residues. Among these were acrylodan, several derivatives of fluorescein (5-iodoacetamidofluorescein, fluorescein-maleimide, and MTS-fluorescein), MTS-sulforhodamine, and two longer-lifetime probes, MTS-EDANS and IAEDANS (the iodoacetamide derivative of the same compound). Structures for these compounds are shown in Figure II.5.

For labeling, protein was diluted to 20 μM in binding site concentration, and 1 μL of 10 mM fluorophore was added into a total volume of 100 μL to achieve a 5-fold molar excess of the label. All labeling reactions were shielded from light. Acrylodan and MTS-reagent labeling were most specific when reacted for 90 or 60 minutes at room temperature, respectively. All other fluorescent derivatives reacted most specifically when labeling was performed for 16-20 hours at 4°C. Unreacted fluorophore was removed from the covalently-labeled protein by size exclusion chromatography using Sephadex G25 coarse resin equilibrated in 0.1 M $NaPO_4$, pH 7.0. Stoichiometry of labeling was assessed by a comparison of fluorophore and protein concentration, as

calculated using absorption and relevant extinction coefficients. The amount of background signal was determined by comparison of emission intensity of the labeled mutant with wild-type protein that was labeled simultaneously.

Good success was had in most cases with acrylodan, however it did not react with all engineered sites. Little success was had with the iodoacetamides or the maleimide. The MTS reagents (Toronto Research Chemicals) worked quite well in most cases (except for the rhodamine derivative), and some worked where acrylodan did not, and the opposite was also true (Table III.1). On several occasions I tried a mild reduction with either DTT (0.25 mM for 30 minutes) or TCEP (0.4 mM for 2 hr before labeling), as this had been successful in labeling of acetylcholinesterase (3), but observed neither an increase in labeling efficiency of the mutant nor in increase in background labeling of the existing cystines. It was generally not predictable which fluorophore would label a given site more effectively, and if the labeling did not work simply with a probe, I was never able to improve on it significantly. These results are most likely due to inaccessibility of the cysteine side chain by a bulky fluorophore.

G. References

1. Brejc, K., van Dijk, W. J., Klaassen, R. V., Schuurmans, M., van Der Oost, J., Smit, A. B., and Sixma, T. K. (2001) *Nature* **411**, 269-276

2. Hansen, S. B., Sulzenbacher, G., Huxford, T., Marchot, P., Taylor, P., and Bourne, Y. (2005) *Embo J* **24**, 3635-3646

3. Shi, J., Boyd, A. E., Radic, Z., and Taylor, P. (2001) *J Biol Chem* **276**, 42196-42204

Chapter IV

Acrylodan Conjugated Cysteine Side Chains Reveal Conformational State and Ligand Site Locations of the Acetylcholine Binding Protein

A. Abstract

We undertook cysteine substitution mutagenesis and fluorophore conjugation at selected residue positions to map sites of ligand binding and changes in solvent exposure of the acetylcholine binding protein from *Lymnaea stagnalis*, a nicotinic receptor surrogate. Acrylodan fluorescence emission is highly sensitive to its local environment, and when bound to protein, exhibits changes in both intensity and emission wavelength that are reflected in the degree of solvent exclusion and the effective dielectric constant of the environment of the fluorophore. Hence, cysteine mutants were generated based on the acetylcholine binding protein crystal structure and predicted ligand binding sites, and fluorescence parameters were assayed on the acrylodan-conjugated proteins. This approach allows one to analyze the environment around the conjugated fluorophore side chain and the changes induced by bound ligand. Introduction of an acrylodan-cysteine conjugate at the 178 position yields a large blue shift with α-bungarotoxin association, whereas the agonists and alkaloid antagonists induce red shifts reflecting solvent exposure at this position. Such residue-selective changes in fluorescence parameters suggest that certain ligands can induce distinct conformational states of the binding protein, and that mutually exclusive binding results from disparate portals of entry to and orientations of the bound α-toxin and smaller acetylcholine congeners at the binding

pocket. Labeling at other residue positions around the predicted binding pocket also reveals distinctive spectral changes for α-bungarotoxin, agonists and alkaloid antagonists.

B. Introduction

The nicotinic acetylcholine receptor (nAChR) is the prototypic member of the superfamily of pentameric ligand-gated ion channels (LGIC), that include γ-aminobutyric acid, glycine and serotonin (5-HT_3) receptors. These receptors are prevalent mediators of neurotransmitter signaling and targets of drug action. nAChR subtypes mediate fast neurotransmission both centrally as well as in the periphery by linkage to an intrinsic cation channel. Since the late 1960's (1-3), structure and function of nAChRs have been under intense study, although these transmembrane proteins have resisted crystallization, precluding high-resolution structures from X-ray crystallography. However, electron microscopy and image reconstruction have detailed the overall shape of the molecule and uncovered potential changes in conformation associated with ligand binding (4,5).

In this family of channels, each subunit contains an extracellular domain encompassing the first ~210 amino acids followed by four transmembrane alpha helical segments; ligand binding sites are formed at subunit interfaces on the extracellular side (1,2). nAChRs are members of the Cys-loop family of LGICs, so named because of a conserved disulfide linkage in their amino-terminal, extracellular domains. In 2001, a soluble protein homologous to the extracellular domain of the nAChR, termed the acetylcholine binding protein (AChBP), was identified, characterized and its structure determined by X-ray crystallography (6,7). While sharing modest sequence identity with all members of the Cys-loop family of LGIC, AChBP most closely resembles the homomeric neuronal nicotinic receptor subunits (α7, ~25% residue identity). In

functional terms, AChBP shares virtually all of the ligand binding characteristics with the nicotinic receptor family, and reveals a structure largely consistent with the electron microscopy image, chemical modification, mutagenesis and spectroscopic data. Based on the position of the associated HEPES buffer molecule (6), the ligand binding site at the subunit interface appeared to be formed from the side chain determinants of binding ascertained previously from mutagenesis and chemical modification (8-12). As a soluble entity of similar overall structure, AChBP provides new opportunities to investigate the structure and function of LGIC at the molecular level. Furthermore, should it be possible to couple AChBP to the receptor transmembrane-spanning region and achieve ligand gating of channel function, the binding protein would possess the conformational capabilities of the extracellular domain of receptors. Hence, conformational changes induced by ligand binding to AChBP may have global implications for ligand gating mechanisms for ion channels.

Another acetylcholine recognition protein with intrasubunit disulfide linkages, acetylcholinesterase (AChE), has multiple high resolution crystal structures of complexes for several ligands bound at its active center and peripheral site (13-15). Although these structures exhibit differences in conformation and side chain orientations, their overlay is likely to reveal only a small fraction of the conformational space of the AChE molecule in solution and the potential structural fluctuations and plasticity of the various ligand complexes (16,17). Cysteine substitution mutagenesis is followed by acrylodan conjugation to the single introduced cysteine, which reveals changes in hydrophobicity and solvent exposure at various acrylodan positions on the AChE molecule associated with ligand binding. Conjugates of longer-lived fluorescein and anilinonaphthalene

fluorophores with the introduced cysteines reveal distinct differences in segmental motion of certain structural domains of AChE upon ligand association (18). The results from these fluorescence-based studies in another system provide evidence for the value of the studies in solution described herein.

We undertook cysteine substitution mutagenesis and fluorophore conjugation at selected positions to describe the immediate environment surrounding the fluorophore, and examine regional flexibility of AChBP, as a nAChR surrogate. Ligand binding in the vicinity of the fluorophore may reveal changes in solvent exposure by ligand occlusion or through conformational changes induced by the ligand. Acrylodan fluorescence emission is highly sensitive to its local environment when bound to protein, and exhibits changes in both intensity and emission wavelength that reflect the effective dielectric constant of the environment around the fluorophore. Hence, cysteine mutants were generated based on the AChBP crystal structure and predicted ligand binding sites, and fluorescence parameters were assayed on the acrylodan-conjugated proteins. This approach allows one to analyze the environment around the conjugated fluorophore side chain and the changes induced by bound ligand. Fluorescence emission data from nine acrylodan-labeled residues residing near the predicted binding pocket in AChBP reveal distinctive spectroscopic changes for α-bungarotoxin and the alkaloid agonists and antagonists, allowing us to describe ligand binding orientations with respect to the distinctive C-loop in the protein.

C. Experimental Procedures

1. Ligands and labeling reagents

(+)Epibatidine, gallamine, α-bungarotoxin, nicotine and carbamylcholine were purchased from Sigma-Aldrich (Fig. IV.1). *d*-Tubocurarine chloride was purchased from ICN Pharmaceuticals, Inc. Methyllycaconitine citrate (MLA) was purchased from Tocris (Ellisville, MO). Metocurine iodide was a gift from the Eli Lilly Co. Acrylodan was obtained from Molecular Probes (Eugene, OR). [^{125}I]-α-Bungarotoxin (specific activity: 80 Ci/mmol) was a product of PerkinElmer Life Sciences, Inc. All other chemicals were of the highest grade commercially available.

2. Expression, mutagenesis and purification of AChBP

Wild-type AChBP from *Lymnaea stagnalis* was expressed from a cDNA synthesized from oligonucleotides selected for mammalian codon usage, as previously described (19,20). Briefly, the AChBP gene was inserted into a p3×FLAG-CMV-9 expression vector (Sigma) containing a preprotrypsin leader peptide followed by a N-terminal 3×FLAG epitope. A C-terminal 6X-histidine tag was attached for radioligand binding assays. Mutant AChBPs were generated by polymerase chain reaction-mediated standard mutagenesis procedures, and cassettes containing the mutation were subcloned into the wild type vector and verified by double stranded sequencing. Wild type and mutant AChBP-transfected HEK-293 cells were selected with G418 to generate stably expressing cell lines. Dulbecco's modified Eagle's medium (MediaTech CellGro) containing 3% FBS was collected at 3-day intervals from multitier flasks for up to 4 weeks. Adsorption onto a FLAG antibody column followed by elution with the 3×FLAG

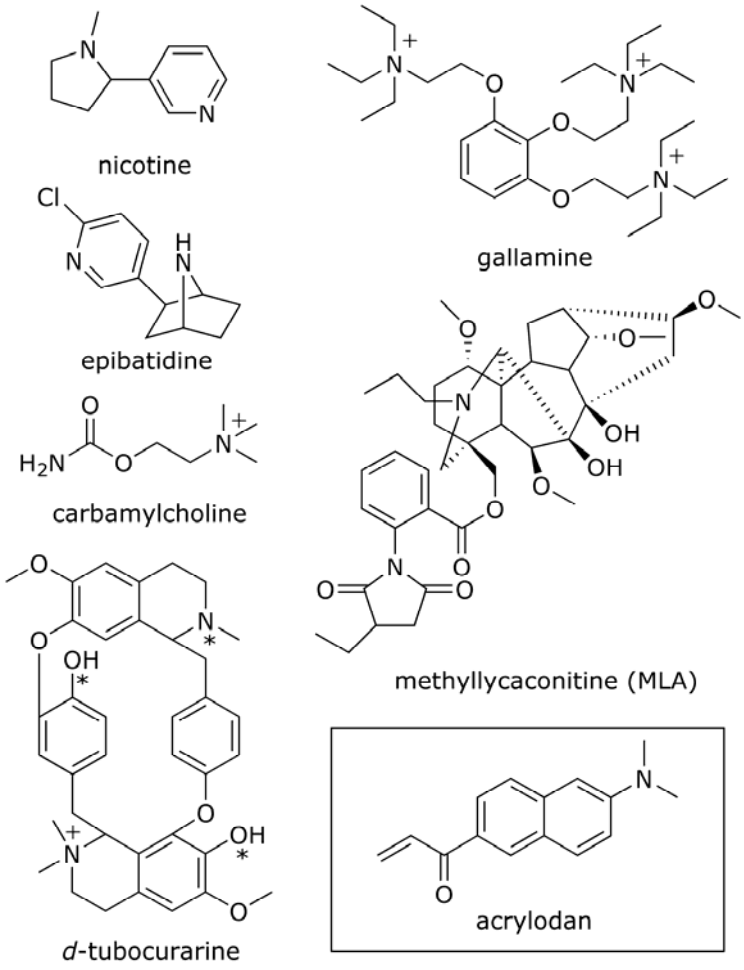

Figure IV.1: Structures of Acrylodan and Ligands Used in Binding Assays. Metocurine (structure not shown) is identical to that of *d*-tubocurarine but contains three additional methyl groups at positions indicated by (*).

peptide yielded purified protein in quantities between 0.5 and 2 mg/liter. Purity and assembly of subunits as a pentamer were assessed by SDS-PAGE and FPLC.

3. Radioligand binding assays

A scintillation proximity assay (SPA, Amersham Biosciences) was adapted for use in a soluble radioligand-binding assay. In 200 μL reaction vessels, AChBP (0.5 nM binding sites) was incubated with increasing concentrations of either [^{125}I]-labeled α-bungarotoxin or (+)epibatidine in a solution of 0.1 mg/mL anti-His SPA beads. In competition assays, [^{125}I]-labeled α-bungarotoxin was held constant at 20 nM and epibatidine was added in variable concentrations. Radioactivity was measured on a Beckman LS 6500 liquid scintillation counter. All radioligand binding data are averages of at least three replicate experiments.

4. Acrylodan labeling

The labeling reactions contained 20 μM AChBP (monomer concentration), 100 μM acrylodan, in 100 μL of 0.1 M $NaPO_4$ buffer, pH 7.0. Labeling reactions ran for 90 minutes at room temperature, after which unreacted label was removed by buffer exchange (4 X 2 mL washes) in Centricon YM-30 spin columns (Amicon). The degree of specific labeling was assessed by comparison with labeling of wild-type AChBP where the four cysteines are disulfide linked as cystines, after normalization to protein concentration by the Bradford assay. Specific labeling for each mutant was as follows: W53C, 90%; L112C, 95%; M114C, 91%; K139C, 88%; E157C, 76%; Y164C, 78%; Q178C, 93%; S182C, 79%. Stoichiometry of labeling for each preparation was estimated from a comparison of acrylodan concentration (by absorption at 372 nm, extinction coefficient ~16,400 $M^{-1}cm^{-1}$) and protein concentration (by absorption at 280 nm,

extinction coefficient ~268,000 $M^{-1}cm^{-1}$). Stoichiometry of labeling for each mutant was as follows: W53C, 79%; L112C, 59%; M114C, 57%; K139C, 55%; E157C, 55%; Y164C, 48%; Q178C, 88%; S182C, 49%.

5. Spectrofluorometric assays

Steady-state emission spectra were measured at room temperature using a Jobin Yvon/Spex FluoroMax II spectrofluorometer (Instrument S.A., Inc., Edison, NJ) with the excitation and emission bandwidths set at 5 nm. The excitation wavelength for acrylodan was set at 359 nm, and emission was monitored between 380 and 600 nm. Saturating ligand concentrations were set at ≥ 10-fold over the K_D for that ligand, or ≥ 5-fold over the concentration of binding sites, whichever was greater. Final ligand concentrations were 2.5 μM for epibatidine, gallamine, α-bungarotoxin, *d*-tubocurarine, metocurine, nicotine and methyllycaconitine, and 25 μM for carbamylcholine. The concentration of binding sites in the spectrofluorometric assays was 0.5 μM. Binding saturation was verified by observation that additional increments in ligand concentration did not result in a further chromic shift or change in quantum yield. For binding site titration experiments, the concentration of binding sites was held constant at 1 μM for epibatidine and α-bungarotoxin titrations, and 3 μM for *d*-tubocurarine and gallamine. Ligand was added in incremental amounts to produce 0.1 μM (for epibatidine and α-bungarotoxin) or 0.3 μM (for *d*-tubocurarine and gallamine) increases until saturation was achieved. Titration data are based on duplicate experiments; all other fluorescence emission data are an average of at least three replicate experiments. Relative quantum yields were

determined from the areas under the emission spectra curves relative to the acrylodan absorption.

6. Stopped-flow kinetics

Stopped-flow kinetic experiments were conducted using an Applied Photophysics SX.18MV (Leatherhead, UK) stopped-flow spectrophotometer. Acrylodan-conjugated AChBP mutants were excited at 372 nm, and a cut-off filter at 420 nm was used to collect the fluorescence signal. Rates of binding of α-bungarotoxin were estimated from the slope of plots of the observed rate of fluorescence change *versus* ligand concentration. Rates of dissociation of α-bungarotoxin were measured by reacting the preformed complex with a large excess of wild-type, unlabeled AChBP to scavenge the dissociated ligand, and observing the time course of the change in fluorescence emission.

D. Results

1. Characterization of the expressed protein

The expressed cysteine-substituted AChBPs were monitored to ascertain assembly as a pentamer of the appropriate molecular weight by elution volume on FPLC size-exclusion chromatography and comparison with corresponding data on wild-type preparations (20). Mutants analyzed further had >90% of the protein eluting as a pentamer rather than as a higher order oligomer or aggregate or as a monomer. Dissociation constants for each AChBP Cys-substituted mutant (see Table IV.1) were

Table IV.1

K_D Values for Each Mutant with α-Bungarotoxin (direct) and Epibatidine (competition)

AChBP Mutant	K_D α-bungarotoxin (M)	K_D epibatidine (M)
WT	1.8E-09	1.6E-10
W53C	9.3E-09	1.8E-10
L112C	4.1E-09	3.0E-10
M114C	4.1E-09	24.8E-10
K139C	15.5E-09	2.2E-10
E157C	3.1E-09	2.1E-10
Y164C	2.2E-09	3.6E-10
Q178C	2.8E-09	2.3E-10
S182C	3.3E-09	6.9E-10
V183C	7.3E-09	1.7E-10

For direct saturation experiments, [^{125}I]-α-bungarotoxin was added in increasing concentrations to AChBP at 0.5 nM in binding sites. For epibatidine competition with α-bungarotoxin binding, the concentration of [^{125}I]-α-bungarotoxin was held constant at 20 nM, and increasing concentrations of cold epibatidine were added to compete with the radioligand. Measurements were done in triplicate and K_D's varied by less than a factor of 2. Conversions from EC_{50} to K_D were made using Prism version 3.00 (from GraphPad Software, Inc.).

determined for two standard ligands, α-bungarotoxin and (+)epibatidine, using the scintillation proximity assay (a version of a traditional radioligand binding assay). Dissociation constants (K_D's) for the snake toxin were determined by direct saturation binding with [^{125}I]-α-bungarotoxin, while K_D's for epibatidine were determined by competition with the radiolabeled α-toxin. K_D's for all the cysteine substitution mutants were within a factor of ~5 of wild-type AChBP for α-bungarotoxin and epibatidine. An exception was the 15-fold change for M114C. Irrespective of these differences in K_D, the ligands retained high affinity for the mutant proteins, indicating that the cysteine substitution at the positions studied does not affect the overall fold of the subunits or their assembly.

To quantitate sites and dissociation constants after fluorophore conjugation, ligands that produced a large chromic shift at a given site of fluorophore labeling were titrated against the labeled protein to determine stoichiometry of binding sites. Representative examples of the wavelength changes in the experimental titrations are shown in Figs. IV.2 and IV.3, which describe both hypsochromic and bathochromic shifts from a single site of modification, Q178C, when titrated with α-bungarotoxin or epibatidine, respectively. In all binding site titration experiments, ligand was found to approach a ratio of ~1:1 with respect to the number of binding sites based on five sites per pentameric assembly (Table IV.2).

The approach to full ligand occupation at the 5 sites and no further fluorescence change, as shown in Fig. IV.3, was not always linear. This likely reflects the slightly different affinities of the acrylodan-labeled protein and the fractional labeling achieved for the particular acrylodan conjugate. The abrupt intersection of the extrapolated

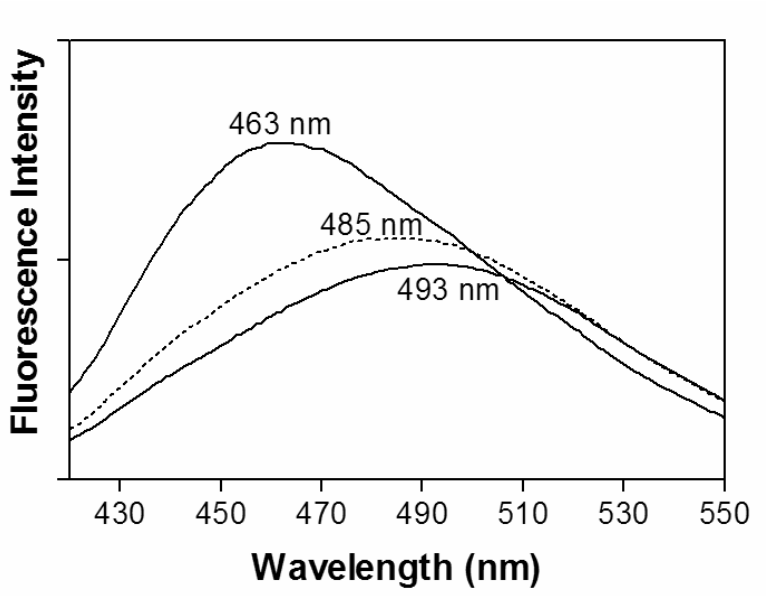

Figure IV.2: Emission Spectra of Q178C-Acrylodan in Unliganded State and After Saturation with Epibatidine or α-Bungarotoxin. With no ligand present (dashed line) emission peak is at 485 nm. α-Toxin association enhances quantum yield and shifts the emission maximum in the blue direction (hypsochromic shift), whereas epibatidine quenches the fluorescence and shifts the emission maximum in the red direction (bathochromic shift). Excitation wavelength = 359 nm.

Table IV.2

Titration of Binding Sites and Calculation of Dissociation Constants

Mutant	Ligand	Chromic Shift (nm)	[ligand]:[sites]	k_{on} ($M^{-1}s^{-1}$)	k_{off} (s^{-1})	K_D (nM)
W53C	α-bungarotoxin	-15	1:0.95	2.0E+05	8.0E-03	40.0
W53C	gallamine	-11	1:1.03			
L112C	epibatidine	-16	1:0.98			
E157C	epibatidine	-10	1:0.89			
Y164C	epibatidine	-9	1:0.90			
Y164C	*d*-tubocurarine	-9	1:1.07			
Q178C	α-bungarotoxin	-22	1:0.95	6.0E+05	8.0E-03	13.0
Q178C	epibatidine	8	1:1.01			

Residue positions with larger emission wavelength changes were titrated with the respective ligands to ascertain stoichiometry and/or dissociation constant for ligand binding to the acrylodan-conjugated binding protein. AChBP binding site concentrations were between 1.0 and 3.0 μM.

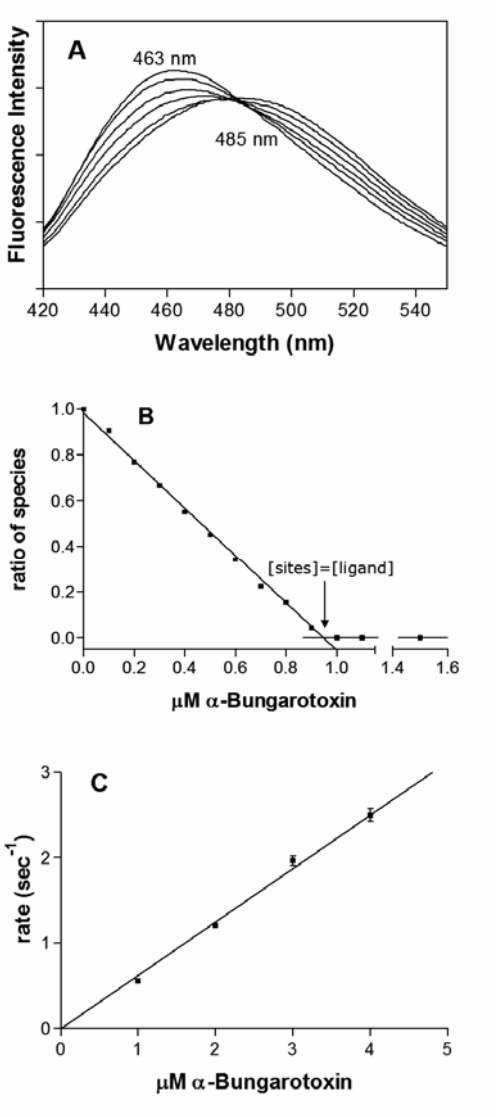

Figure IV.3: Titration of Binding Sites and Kinetics of Association for α-Bungarotoxin at Q178C-Acrylodan. Equilibrium emission spectra are presented in **A**. The ratio of species in **B** was determined from the wavelength intensities according to the following equation: $[(I_{463}-I_{485})-(I_{463}-I_{485})_\infty]/[(I_{463}-I_{485})_0-(I_{463}-I_{485})_\infty]$, where I is intensity at the specified wavelength and the subscripts (0, ∞) denote in the absence of ligand and saturating ligand conditions. In **C** the rate of association by measured by stopped-flow of α-bungarotoxin at Q178C-acrylodan was calculated from the slope plotted as the observed rate of fluorescence change *versus* concentration of α-bungarotoxin.

titration lines in Fig. IV.3B reflects the high affinity of the α-toxin complex, since virtually all of the added α-bungarotoxin binds until the five sites are fully occupied. In some cases, we have estimated the α-bungarotoxin dissociation constant from its component rate constants, showing that it retains its high affinity for the acrylodan-conjugated AChBPs (Table IV.2).

2. Effect of α-bungarotoxin binding on acrylodan fluorescence emission

Although the subunits in AChBP are identical, the subunit interface can best be related to the heteromeric receptor where the C-loop face, which contains the vicinal cysteines at 187 and 188, corresponds to the α1 subunit in muscle and the complementary face corresponds to that of the muscle γ, δ or ε subunit. These subunit positions are shown in gray (α) and orange (γ, δ or ε), respectively, in Fig. IV.4.

Changes in acrylodan fluorescence emission initiated by binding of α-bungarotoxin are listed in Table IV.3. In these fluorescence studies, chromic shifts of 2 nm or more in emission maxima were considered significant. α-Bungarotoxin binding produced a large blue shift (15 nm) in emission from the fluorophore side chain buried internally to loop C, W53C, a region of the putative binding pocket (6,8). Interestingly, minimal (M114C) or small (L112C) shifts in the opposite direction, indicating greater solvent accessibility, are induced in acrylodan-conjugated residues located apical to the binding pocket at the subunit interface. These residues are found on the subunit face complementary to the C-loop. Data from residues on the membrane side of the pocket (E157C, Y164C, Q178C) reveal emission shifts consistent with a significant decrease in

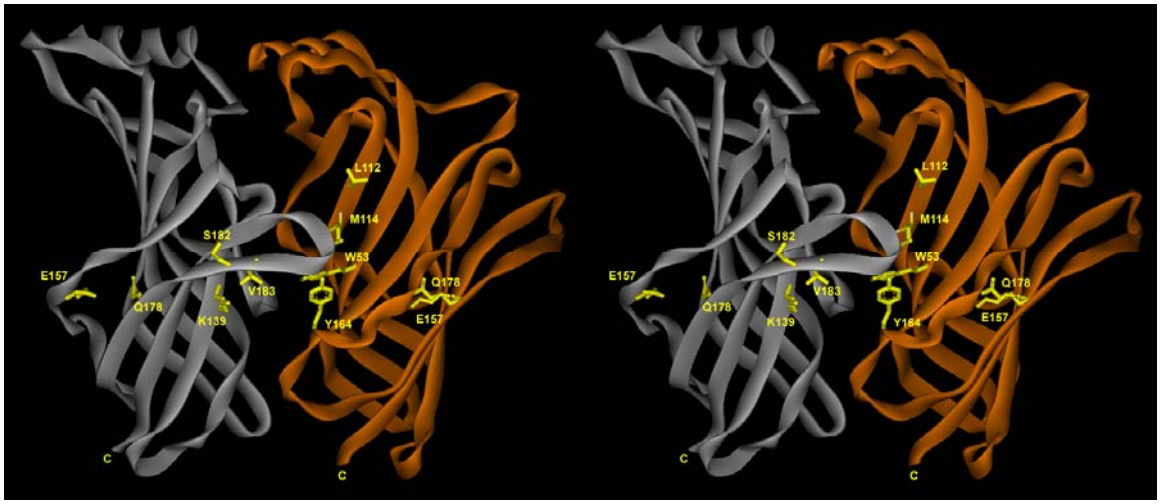

Figure IV.4: 3-Dimensional (Stereo) Image of AChBP Subunit Interface Viewed from its External Radial Perimeter. The model was built from crystallographic coordinates (PDB ID: 1I9B). Although the subunits are identical in AChBP, the positioning illustrated by the color-coding would make the gray subunit interface comparable to that in the α-subunit (with the protruding vicinal cysteine or C-loop), and the orange interface comparable to that in the γ or δ subunit positions in the $\alpha_2\beta\gamma\delta$ arrangement of the muscle nicotinic receptor. Side chains shown are those mutated to cysteine and conjugated to acrylodan and are indicated by their single letter amino acid code (W53; L112; M114; K139; E157; Y164; Q178; S182; V183). The "C-loop" contains the disulfide bond from the vicinal cysteines that are important for ligand binding. Apical region is at the top and the α-carbon chain linkage to the membrane spans is noted by the carboxyl-terminus, labeled by C. Homologous residues in the nicotinic receptor and AChBP family for several of the regions are shown in Table IV.6.

Table IV.3

*Fluorescence emission parameters of acrylodan-labeled AChBP mutants in the presence of α-bungarotoxin**

	Acrylodan Emission Maxima (nm)			
AChBP Mutant	(-)ligand	α-Bungarotoxin	Chromic Shift	Relative Quantum Yield
W53C	489	474	-15	1.46
L112C	499	503	4	1.30
M114C	486	487	1	1.04
K139C	491	492	1	1.13
E157C	508	503	-5	1.36
Y164C	508	503	-5	1.43
Q178C	485	463	-22	1.36
S182C	482	484	2	0.99
V183C	476	477	1	0.98

*Data were collected from spectra similar to those shown in Figs. IV.2 and IV.3 for the respective acrylodan-conjugated mutant binding protein and 2.5 μM α-bungarotoxin.

Table IV.4

*Fluorescence emission parameters of acrylodan-labeled AChBP mutants in the presence of agonists**

	Acrylodan Emission Maxima (nm)			
AChBP Mutant	(-)ligand	Epibatidine	Chromic Shift	Relative Quantum Yield
W53C	489	484	-5	1.09
L112C	499	483	-16	1.92
M114C	486	487	1	1.08
K139C	491	489	-2	1.08
E157C	508	498	-10	1.72
Y164C	508	499	-9	1.70
Q178C	485	493	8	0.90
S182C	482	484	2	0.97
V183C	476	478	2	0.95

AChBP Mutant	(-)ligand	Nicotine	Chromic Shift	Relative Quantum Yield
W53C	489	480	-9	1.02
L112C	499	492	-7	1.25
M114C	486	486	0	0.99
K139C	491	493	2	0.96
E157C	508	503	-5	1.21
Y164C	508	502	-6	1.29
Q178C	485	492	7	0.91
S182C	482	483	1	0.94
V183C	476	476	0	0.95

AChBP Mutant	(-)ligand	Carbamylcholine	Chromic Shift	Relative Quantum Yield
W53C	489	485	-4	0.94
L112C	499	499	0	0.95
M114C	486	486	0	0.96
K139C	491	493	2	0.95
E157C	508	502	-6	1.05
Y164C	508	506	-2	1.00
Q178C	485	491	6	0.92
S182C	482	480	-2	0.95
V183C	476	477	1	0.94

*Data were collected from spectra similar to those shown in Figs. IV.2 and IV.3 for the respective acrylodan-conjugated mutant binding protein and agonist using 2.5 μM nicotine and epibatidine and 25 μM carbamylcholine.

solvent exposure for a residue located directly internal to the pocket (Y164C), as well as those around the exterior face of the subunits (E157C, Q178C). Little to no change in solvent exposure on the membrane side of the pocket on the C-loop face was observed (K139C; see Fig. IV.4 for structural orientation). Somewhat surprisingly, the largest chromic shift at all of the sites for any ligand was a 22 nm blue shift at Q178C, by α-bungarotoxin. This indicates a potentially extensive interaction on the α-toxin with an area on the C-loop side of the interface, but at some distance from the pocket and well removed from predicted binding site region for small ligands (6,21-25). All other ligands assayed induce a chromic shift to longer wavelength at the Q178C site. These data distinguish the binding site or conformation for the α-bungarotoxin-bound complex from the conformations of the smaller agonists and competitive antagonists. A minimal change in solvent exposure around the E157C site of acrylodan conjugation, relative to other ligands, is consistent with the greater solvent occlusion by α-bungarotoxin on the C-loop positioned subunit face than the complementary face.

3. Effect of agonist binding on acrylodan fluorescence emission

Epibatidine, nicotine and carbamylcholine (Table IV.4) all induced blue shifts in acrylodan emission wavelength at the W53C and Y164C sites. Carbamylcholine, having more torsional flexibility in its bonds and occupying a smaller molar volume than the other two agonists, generally produced smaller shifts in emission wavelength. Epibatidine and nicotine decreased solvent exposure in the apical region of the pocket at the L112C position, while carbamylcholine did not influence this region. This class of ligands also exerted marked effects on solvent exposure at two positions of fluorophore conjugation presumed to be outside of the pocket; all three agonists significantly

decreased polarity of the acrylodan environment at the E157C position, and increased polarity at the Q178C position. These changes in emission wavelength for residues distant from the pocket were also seen for the alkaloid antagonists, with the effect of α-toxin on the Q178C position being the notable exception. Little change in emission wavelength is evident for acrylodan conjugated at S182C and V183C. These side chains reside in a hydrophobic environment and presumably stay fixed in their locations after ligand binding.

4. Effect of alkaloid antagonist binding on acrylodan fluorescence emission

Gallamine, *d*-tubocurarine, metocurine, methyllycaconitine (MLA), and metocurine (Table IV.5) induced a blue shift in acrylodan emission wavelength from the W53C position, consistent with the bound ligand displacing solvent from this location. Metocurine induced a larger blue shift at this position (11 nm) than its des-methyl structural congener, *d*-tubocurarine (6 nm); otherwise, these two ligands produce very similar acrylodan emission profiles. Detailed studies of the influence of mutations on the binding energetics of *d*-tubocurarine and its bisquaternary, methylated derivative, metocurine, suggest that the two ligands are oriented differently in the binding site (26). MLA is unique in its promotion of a red shift in acrylodan emission wavelength from the K139C position. This ligand decreases solvent accessibility to areas in the pocket (W53C, Y164C), as well as immediately apical to the pocket likely due to its large size (L112C, M114C), but appears to open up the regions examined between the pocket and the membrane (Q178C, K139C) at both subunit interfaces.

Table IV.5

*Fluorescence emission parameters of acrylodan-labeled AChBP mutants in the presence of alkaloid antagonists**

	Acrylodan Emission Maxima (nm)			
AChBP Mutant	(-)ligand	Gallamine	Chromic Shift	Relative Quantum Yield
W53C	489	478	-11	1.20
L112C	499	496	-3	1.17
M114C	486	485	-1	1.05
K139C	491	493	2	0.96
E157C	508	505	-4	1.04
Y164C	508	505	-3	1.01
Q178C	485	492	7	1.00
S182C	482	484	2	0.93
V183C	476	477	1	0.94

AChBP Mutant	(-)ligand	*d*-Tubocurarine	Chromic Shift	Relative Quantum Yield
W53C	489	483	-6	1.00
L112C	499	496	-3	1.02
M114C	486	485	-1	0.97
K139C	491	490	-1	1.08
E157C	508	487	-21	1.55
Y164C	508	499	-9	1.35
Q178C	485	490	5	1.03
S182C	482	483	1	0.97
V183C	476	476	0	0.97

AChBP Mutant	(-)ligand	Metocurine	Chromic Shift	Relative Quantum Yield
W53C	489	478	-11	0.97
L112C	499	495	-4	1.15
M114C	486	485	-1	1.06
K139C	491	492	1	1.05
E157C	508	495	-13	1.43
Y164C	508	501	-7	1.30
Q178C	485	491	6	1.04
S182C	482	483	1	0.95
V183C	476	476	0	0.94

AChBP Mutant	(-)ligand	Methyllycaconitine	Chromic Shift	Relative Quantum Yield
W53C	489	482	-7	1.17
L112C	499	490	-9	1.53
M114C	486	482	-4	1.20
K139C	491	497	6	1.05
E157C	508	500	-8	1.54
Y164C	508	503	-5	1.38
Q178C	485	491	6	1.01
S182C	482	484	2	0.98
V183C	476	477	1	0.95

Data were collected from spectra similar to those shown in Figs. IV.2 and IV.3 for the respective acrylodan-conjugated mutant binding protein and 2.5 μM antagonist.

E. Discussion

1. Characteristics of fluorescence emission from acrylodan-conjugated cysteine residues

Employing cysteine substitution mutagenesis and selective fluorophore conjugation at the introduced cysteine in crystallographically-defined protein templates expands structural analyses to solution-based considerations. When the endogenous cysteines in a protein are disulfide linked as cystines, the relatively selective tethering of acrylodan through a Michael addition to an introduced single cysteine nucleophile provides a site-directed and regionally localized spectroscopic handle. Upon excitation of acrylodan to form an excited-state dipole, its fluorescence emission is sensitive to reorientation of local neighboring or solvent dipoles. These polarity-sensitive fluorescence characteristics give rise to distinctive Stokes' shifts for acrylodan conjugated to the protein, revealed in the difference between excitation and emission wavelengths (27). While the number of cysteine substitutions on AChBP is still limited to regions around the ligand binding site ascertained from the crystal structure and a variety of mutagenesis and chemical modification studies, several interesting observations emerge that are predictive of the binding determinants of the site and potential conformational changes accompanying ligand binding.

2. Fluorescence characterization of residues in the unliganded protein

In the absence of ligand, emission maxima from the nine described acrylodan-labeled mutants reveal the Y164C and E157C positions to be in the most hydrophilic environment, with peak emission wavelengths at 508 nm. The crystal structure shows both of these native side chains to be on the surface of the protein with their surfaces

largely exposed to the solvent. The fluorescent moiety of acrylodan is tethered through an extended thioether linkage and can explore a wider range of positions than the natural side chain. Presumably, extensive interaction with solvent molecules or proximal polar residues on the protein lowers the excited state energy of the fluorophore to yield longer wavelength emission.

In contrast to these relatively hydrophilic positions, acrylodan molecules tethered at M114C, Q178C, S182C and V183C have emission maxima at the blue end of the spectrum, indicative of a hydrophobic environment and far lower solvent exposure. Referring to the crystal structure, the Q178C position is buried between two β-sheets and points somewhat inward to the protein core, and M114C in the apical entry area of the binding pocket is wedged into the subunit interface. S182C is located on the outside of the C-loop where it could fold over the pocket, and V183C is adjacent to S182C but points into the pocket. The crystal structure reveals a high degree of solvent accessibility at the S182C site, however the fluorescence emission data for acrylodan conjugated at S182C suggest otherwise. In this case, it seems likely that the fluorophore is oriented toward the core of the protein, packing into a more hydrophobic area. This position is consistent with a minimal change in emission wavelength or quantum yield at this site upon ligand binding.

3. Shifts in emission maxima induced by ligand binding

A comparison of the shifts induced by the three agonists (Table IV.4) and the four synthetic and natural alkaloid antagonists (Table IV.5) does not reveal a pattern distinctive for agonists versus antagonists. Perhaps this is not unexpected, as the binding affinities of the various ligands and the structure of AChBP might best reflect that of a

desensitized state of the receptor (5,19). Nevertheless, several distinctive characteristics of ligand-induced changes in the emission spectra are evident. First, blue shifts are evident for residues positioned on the surface complementary to the C-loop containing subunit, W53 and L112 (Fig. IV.4, in orange). These positions of fluorophore conjugation are also found apical to the C-loop. Amino acid residues in the muscle γ- and δ-subunits conserved as γW55 and γL119, and δW57 and δL121, that are homologous to W53 and L112 in AChBP, appear as important determinants of agonist and antagonist binding (23). Hence, these residues are likely to be occluded from solvent when ligands bind, either by the ligand itself or through displacement by the side chain position of acrylodan. The spectroscopic changes observed are consistent with the W53, L112 surface being within the proximal ligand binding region as seen for the HEPES site in the crystal structure (6).

A consistent change for the binding of all of these ligands is the 5-9 nm red (bathochromic) shift for acrylodan at the Q178C position. This shift is indicative of increased exposure to the polar solvent and would be consistent with conformational changes induced by ligand in channel opening and desensitization (5,28). If binding induces a rotation of one subunit about an axis extending from the extracellular side through the subunit and normal to the membrane, then it is quite possible for the 178 residue, despite its distance from the proposed binding site, to become more solvent exposed. Accordingly, the fluorescence change is indicative of a change in conformation induced by ligand occupation.

The bathochromic shift in emission at the Q178C position might also be compared with the hypsochromic shift at E157C. The same clockwise subunit rotation

alluded to above could cause the E157C side chain to become buried or less exposed to solvent. In general, while the Q178C-acrylodan conjugate shifts in a red direction, acrylodan at E157C shows a blue, hypsochromic shift. However, the region of E157C (155-160) is unresolved in the crystal structure suggesting a lack of structural rigidity and thermal stability (6). Moreover, lysine substitution mutagenesis also reveals that this region lacks defined β-pleated sheet structure (29). Interestingly, while in all cases acrylodan at the 157 position shows a hypsochromic shift, its peak emission wavelength appears to be the most sensitive to the structures of the bound ligand (Tables IV.3-5).

4. α-Bungarotoxin induced shifts in acrylodan emission

α-Bungarotoxin yields the most distinctive wavelength shifts among the ligands studied to date. In part, this would be reflected in its larger size and greater potential for solvent exclusion. Also, substantial kinetic data reveal slow association and dissociation rates for α-neurotoxin binding that would suggest a kinetic limitation in formation of a distinct conformational state. The slower rates, reported long ago for the muscle type receptor (30,31), are also observed with AChBP (19). No evidence for wavelength shifts in the direction of solvent exclusion upon α-bungarotoxin binding is found for residues in the region apical to the C-loop (L112C, M114C). If anything, these two residues apical to the binding pocket show an increase in solvent exposure. In contrast, unusually large hypsochromic shifts are observed for acrylodan at W53C and Q178C. Smaller shifts are seen for the E157C and Y164C side chains. Taken together, these findings reveal that α-bungarotoxin binds from the membrane side of the C-loop in contrast to the small ligands that enter from the apical side.

Our findings on the distinctive changes in acrylodan emission induced by α-bungarotoxin at multiple locations around its binding site might be compared with studies on residue proximity to the α-toxin binding site on the muscle receptor and the neuronal α7 receptor. Thermodynamic mutant cycle analysis has been used to analyze pairwise interactions between α-toxin (*Naja mossambica mossambica*; *Nmm*) residues and receptor subunit determinants that influence binding affinity (23,32). These studies, which analyze the interaction or linkage free energy between paired residues, reveal that the tip of loop II of the *Nmm* α-toxin, with its extended Arg 33 side chain (see Fig. IV.5), interacts with the α-subunit residues 188, 190, and 198, and with residues 55, 119, and 176 on the γ-subunit. Since the homologous residues in AChBP (Table IV.6), 183, 188 and 193 in the C-loop-containing subunit and 53, 112 and 171 on the complementary face, are in close proximity, it is likely that this long loop intersects or bisects at the subunit interface. Similar coupling was found for the arginine at the tip of loop II in α-cobratoxin in its interaction with C-loop residues in the α7 nicotinic receptor (25).

A similar conclusion was reached through crystallographic and NMR studies (21,22,24,33), that examined the structure of α-subunit peptides of 13 and 21 amino acid residues from the C-loop when bound to the α-toxin. Although the limited segment of peptide studied enabled a direct examination of only a small fraction of the potential interacting surface of the receptor subunits with α-toxin, the position of the C-loop with

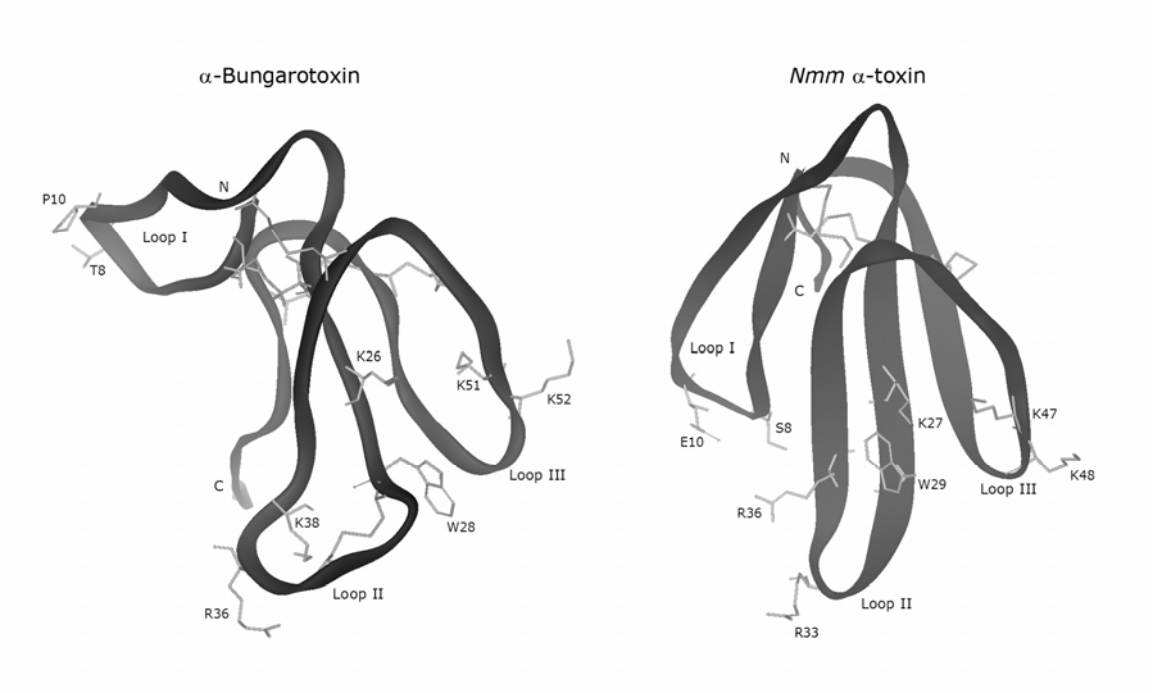

Figure IV.5: Structures of α-Bungarotoxin (NMR, PDB ID: 1IDI) and *Nmm* α-Toxin from *Naja mossambica mossambica* (energy minimized model (23)). Disulfide linkages for α-bungarotoxin and for *Nmm* α-toxin are shown along with residues that are stuctural landmarks and binding determinants on the two molecules. In α-bungarotoxin, disulfides link residues 3 with 23, 29 with 33, 16 with 44, 48 with 59, and 60 with 65. In the Nmm α-toxin, disulfides link residues 3 with 24, 17 with 41, and 43 with 54. α-Bungarotoxin is a 74 amino acid peptide while *Nmm* has 62 amino acids.

Table IV.6

Sequence alignments of interacting residues from AChBP and nAChR subtypes

	Segment A	Segment B	Segment (loop) C	
AChBP	^{89}YNAISKPEV^{97}	^{143}WTHHSREIS^{151}	^{176}VTQKKNSVTYSCCPE-AYED^{194}	
α7 (chick)	^{92}YNSADER^{98}	^{148}WTYGG^{152}	^{178}IPGKRTESFYECCKE-PYPD^{196}	A
α1 (mouse)	^{93}YNNADGD^{99}	^{149}WTYDGSVV^{156}	^{180}EARGWKHWVFYSCCPTTPYLDIT^{200}	B

	Segment D	Segment E	Segment F	Segment F*
AChBP	^{53}WQQTTWS^{59}	^{105}VVSDGEVLYM^{114}	^{160}DDSEYFSQYSRF^{171}	^{32}SLKFI^{36}
α7 (chick)	^{54}WLQMYWT^{60}	^{110}NSSGHCQYLP^{119}	^{163}DISGY^{167}	^{33}LLKNY^{37}
γ (mouse)	^{54}VWIEMQWC^{61}	^{111}SPDGCIYWLP^{120}	^{172}FIDPEAF^{178}	^{31}SLKLT^{35}
δ (mouse)	^{56}VWIDHAWV^{63}	^{113}YDSGYVTWLP^{122}	^{178}IIDPEGF^{184}	^{33}ALSLT^{37}
ε (mouse)	^{54}VWIGID^{59}	^{111}YEGGYVSWLP^{120}	^{173}DIDTAAF^{179}	^{31}TLKVT^{35}

[A] Peptides (residues 178-196) studied by (22).
[B] Peptides from *Torpedo californica* (residues 181-198 and 182-202) studied by (21,33).

Segment F*, while not recognized in all models, is in spatial proximity to segment F and these two regions have a synergistic influence on α-conotoxin association (36,37).

respect to the surrounding subunit interface allowed constraints to be placed on the positions of neighboring residues not on the C-loop itself. Hence, it was proposed that Arg 36 at the loop tip in α-bungarotoxin and the choline moiety in acetylcholine are sandwiched between the aromatic groups of the C-loop at αY190 and αY198 and the complementary face at γW57 and γL119 (33). Other NMR studies with α-bungarotoxin and a C-loop peptide from the α7 subunit of 19 residues show similar interactions with the C-loop extending from the loop tip at Arg 36 to residue 40 (22). These studies with the synthetic peptide also identify a potential contact zone for loop I in the α-toxin.

Mutant cycle analysis with *Nmm* α-toxin allows for an analysis of interacting residue pairs in additional loops or regions of the α-toxin structure and the receptor subunit interface. Strong interactions were found between Lys 27 and Arg 33 on loop II of *Nmm* α-toxin with γGlu176, γL119, and γTrp55 of the muscle receptor (Table IV.6). Arg 36 in *Nmm* α-toxin does not partner with γ-subunits, but with the α-subunit face (23,32). Hence, with *Nmm* α-toxin, residues N-terminal to Arg 33 and proximal to loop III (Fig. IV.5) have a primary interaction with the γ-subunit, whereas residues C-terminal to Arg 33 and proximal to loop I interact with the α-subunit. Finally, interaction energies are found between loop I (E8 and E10) and residues αV188, αY190 and αY198; as well as between loop III (K47 and K48) and γE176, γD184 and γW55. Thus, the disc shaped α-toxin likely lies with an orientation close to parallel with the membrane rather than perpendicular to it. This toxin orientation is also consistent with structure-activity studies of Menez and colleagues with the short α-neurotoxins (34). In fact, the proposed residue

placement of Samson et al. (33) places loop I and the portion of loop II facing loop I in the vicinity of Q178, consistent with *Nmm* residue pairs.

Our findings suggest that acrylodan extending from the Q178C may be occluded from solvent by loop I interactions. The α-carbon positions of Q178 and W53 are ~26 Å apart as measured through space, revealing that α-toxin binding covers a substantial area of the receptor subunit interface. α-Bungarotoxin acquires much of its interaction energy through Van der Waals contact with the subunit face bearing the C-loop rather than the complementary γ, δ surface. The data presented here support recent NMR-based models of α-bungarotoxin binding (22,33), where the primary interaction surface with α-toxin arises from the subunit face bearing the C-loop and involves loop I and the position of loop II that faces loop I.

An alternative explanation of our data that should be considered relates to the α-bungarotoxin actually perturbing the C-loop position so that it protrudes radially. In this case, the side chain on residue 178 is forced in the direction of the protein core with the partial opening of the C-loop cover. A potential hinge region in the vicinity of residue 178 would be influenced by the large α-bungarotoxin molecule dislodging and opening the C-loop or flap, while the flap may close down upon the smaller ligands when bound, exposing the side chain in the 178 hinge region. Such an explanation would be consistent with the opposing directions of the emission wavelength shift of acrylodan at Q178C elicited by small ligands and α-toxin (Fig. IV.2).

While several docking models of the α-toxin-receptor interaction have been proposed (21-23,25,33,35), experimental data positioning the α-toxin or other antagonists

and agonists are only beginning to emerge. The fluorescence approach, while lacking atomic level resolution, provides spectroscopic parameters useful for further monitoring the interaction and local conformational changes induced around the inserted fluorophore of the complex in solution. Such solution-based studies should also allow for subsequent analyses of torsional and segmental motion in the respective localized regions of the interacting molecule (18). Finally, through a comparison of the spectral perturbations achieved by various classes of alkaloid and peptide ligands, the positions of the bound ligand and differences in AChBP conformation associated with ligand binding can be deduced.

F. Acknowledgements

This chapter is material as it appears in: Ryan E Hibbs, Todd T Talley, and Palmer Taylor "Acrylodan conjugated cysteine side chains reveal conformational state and ligand site locations of the acetylcholine binding protein," *Journal of Biological Chemistry* (2004) Jul 2;279(27):28483-91. The dissertation author was the primary investigator in the development and execution of the study, and the principal author of this paper.

I thank Dr. Zoran Radić for assistance with stopped-flow kinetic measurements of ligand binding, Dr. Scott Hansen for synthesis of *L. stagnalis* AChBP cDNA, and Dr. David Johnson for helpful discussion.

G. References

1. Corringer, P. J., Le Novere, N., and Changeux, J. P. (2000) *Annu Rev Pharmacol Toxicol* **40**, 431-458

2. Karlin, A. (2002) *Nat Rev Neurosci* **3**, 102-114

3. Changeux, J. P., Kasai, M., and Lee, C. Y. (1970) *Proc Natl Acad Sci U S A* **67**, 1241-1247

4. Miyazawa, A., Fujiyoshi, Y., Stowell, M., and Unwin, N. (1999) *J Mol Biol* **288**, 765-786

5. Miyazawa, A., Fujiyoshi, Y., and Unwin, N. (2003) *Nature* **424**, 949-955

6. Brejc, K., van Dijk, W. J., Klaassen, R. V., Schuurmans, M., van Der Oost, J., Smit, A. B., and Sixma, T. K. (2001) *Nature* **411**, 269-276

7. Smit, A. B., Syed, N. I., Schaap, D., van Minnen, J., Klumperman, J., Kits, K. S., Lodder, H., van der Schors, R. C., van Elk, R., Sorgedrager, B., Brejc, K., Sixma, T. K., and Geraerts, W. P. (2001) *Nature* **411**, 261-268

8. Taylor, P., Osaka, H., Molles, B., Keller, S. H., and Malany, S. (2000) in *Handbook of Experimental Pharmacology: Neuronal Nicotinic Receptors* (Gotti, C., ed) Vol. 144, pp. 79-100, Springer-Verlag

9. Dennis, M., Giraudat, J., Kotzyba-Hibert, F., Goeldner, M., Hirth, C., Chang, J. Y., Lazure, C., Chretien, M., and Changeux, J. P. (1988) *Biochemistry* **27**, 2346-2357

10. Reiter, M. J., Cowburn, D. A., Prives, J. M., and Karlin, A. (1972) *Proc Natl Acad Sci U S A* **69**, 1168-1172

11. Sine, S. M. (2002) *J Neurobiol* **53**, 431-446

12. Martin, M., Czajkowski, C., and Karlin, A. (1996) *J Biol Chem* **271**, 13497-13503

13. Silman, I., and Sussman, J. L. (2000) in *Cholinesterases and Cholinesterase Inhibitors* (Giacobini, E., ed), pp. 9-25, Martin Dunitz LTD

14. Sussman, J. L., Harel, M., Frolow, F., Oefner, C., Goldman, A., Toker, L., and Silman, I. (1991) *Science* **253**, 872-879

15. Bourne, Y., Taylor, P., and Marchot, P. (1995) *Cell* **83**, 503-512

16. Bourne, Y., Kolb, H. C., Radic, Z., Sharpless, K. B., Taylor, P., and Marchot, P. (2004) *Proc Natl Acad Sci U S A* **101**, 1449-1454

17. Shi, J., Boyd, A. E., Radic, Z., and Taylor, P. (2001) *J Biol Chem* **276**, 42196-42204

18. Shi, J., Tai, K., McCammon, J. A., Taylor, P., and Johnson, D. A. (2003) *J Biol Chem* **278**, 30905-30911

19. Hansen, S. B., Radic, Z., Talley, T. T., Molles, B. E., Deerinck, T., Tsigelny, I., and Taylor, P. (2002) *J Biol Chem* **277**, 41299-41302

20. Hansen, S. B., Talley, T. T., Radic, Z., and Taylor, P. (2004) *Submitted for publication*

21. Zeng, H., Moise, L., Grant, M. A., and Hawrot, E. (2001) *J Biol Chem* **276**, 22930-22940

22. Moise, L., Piserchio, A., Basus, V. J., and Hawrot, E. (2002) *J Biol Chem* **277**, 12406-12417

23. Malany, S., Osaka, H., Sine, S. M., and Taylor, P. (2000) *Biochemistry* **39**, 15388-15398

24. Harel, M., Kasher, R., Nicolas, A., Guss, J. M., Balass, M., Fridkin, M., Smit, A. B., Brejc, K., Sixma, T. K., Katchalski-Katzir, E., Sussman, J. L., and Fuchs, S. (2001) *Neuron* **32**, 265-275

25. Fruchart-Gaillard, C., Gilquin, B., Antil-Delbeke, S., Le Novere, N., Tamiya, T., Corringer, P. J., Changeux, J. P., Menez, A., and Servent, D. (2002) *Proc Natl Acad Sci U S A* **99**, 3216-3221

26. Gao, F., Bern, N., Little, A., Wang, H. L., Hansen, S. B., Talley, T. T., Taylor, P., and Sine, S. M. (2003) *J Biol Chem* **278**, 23020-23026

27. Lakowicz, J. R. (1999) *Principles of Fluorescence Spectroscopy*, 2nd Ed., Kluwer Academic Publishers and Plenum Publishing Corp., New York

28. Unwin, N., Miyazawa, A., Li, J., and Fujiyoshi, Y. (2002) *J Mol Biol* **319**, 1165-1176

29. Sine, S. M., Wang, H. L., and Bren, N. (2002) *J Biol Chem* **277**, 29210-29223

30. Weber, M., and Changeux, J. P. (1974) *Mol Pharmacol* **10**, 15-34

31. Weiland, G., Georgia, B., Lappi, S., Chignell, C. F., and Taylor, P. (1977) *J Biol Chem* **252**, 7648-7656

32. Osaka, H., Malany, S., Molles, B. E., Sine, S. M., and Taylor, P. (2000) *J Biol Chem* **275**, 5478-5484

33. Samson, A., Scherf, T., Eisenstein, M., Chill, J., and Anglister, J. (2002) *Neuron* **35**, 319-332

34. Teixeira-Clerc, F., Menez, A., and Kessler, P. (2002) *J Biol Chem* **277**, 25741-25747

35. Lozzi, L., Lelli, B., Runci, Y., Scali, S., Bernini, A., Falciani, C., Pini, A., Niccolai, N., Neri, P., and Bracci, L. (2003) *Chem Biol* **10**, 411-417

36. Quiram, P. A., McIntosh, J. M., and Sine, S. M. (2000) *J Biol Chem* **275**, 4889-4896

37. Sugiyama, N., Marchot, P., Kawanishi, C., Osaka, H., Molles, B., Sine, S. M., and Taylor, P. (1998) *Mol Pharmacol* **53**, 787-794

Chapter V

Structural Dynamics of the α-Neurotoxin-Acetylcholine-Binding Protein Complex: Hydrodynamic and Fluorescence Anisotropy Decay Analyses

A. Abstract

The three-fingered α-neurotoxins have played a pivotal role in elucidating the structure and function of the muscle-type and neuronal α7 nicotinic acetylcholine receptors (nAChRs). To advance our understanding of the α-neurotoxin-nAChR interaction, we examined the flexibility of α-neurotoxin bound to the acetylcholine binding protein (AChBP), which shares structural similarity and sequence identities with the extracellular domain of nAChRs. Because the crystal structure of five α-cobratoxin molecules bound to AChBP shows the toxins projecting radially like propeller 'blades' from the perimeter of the donut-shaped AChBP, the toxin molecules should increase the frictional resistance and thereby alter the hydrodynamic properties of the complex. α-Bungarotoxin binding had little effect on the frictional coefficients of AChBP measured by analytical ultracentrifugation suggesting that the bound toxins are flexible. To support this conclusion, we measured the anisotropy decay of four site-specifically labeled α-cobratoxins (conjugated at positions Lys^{23}, Lys^{35}, Lys^{49} and Lys^{69}) bound to AChBP and free in solution and compared their anisotropy decay properties with fluorescently-labeled cysteine mutants of AChBP. The results indicated that the core of the toxin molecule is relatively flexible when bound to AChBP. Taken together, hydrodynamic and anisotropy decay analyses indicate that only one face of the second loop of the α-

neurotoxin is immobilized significantly by its binding. The results indicate that bound α-neurotoxin is not rigidly oriented on the surface of AChBP but rather exhibits segmental motion by virtue of flexibility in its finger-like structure.

B. Introduction

Nicotinic acetylcholine receptors (nAChRs) are prototypic members of the Cys-loop superfamily of pentameric ligand-gated ion channels, so named by a conserved disulfide linkage in the extracellular domain of the receptors (*1*). Other members of this family include the $GABA_A$, $GABA_C$, $5\text{-}HT_3$, and glycine receptors. nAChRs are responsible for fast neurotransmission via acetylcholine-induced cation permeability at the skeletal neuromuscular junction, as well as at ganglionic and central nervous system synapses. Various subtypes of nAChRs are defined by the subunit composition of the homo- or hetero-pentameric subunit assemblies; ligand specificity is governed by binding determinants at the subunit interface.

Our understanding of the structure and function of nAChRs in particular, and ligand-gated ion channels in general, has been greatly facilitated by studies of the muscle-type nAChR and snake venom α-neurotoxins from *Elapidae* species, which display high specificity for muscle-type nAChRs (*2*). α-Bungarotoxin, a member of this family of over 100 α-neurotoxins, enabled the first isolation and characterization of a nAChR (*3*). Other *Elapidae* α-neurotoxins have also been of great value in the identification and *in situ* localization of nAChRs (*4*). Structurally, α-neurotoxins consist of a core region from which three loops extend outward like fingers from a hand. The secondary structure consists of two anti-parallel β-sheets, one of which is a three-stranded β-sheet with two

strands associated with the central finger (loop II). Functionally, the α-neurotoxins are defined by their ability to compete with acetylcholine at post-synaptic nicotinic receptors and were hence originally denoted "curaremimetic toxins." α-Bungarotoxin and α-cobratoxin fall into the category of long-chain (Type II) α-neurotoxins, which contain four internal core disulfides and one residing at the tip of their central loop (loop II). These long chain family members share a high affinity for the skeletal muscle-type and the homomeric α7 neuronal nAChR.

Recently the crystal structure for the acetylcholine binding protein (AChBP), a valuable structural (*1, 5*) and functional (*6*) surrogate of the nicotinic receptor ligand-binding domain, complexed with α-cobratoxin, was solved at 4.2 Å resolution (*7*). This structure complemented longstanding biochemical, mutagenesis and structure-based modeling studies on α-neurotoxin binding to nAChRs (*8-12*), and suggested new, unpredicted atomic interactions of the toxin with the receptor.

To advance our understanding of the interaction of α-neurotoxins with nicotinic receptors, we examined the conformational flexibility of α-neurotoxins bound to AChBP, focusing on the orthologous peptides α-cobratoxin and α-bungarotoxin. Because the crystal structure of five α-cobratoxin molecules bound to AChBP shows the toxins projecting radially, like propeller 'blades,' from the outer perimeter of the cylindrical AChBP, we reasoned that, if the 'blades' were rigid, they should dramatically increase the hydrodynamic, frictional drag or resistance of the α-neurotoxin-AChBP complex. Hydrodynamic properties of detergent-solubilized receptors from *Torpedo* have been studied (*13*), however by examining only the extracellular domain of this protein family,

the subunit size falls in a range where bound α-neurotoxin molecules should influence hydrodynamic characteristics.

The diffusion and frictional coefficients of the α-neurotoxin-bound and unliganded AChBP were measured using analytical ultracentrifugation. We found that α-neurotoxin binding had little effect on the frictional coefficients revealing minimal apparent difference in dimensional asymmetry between AChBP and its toxin complex. This suggested a significant level of flexibility of the bound α-neurotoxin in the time domain of translational diffusion of AChBP. To confirm independently the flexibility of the bound α-neurotoxins, we measured the anisotropy decay of four site-specifically FITC (fluorescein isothiocyanate)-labeled α-cobratoxins bound to AChBP and free in solution and compared their decays to those of fluorescently-labeled cysteine mutants of AChBP. The results indicate that the internal core and most finger residue positions of the toxin molecule are relatively flexible when bound to AChBP.

C. Materials and Methods

1. Ligands and labeling reagents

α-Bungarotoxin was purchased from Sigma-Aldrich (St. Louis, MO). [^{125}I]-α-Bungarotoxin (specific activity: 130 Ci/mmol) was a product of PerkinElmer Life Sciences, Inc (Wellesley, MA). α-Cobratoxin was isolated as previously described from the venom of *Naja naja siamensis* (Miami Serpentarium, Salt Lake City, UT)(*14*). 2-[(5-Fluoresceinyl)aminocarbonyl]ethyl methanethiosulfonate (MTS-Fl) and N-(methanethiosulfonylethylcarboxamidoethyl)-5-naphthylamine-1-sulfonic acid (MTS-

EDANS, Figure V.1) were purchased from Toronto Research Chemicals, Inc (Ontario, Canada). All other chemicals were of the highest grade commercially available.

2. Expression, mutagenesis and purification of AChBP

Wild-type AChBP from *Lymnaea stagnalis* was expressed from a cDNA synthesized from oligonucleotides selected for mammalian codon usage, as previously described (*15*). Briefly, the cDNA was inserted into a p3×FLAG-CMV-9 expression vector (Sigma) containing a preprotrypsin leader peptide followed by an NH_2-terminal 3×FLAG epitope. A COOH-terminal 6×-histidine tag was attached for radioligand binding assays. Stable cell lines of single cysteine mutants of AChBP were generated as previously described (*16*). For protein used in the hydrodynamic assays, wt-AChBP was also transfected and stably selected in an HEK 293 cell line deficient in the N-acetylglucosaminyltransferase I gene ('GnTI$^-$ cells'), which should result in homogeneous glycosylation of limited oligosaccharide length (*17, 18*). The expression vector for AChBP differed slightly in the GnTI$^-$ cell line in that the construct contained a 1×NH_2-terminal FLAG epitope and no COOH-terminal tag. AChBP was purified from tissue culture medium by adsorption onto an α-FLAG antibody column and elution with FLAG peptide as previously described (*16*). Purity and assembly of subunits as a pentamer were assessed by SDS-PAGE and fast protein liquid chromatography.

3. Fluorophore labeling

Four site-specifically FITC-conjugated α-cobratoxins, labeled at positions of Lys^{23}, Lys^{35}, Lys^{49}, and Lys^{69}, were prepared as previously described (*19*). MTS-Fl and MTS-EDANS labeling of two cysteine-substituted AChBPs at positions N158C and D194C was carried out in a 100 μL volume containing 20 μM AChBP (subunit or

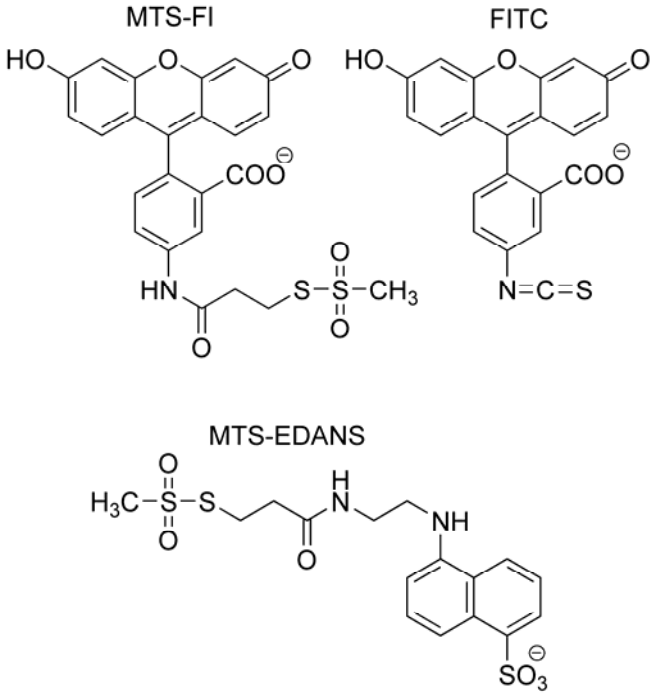

Figure V.1: Chemical Structures of Fluorescent Probes Used in Protein Labeling. FITC was conjugated to lysine residues in α-cobratoxin, MTS-fluorescein and MTS-EDANS to cysteine residues in AChBP for anisotropy decay analysis.

binding site concentration) and 100 μM fluorophore in 50 mM Tris-HCl, 150 mM NaCl, 0.02% NaN_3, pH 7.4. Labeling reactions ran for 90 min at room temperature shielded from light, after which free fluorophore was removed by buffer exchange (4×2 mL washes) into 0.1 M $NaPO_4$, pH 7.0 in Centricon YM-30 spin columns (Millipore, Billerica, MA). Specific labeling was assessed by comparison of fluorophore emission from the labeled mutant with that of a sample of wt-AChBP that was labeled in parallel with the mutant, after standardization to protein concentration by the Bradford assay. In all cases, non-specific labeling was ≤5%. Stoichiometry of labeling for each preparation was estimated from a comparison of fluorophore concentration (absorbance at 340 nm for MTS-EDANS, extinction coefficient ~5700 M^{-1} cm^{-1}, and at 496 nm for MTS-4-fluorescein, extinction coefficient 85,000 M^{-1} cm^{-1}) and protein concentration (by absorbance at 280 nm, extinction coefficient 268,000 M^{-1} cm^{-1}). Stoichiometry of subunit labeling in each mutant preparation ranged between 20-25%.

4. Mass spectrometry

Matrix-assisted laser desorption/ionization time-of-flight mass spectrometry was performed on a PE Biosystems Voyager DE-STR instrument (Framingham, MA). Purified recombinant AChBPs at 2 mg/mL in 60% acetonitrile, 0.1% (v/v) trifluoroacetic acid were mixed 1:1 with a matrix of 10 mg/mL saturated sinapinic acid (3,5-dimethoxy-4-hydroxycinnamic acid) dissolved in 50% acetonitrile, 0.1% trifluoroacetic acid, pH 2.2. One-μL droplets of AChBP/matrix mixture, containing approximately 6 pmol of protein, were spotted and dried by slow evaporation. Mass spectra were collected using the linear mode and external calibration was performed using yeast enolase protein (+1 and +2 monomer m/z species) and horse skeletal apomyoglobin (+1 monomer m/z).

5. Analytical ultracentrifugation

Sedimentation equilibrium and velocity experiments were conducted at 20°C using a Beckman Optima XL-1 analytical ultracentrifuge equipped with absorbance optics at 280 nm and an An60Ti rotor. Sedimentation equilibrium experiments were performed with protein solutions of 200 μg/mL centrifuged at 8, 10, and 12 krpm, in charcoal-filled Epon 6 channel centerpieces loaded with 110 μL of sample and 125 μL of reference buffer (50 mM Tris-HCl, 150 mM NaCl, 0.02% NaN_3, pH 7.4). Individual samples were centrifuged for 16 h at each speed with an absorbance scan conducted every 2 h. Data were collected in step mode with a spacing of 0.001 cm. Values presented are an average of at least three absorbance scans at each speed. Equilibrium was achieved as judged by comparison of overlays of three subsequent absorbance scans. The partial specific volume of the AChBPs was calculated using the Sednterp computer program (version 1.07, Hayes, Laue, Philo, University of New Hampshire 2002) to be 0.71 with no ligand present and with α-bungarotoxin bound. Ligand was added to achieve a slight excess of binding stoichiometry (1.2 molecules ligand per binding site). Stoichiometry of α-neurotoxin binding to AChBP was demonstrated previously using SDS-PAGE (*7*).

Sedimentation velocity experiments were performed at 30K rpm in charcoal-filled Epon double-sector centerpieces loaded with 400 μL of sample (200 μg/mL) and 425 μL of reference buffer (as above). Migration rates were monitored in a continuous scan mode, and were analyzed using the DCDT+ computer program (version 1.16, Philo). The reported weight average sedimentation coefficients ($S_{20,w}$) obtained from DCDT+ are

calculated by a weighted integration over the entire range of sedimentation coefficients covered by the $g(s)$ distribution (*20*) and corrected for the solution density and viscosity (*21*). Sedimentation data were collected on samples at two concentrations (0.2 A units and 0.4 A units) and concentration-dependence of s was not observed (data not shown).

From an experimentally-determined sedimentation coefficient (s), the apparent frictional coefficient f can be calculated with the expression:

$$f = \frac{M(1-\bar{V}\rho)}{N_A s} \tag{1}$$

and a frictional coefficient ratio f/f_0 equal to the Perrin shape factor (F) where f_0 is a theoretical minimum frictional coefficient for a non-hydrated sphere of a given molecular weight:

$$f_0 = 6\pi\eta r_0, \tag{2}$$

$$\text{where } r_0 = (3M\bar{V}/4\pi N_A)^{1/3} \tag{3}$$

and M is the molecular weight of the protein, $\bar{V}$ the partial specific volume of the protein, ρ the density of protein in g/cm^3, N_A equals 6.02×10^{23}, and η is the solution viscosity. For our analysis, M was determined by mass spectrometry, $\bar{V}$, ρ, and η were calculated based on amino acid content with the Sednterp computer program. From f, a diffusion constant D can be calculated with the expression:

$$D = \frac{kT}{f} \tag{4}$$

where k equals 1.38×10^{-16} erg $\times$ deg^{-1} and T is the absolute temperature (*22*).

6. Radioligand Binding Assays

A scintillation proximity assay (SPA, Amersham Biosciences) was adapted for use in a soluble radioligand-binding assay (*16*). Briefly, AChBP (0.5 nM binding sites) was incubated with 20 nM [^{125}I]-labeled α-bungarotoxin in a solution of 0.1 mg/mL anti-His SPA beads, and FITC-labeled α-cobratoxin was added in increasing concentrations. Binding data were fit to a one-site competition model using the Prism 4 computer program (GraphPad Software, Inc.). All radioligand binding data are averages of at least three replicate experiments.

7. Time-resolved fluorescence anisotropy

Emission anisotropy was determined by time-correlated single photon-counting with an HORIBA Jobin Yvon IBH Ltd. (Glasgow, U.K.) 470-nm NanoLED^{TM} laser (with FITC of MTS-Fl conjugates) or a 375-nm NanoLED^{TM} laser (with the MTS-EDANS conjugate) run at 1 MHz, an HORIBA Jobin Yvon IBH Ltd. model TBX-04 photon detector, a rotatable Glan-Thomson polarizer placed in the path of the excitation beam and a rotatable Polaroid HNP′B dichroic film polarizer placed in front of the photon detector. A depolarizing filter was also placed between the emission polarizer and photon detector to minimize the polarization bias of the photon detector. Vertically, $I_{\parallel}(t)$, and orthogonally, $I_{\perp}(t)$, polarized emission components were collected at 22°C while the samples were excited with vertically polarized light. For FITC and MTS-Fl, excitation and emission bands were selected with Omega 470DF35 and Omega 510DF23 filters, respectively. For MTS-EDANS, excitation and emission bands were selected with Corning 4-70 and Oriel 470 nm cuton filters, respectively. Typically, 4-6 × 10^4 peak counts were collected (in 2 min) with the emission polarizer oriented vertically. The orthogonal emission decay profile was generated over the same time interval. To

minimize convolution artifacts, laser profiles were recorded by removing the emission filter and monitoring light scatter from a suspension of latex beads. The data analysis software corrected for the wavelength-dependent temporal dispersion of the photoelectrons by the photon detector. The polarization bias (G) of the detection instrumentation was determined by measuring the integrated photon counts/6×10^6 lamp flashes while the samples were excited with orthogonally polarized light and the emission was monitored with a polarizer oriented in the vertical and orthogonal directions (G equals 1.015).

Unless stated otherwise, emission anisotropy decay was analyzed with the impulse reconvolution method implemented in the DAS6^{TM} software package from HORIBA Jobin Yvon IBH Ltd. (Glasgow, U.K.) described elsewhere (*23*). Briefly and simply, this approach splits the analysis into two steps − analysis of the total emission decay, S(t), followed by analysis of the vertical/perpendicular difference emission decay, D(t). S(t), free of anisotropy effects, is given by the expression

$$S(t) = I_{\parallel}(t) + G \bullet I_{\perp}(t) \tag{5}$$

and was analyzed as a biexponential function. D(t*)*, which includes both fluorescence and anisotropy parameters, is given by the expression

$$D(t) = I_{\parallel}(t) - G \bullet I_{\perp}(t). \tag{6}$$

D(t) is deconvolved with the results from the *S(t)* analysis as a constraint yielding

$$r(t) = \beta_1 \exp(-t/\phi_{fast}) + \beta_2 \exp(-t/\phi_{slow}). \tag{7}$$

Here, β_1 and β_2 are the amplitudes of the anisotropy at time zero for the fast and slow anisotropy decay processes, respectively. ϕ_{fast} and ϕ_{slow} are the fast and slow rotational correlation times of the anisotropy decay, respectively. A nonassociative model was assumed, where the emission relaxation times are common to all the rotational correlation times. Goodness of fit was evaluated from the values of the reduced χ^2_r and by visual inspection of the weighted-residual plots.

D. Results

1. Hydrodynamic analyses of AChBP and the α-neurotoxin complex

In sedimentation equilibrium (Figure V.2A), sample solutions are centrifuged until equilibrium is approached where concentration from the centrifugal force is balanced by diffusion from a concentration gradient extending in the opposite direction. As dimensional asymmetry of the macromolecule affects both of these forces equally, sedimentation equilibrium measurements provide an estimate of molecular weight independent of the volume and shape of the hydrated macromolecule. Mass spectrometry was used as an independent assessment of molecular weight to verify the hydrodynamic results. In all cases measurements from the two methods yielded data within 5% (Table V.1).

To serve as an internal control, AChBP produced in an HEK 293 cell line deficient in the glycosylation processing enzyme, N-acetylglucosaminyltransferase I ($GnTI^-$), was also examined by mass spectrometry and analytical ultracentrifugation. The corresponding molecular weight difference between this protein species and that produced in standard HEK 293 cells can be attributed to the mass difference in the conjugated affinity tags and the oligosaccharide trimming to 5 mannose residues and 2 N-

Table V.1: Experimentally-determined Sedimentation Parameters[a]

	MW by Mass Spectrometry[b]	MW by Sedimentation Equilibrium	S ($\times 10^{-13}$ s)	D (cm^2/s)	f/f_0
Apo	151,945	151,000	6.9	3.9	1.5
+Epibatidine	152,990	152,000	6.8	3.8	1.6
+ α-Bungarotoxin	191,868	188,000	8.1	3.6	1.5
Apo GnTI$^-$	130,305	127,000	6.8	4.5	1.4
+ α-Bungarotoxin GnTI$^-$	170,229	164,000	8.3	4.3	1.3

[a]Molecular weights were determined by mass spectrometry and sedimentation equilibrium. Sedimentation coefficients in Svedbergs (S), diffusion constants in cm^2/s and frictional coefficients were determined by sedimentation velocity and the MW from mass spectrometry. [b]Increase in MW upon ligand binding is the calculated sum of the apo-receptor measured value plus the projected addition of five ligand molecules.

acetylglucosamine residues per AChBP subunit derived from GnTI$^-$ HEK cells (*18*). The respective mass differences are 3×FLAG plus 6×His in the standard protein species, versus 1×FLAG: 12,800 Da, and the absence of oligosaccharide processing, 6,800 Da in the glycosylation processing deficient species. Differences in molecular weight and the mass uniformity of the trimmed oligosaccharide structure are qualitatively evident upon SDS gel electrophoresis (Figure V.2B).

Sedimentation velocity measurements were used to measure the effect of ligand binding on the overall volume and shape of AChBP. Here, differences in dimensional asymmetry are monitored for molecules of established molecular weight, and the protein concentration change over the length of the sample cell in relation to time (Figure V.3) is used to determine sedimentation, translational diffusion, and frictional coefficients.

We also used sedimentation velocity to monitor the effect of α-bungarotoxin (Figure V.4) binding on the macromolecular translational diffusion parameters of AChBP. Binding of five 8-kD toxin molecules to AChBP slightly increased the sedimentation coefficient from 6.9 S to 8.1 S (Table V.1). A similar small increase from bound α-neurotoxin was observed in the sedimentation coefficient for the differentially-glycosylated AChBPs. The diffusion coefficients associated with AChBP from GnTI$^-$ cells were slightly higher than for the heavily glycosylated form, consistent with a trimming of an extended and presumably more heterogeneous oligosaccharide as well as the histidine tag. Notably, there was no significant change in the frictional coefficient ratio f/f_0 upon α-neurotoxin binding to either species of AChBP. As an internal control, parallel hydrodynamic experiments were performed using α-cobratoxin, and indistinguishable sedimentation parameters were obtained (data not shown). Binding of

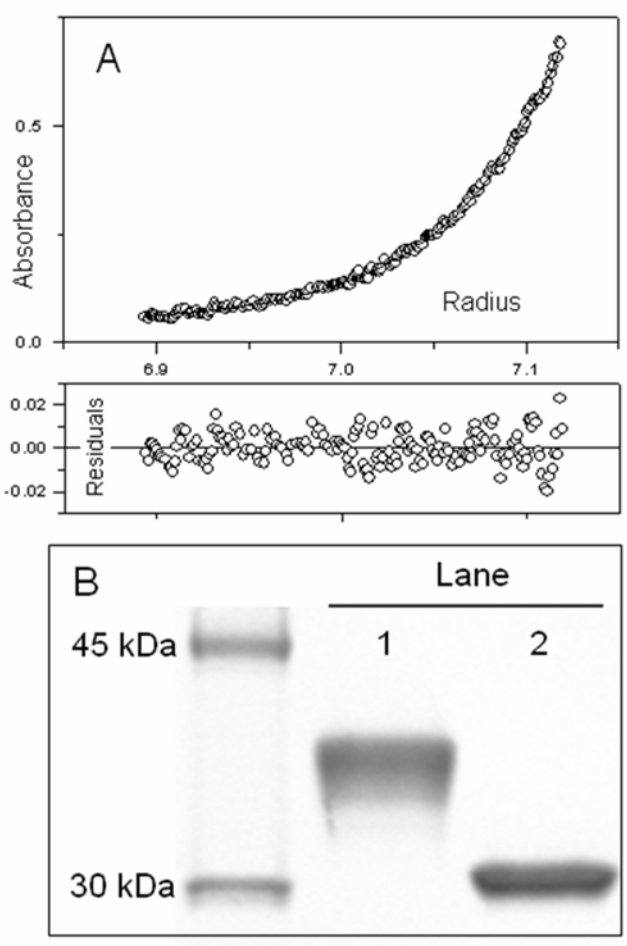

Figure V.2: Characterization of AChBP by Sedimentation and Gel Electrophoresis. (A) Sedimentation equilibrium of AChBP from HEK 293 cells with α-bungarotoxin present. Samples of 110 μg/mL AChBP and a 1.2 molar excess of α-bungarotoxin (in 50 mM Tris-HCl, 150 mM NaCl, pH 7.4) were centrifuged at 10,000 rpm until a constant profile was established as determined by an overlay of consecutive absorbance scans. These data were fit to an equation corresponding to a molecular weight of 188,000 Da for the complex. (B) SDS-PAGE of the purified AChBPs from HEK 293 cells (lane 1) and GnTI$^-$ cells (lane 2). One μg of protein was run in each lane of a 16% polyacrylamide gel.

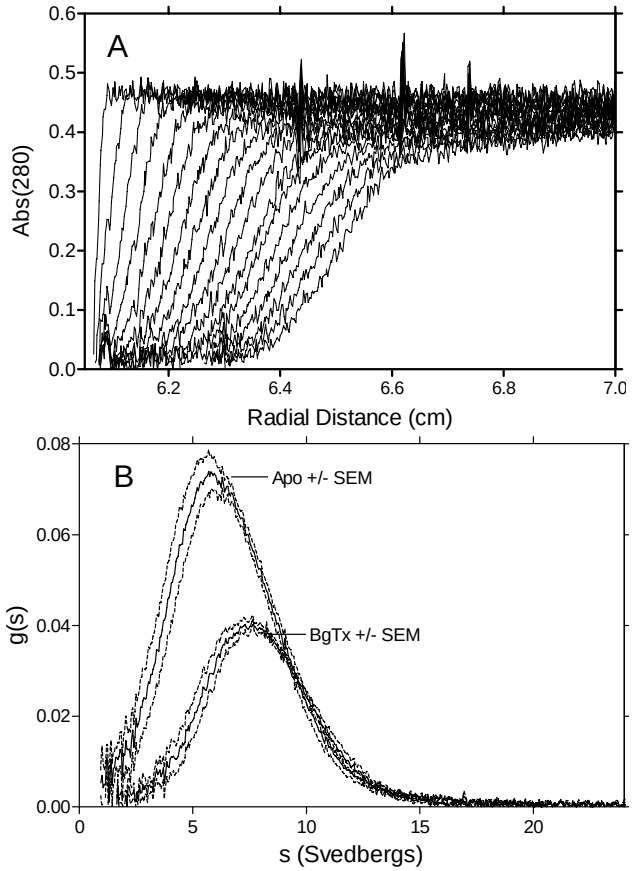

Figure V.3: Sedimentation Velocity of AChBP from HEK 293 Cells. (**A**) Raw data taken as radial absorbance scans at 10 minute intervals with apo protein (no ligand present). (**B**) Analyzed values ± SEM presented as g(s) vs. s comparing apo protein to that with α-bungarotoxin added. The difference in curve amplitude here is due to a two-fold higher concentration used for apo protein data. Weight-averaged sedimentation coefficients (s) were calculated using the fitting equation described in the Methods section to be 6.9 S and 8.1 S for apo and the α-bungarotoxin complex, respectively.

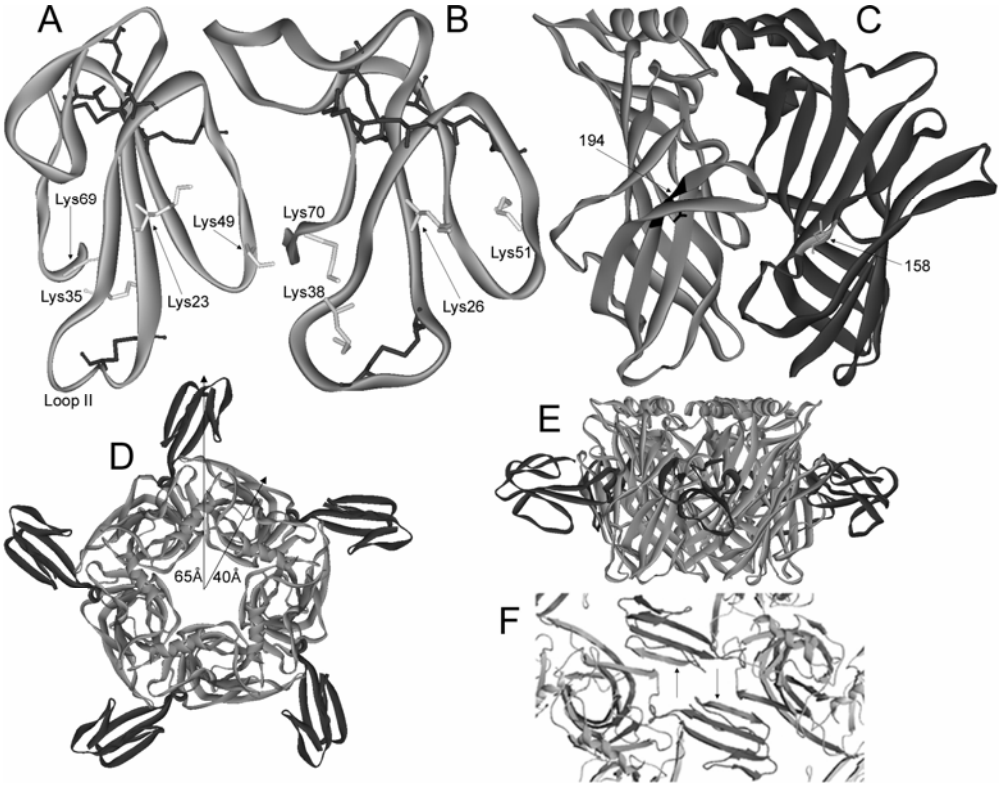

Figure V.4: Ribbon Diagram of the X-ray Structures of α-Neurotoxins and AChBP. Panel A: α-cobratoxin (PDB accession code 2CTX (*40*)). Average B factors for the Lys^{23}, Lys^{35}, Lys^{49}, and Lys^{69} residues from the X-ray coordinates are, respectively, 7.1, 16.3, 27.5, and 54.8, with higher values corresponding to increased disorder. Panel B: α-bungarotoxin (PDB accession code 1IDI (*41*)); Panel C: side view of the interface of two AChBP subunits (PDB accession code 1I9B (*5*)). Cysteine substitutions were made at residues D194C and N158C on opposing sides of the subunit interface and conjugated with the sulfhydryl-reactive probes, MTS-Fl and MTS-EDANS; Panels D-F: apical (D), side (E) and crystal lattice packing (F) views of the α-cobratoxin-AChBP complex (PDB accession code 1YI5; figure adapted from (*7*)). Note the interaction between the core structure of the toxin molecule with the core toxin structure in the symmetry-related molecule (arrows in panel F). α-Carbon backbone and selected side chains are shown in light grey and disulfide bonds are shown in dark grey.

the high-affinity agonist epibatidine (MW: 209 D) had no detectable effect on the sedimentation parameters.

2. Fluorescence anisotropy

To examine more directly the flexibility of the bound α-neurotoxin, time-resolved anisotropy decay of reporter groups specifically conjugated to sites on α-cobratoxin and sites of cysteine substitution on AChBP were measured free in solution and in a complexed state. We have previously reported that it is often possible to resolve to a significant degree tether arm torsional motions of the reporter groups about their linkages to the α-carbon backbone (< 1 ns; very fast), local segmental mobility of the α-carbon backbone (low ns; fast), and global rotation of the macromolecule (slow) (*24-27*). Here, FITC was separately conjugated to the ε-amino groups of four lysines in α-cobratoxin (FITC-Lys^{23}, FITC-Lys^{35}, FITC-Lys^{49} and FITC-Lys^{69}, Figure V.4A). Lys^{23} is located in loop II in the center of three anti-parallel β-strands, Lys^{35} is in a less structured region near the tip of loop II, Lys^{49} is positioned on loop III, and Lys^{69} is near the C-terminus of the toxin. For comparison, MTS-Fl was conjugated to the sulfhydryl side chains of substituted cysteines on two AChBP mutants (N158C and D194C). Additionally, MTS-EDANS, a long lifetime reporter group, was conjugated to the substituted cysteine in the D194C AChBP mutant to better assess the averaged whole-body rotational correlation time of the α-neurotoxin-AChBP complex. Radioligand binding assays on the fluorescent α-cobratoxin derivatives were performed with AChBP and showed that covalent modification did not alter the binding parameters by more than five fold. (Table V.2).

Table V.2: Dissociation Constants for Binding of α-Neurotoxins to AChBP[a]

	K_D (nM)
α-Bungarotoxin	1.8[b]
α-Cobratoxin	3.2[b]
FITC-Lys^{23}-α-Cobratoxin	2.5 ± 0.1
FITC-Lys^{35}-α-Cobratoxin	12.6 ± 0.1

[a]Comparison of affinities ± SEM of FITC-labeled α-cobratoxins for AChBP by radioligand binding competition with [^{125}I]-α-Bungarotoxin. [b]Data from (*15*).

The anisotropy decays of the FITC-α-cobratoxins free in solution were well fit to a biexponential expression (eq. 7) with the slow rotational correlation times (ϕ_{slow}) ranging between 3.5 ns and 4.5 ns (Figure V.5; Table V.3). These values are close to the value predicted by the Stokes-Einstein equation (3.2 ns) for an 8 kD spherical protein, strongly suggesting that the ϕ_{slow} values reflect the average rotational correlation time of the toxin with its modest dimensional asymmetry (*28*). With the exception of the FITC-Lys^{23} derivative, the ϕ_{fast} values were < 1 ns indicating a high level of mobility of the reporter groups (at Lys^{35}, Lys^{49}, and Lys^{69}) and that rates of the tether arm and local α-carbon backbone motions around sites of conjugation overlap one another and are irresolvable (*29*). The ϕ_{fast} value of the FITC conjugated to Lys^{23}, however, was significantly greater than 1 ns (1.8 ns). With the ϕ_{slow} value of the FITC-Lys^{23} derivative reflecting the whole-body rotational correlation time, the ϕ_{fast} value for this conjugate largely reflects local backbone diffusional processes around Lys^{23}. All this indicates that the backbone motions around Lys^{23} are significantly less than that of the other sites of conjugation examined, which is not surprising given the position of the Lys^{23} residue centrally-located within three anti-parallel β-strands and the low thermal (B) factor values of both the main-chain and side-chain atoms of this residue compared to the other lysines (Figure V.4A, PDB accession code 2CTX). Due to the short global rotational correlation times, we were not able to resolve to distinguish differences in the backbone mobility of the other labeling positions; however, our results with position Lys^{23} are consistent in showing the least mobility of the four lysine-labeling sites.

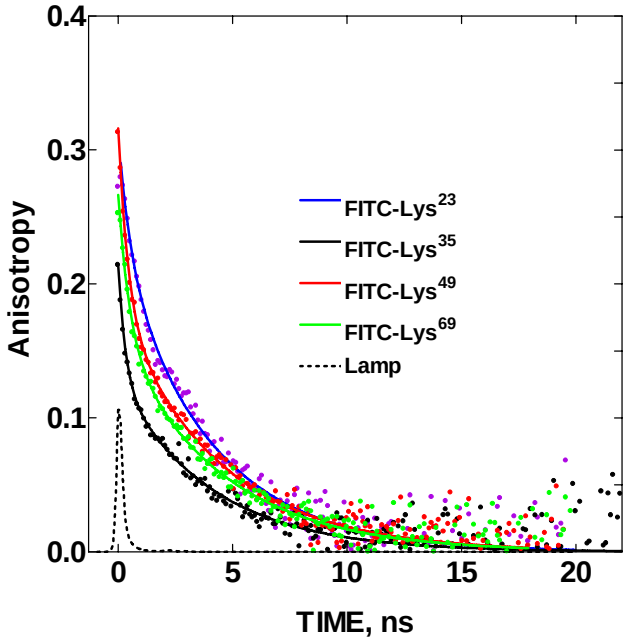

Figure V.5: Time-Resolved Fluorescence Anisotropy Decay for FITC-labeled-α-Cobratoxins Free in Solution.

Table V.3: Anisotropy Decay Parameters of FITC-labeled α-Cobratoxins[a]

Toxin conjugate	Condition	β_1	β_2	ϕ_{fast} (ns)	ϕ_{slow} (ns)	χ^2_r	$\langle\tau\rangle$ (ns)
FITC-Lys^{23}	Free	0.04±0.02	0.17±0.02	1.8±0.2	4.2±0.3	1.6±0.2	2.5±0.1
	Bound	0.05±0.01	0.18±0.01	2.6±0.8	69±15	1.6±0.3	3.0±0.1
FITC-Lys^{35}	Free	0.10±0.02	0.13±0.01	0.1±0.0	3.5±0.2	1.4±0.2	3.7±0.2
	Bound	0.12±0.01	0.11±0.02	2.8±0.2	25±5	1.6±0.2	3.6±0.1
FITC-Lys^{49}	Free	0.06±0.02	0.16±0.01	0.6±0.1	4.5±0.5	2.0±0.2	3.1±0.1
	Bound	0.10±0.01	0.12±0.01	0.8±0.1	17±2	2.1±0.2	2.8±0.1
FITC-Lys^{69}	Free	0.06±0.01	0.15±0.01	0.5±0.1	4.3±0.7	1.7±0.2	3.5±0.1
	Bound	0.08±0.01	0.14±0.01	1.0±0.1	20±2	2.2±0.6	3.4±0.1

[a]To assess regional variations in toxin flexibility, anisotropy decay of free and AChBP-bound FITC-α-cobratoxins was monitored and fit to a biexponential decay equation as described in Methods section. β_1 and β_2 are the magnitudes of the decay associated with fast and slow processes, respectively. ϕ_{fast} and ϕ_{slow} are the fast and slow rotational correlation times, respectively. χ^2_r is the reduced χ^2 of the anisotropy decay analysis. $\langle\tau\rangle$ is the quantum-yield weighted fluorescence lifetime. In all experiments, α-neurotoxins were present at 0.1 μM, and when applicable AChBP was present at 0.2 μM in binding site concentration. All data are the average of at least three replicate experiments ± standard deviation.

When AChBP-bound, the anisotropy decays of the FITC-toxins were again described by a biexponential expression (eq. 7) with the ϕ_{slow} values of the FITC-Lys^{35}, -Lys^{49}, and -Lys^{69} conjugates ranging between 17 and 25 ns and 69 ns for the FITC- Lys^{23} conjugate (Figure V.6; Table V.3). The ϕ_{slow} values of the FITC-Lys^{35}, -Lys^{49}, and -Lys^{69} conjugates are significantly lower than what is predicted by the Stokes-Einstein equation (81 ns) for a spherical protein with a molecular mass of ~190 kD or the experimental value (142 ns) determined with a longer lifetime reporter group (EDANS) conjugated to the surface of the toxin-bound AChBP (described below). This disparity indicates that the bound-toxin ϕ_{slow} values do not reflect solely whole-body rotational processes but probably a merging of large amplitude α-carbon backbone fluctuations of the AChBP-bound α-neurotoxins with rotational diffusion of the toxin-AChBP complex. The merging of the bound-toxin backbone fluctuations with whole-body diffusional processes makes quantitative assessment of the backbone mobility of the bound α-neurotoxins problematic, but visual inspection of the time course of the anisotropy decays (Figure V.6) suggests the rank order of mobility of the reporter groups is Lys^{49} > Lys^{69} > Lys^{35} >> Lys^{23}. Additionally, the total deconvolved amplitudes of the observable anisotropy decay ($\beta_1 + \beta_2$; Table V.3) showed little or no effect from AChBP binding indicating that the bound reporter group was not immobilized between the toxin and AChBP.

To support our interpretation of the fast ϕ_{slow} values for the AChBP-bound FITC-Lys^{35}, -Lys^{49}, and -Lys^{69} conjugates, the anisotropy decay of fluorescein conjugated to two sites on the surface of α-toxin-bound AChBP (Fl-N158C and Fl-D194C) were measured and compared to that of the AChBP-bound FITC-α-neurotoxins. The

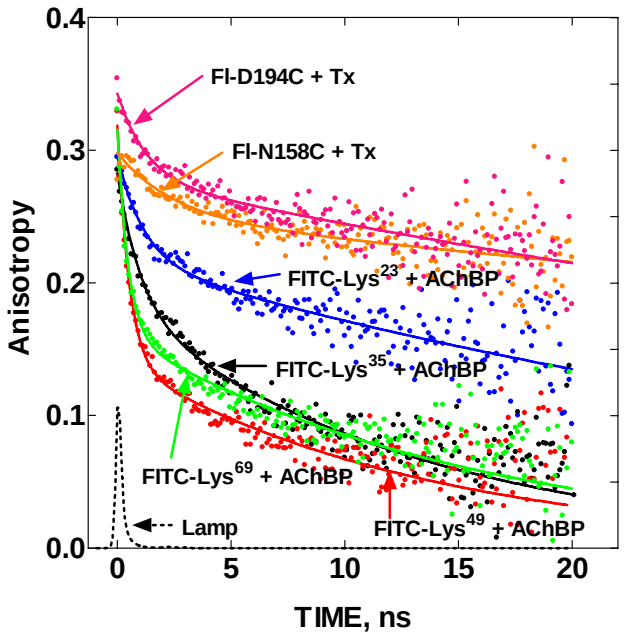

Figure V.6: Comparison of the Time-resolved Fluorescence Anisotropy Decay for AChBP-bound FITC-labeled α-Cobratoxins with Fl-N158C-AChBP and Fl-D194C-AChBP Complexed with α-Bungarotoxin.

anisotropy decay of the Fl-AChBP conjugates was measured in the absence and presence of a stoichiometric excess of α-neurotoxin (Table V.4, Figure V.7). Similar to the FITC-α-neurotoxins, the anisotropy decays of the Fl-N158C and Fl-D194C mutants were well fit to an expression for biexponential decay (eq. 7). The presence of excess α-neurotoxin was associated with significant changes in virtually all of the anisotropy decay parameters (Table V.4) indicating that the α-toxin binds to the conjugated AChBP mutants. Focusing on the rotational correlation times of the slow depolarization processes, the ϕ_{slow} values of the Fl-N158C and Fl-D194C conjugates ranged between 86 ns and 156 ns, which are substantially greater than the comparable values of the AChBP-bound FITC-Lys^{35}, -Lys^{49}, and -Lys^{69} conjugates (range between 17 and 25 ns). The ϕ_{slow} value for the AChBP-bound FITC-Lys^{23} conjugate was intermediate in magnitude (69 ns) between the other FITC and Fl conjugates as described above. Relative to the sites of Fl conjugation on AChBP, three of the four sites of FITC conjugation (Lys^{35}, Lys^{49}, and Lys^{69}) on the AChBP-bound α-neurotoxin were dramatically more flexible than AChBP-surface sites examined and demonstrate the high level of flexibility of much of the AChBP-bound α-neurotoxin.

To obtain a more accurate measure of the averaged whole-body rotational correlation time of α-neurotoxin-bound and free AChBP, the D194C AChBP mutant was conjugated with MTS-EDANS, whose longest emission lifetime is ~20 ns. The anisotropy decay of this conjugate was measured in the presence and absence of excess α-toxin (Table V.4, Figure V.7). In the absence of α-neurotoxin it was possible to fit the anisotropy decay by using the impulse reconvolution method discussed in the Methods section, which yielded a ϕ_{slow} value of 124 ns. When α-neurotoxin was bound the

Table V.4: Anisotropy Decay Parameters for MTS-Fl- and MTS-EDANS-labeled AChBP[a]

AChBP Construct	Ligand	β_1	β_2	ϕ_{fast} (ns)	ϕ_{slow} (ns)	χ^2_r	$\langle\tau\rangle$
Fl-N158C	None	0.06±0.01	0.18±0.02	3.0±0.5	90±19	1.7±0.2	3.5±0.1
	α-Bungarotoxin	0.03±0.01	0.24±0.01	6.2±0.3	156±14	2.3±0.3	3.8±0.1
Fl-D194C	None	0.05±0.02	0.21±0.02	5.4±1.4	76±16	2.0±0.3	3.0±0.1
	α-Bungarotoxin	0.03±0.01	0.26±0.02	3.7±0.2	86±14	1.9±0.7	3.1±0.1
EDANS-D194C	None	0.02±0.01	0.28±0.01	15.0±4.0	124±12	1.0±0.2	17.0±0.1
	α-Bungarotoxin[b]	0.01±0.00	0.27±0.01	4.4±0.8	142±14	1.0±0.1	16.8±0.2

[a]To assess regional variations in α-carbon backbone flexibility of AChBP ± α-neurotoxin, anisotropy decays of MTS-Fl-labeled AChBPs were monitored and fit to a biexponential decay equation as described in Methods section. The same approach was taken with MTS-EDANS-labeled AChBP to better estimate the effect of α-toxin binding on the rotational correlation times of AChBP. β_1 and β_2 are the magnitudes of the decay associated with fast and slow processes, respectively. ϕ_{fast} and ϕ_{slow} are the fast and slow rotational correlation times, respectively. χ^2_r is the reduced χ^2 of the anisotropy decay analysis. $\langle\tau\rangle$ is the quantum-yield weighted fluorescence lifetime. All data are the average of at least three replicate experiments ± standard deviation. [b]In the case of α-bungarotoxin bound to EDANS-D194C, anisotropy decay data were analyzed by fitting to eq. 7 (see Methods) without deconvolution of the lamp pulse starting at a time point 0.8 ns after the peak lamp intensity. Similar experiments were done with α-cobratoxin and no significant difference between the two α-neurotoxins was observed. Fl-N158C and Fl-D194C were present at 1-2 μM in binding site concentration, EDANS-D194C was present at 3-5 μM, and when applicable α-bungarotoxin was added to achieve a 1.5-fold stoichiometric excess.

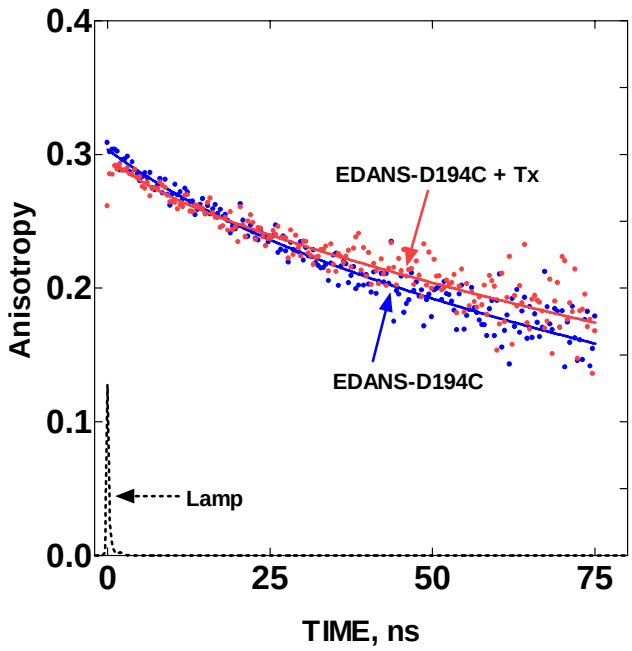

Figure V.7: Comparison of the Time-resolved Fluorescence Anisotropy Decay Curves for EDANS-D194C-AChBP Alone and Complexed with α-Bungarotoxin.

anisotropy increased slightly during the initial 0.6 ns and then decreased almost monoexponentially. Consequently, for this sample the anisotropy decay was fit to eq. 7 without impulse reconvolution utilizing the data points starting just after the end of the lamp pulse (t = 0.8 ns), which yielded a ϕ_{slow} value of 142 ns, a 15% increase of the value of apo-AChBP.

E. Discussion

1. Hydrodynamic characteristics of an oligomeric pore protein

The unique structure of AChBP as a homomeric pentamer with a C_{5v} axis of symmetry (*30*) protruding through what serves as an open vestibule in the nAChR (*31*) presents some new considerations in the hydrodynamic analysis of oligomeric proteins. Comparable tabulated f/f_0 values for prolate and oblate ellipsoids yield axial ratios between 6 and 10 (*32*), a dimensional asymmetry far greater than one would estimate based simply on dimensions from the crystal structure of the cylindrical pentamer (62 Å in length and 80 Å in diameter). One conclusion is that the expanded hydrodynamic radius due to structured water in the central vestibule contributes significantly to the frictional drag that the AChBP pentamer experiences in translational diffusion. In high resolution X-ray structures of AChBP, one observes symmetrically structured water molecules at the narrow portion of the vestibule that could form a constriction point for ion flow in the full-length receptor (*33-35*).

As an initial approximation of molecular dimensions, AChBP might be considered in terms of two concentric cylinders. The inner cylinder would define the volume and surface area of the internal vestibule whereas the outer cylindrical surface area would define the external solvent exposure. The volume difference between the two

cylinders is where the protein mass lies. With an averaged vestibule radius of 9 Å, the internal volume is 16,000 $Å^3$ and the internal surface area is 3500 $Å^2$. The overall volume including the vestibule is 311,000 $Å^3$ and the corresponding surface area is 15,600 $Å^2$. Hence, the volume of the outer cylinder is 295,000 $Å^3$ and its surface area is 12,100 $Å^2$. Estimated from the central axis of the vestibule to the outer Connolly surface toxin binding would extend the overall radius of AChBP from 40 Å to 65 Å with the maximal length at the tips (Figure V.4D).

2. Structural fluctuations in AChBP-bound α-neurotoxin

Combining hydrodynamic analyses with measurements of fluorescence anisotropy decay enabled us to consider torsional and segmental motion within the molecule in relation to global rotational and translational diffusion parameters revealed by the two experimental approaches.

Based on the radial propeller blade-like positioning of five α-neurotoxin molecules around the perimeter of AChBP as shown in the recent X-ray crystal structure (*7*), we anticipated that binding of α-neurotoxin would have a marked influence on the sedimentation properties of AChBP. We assessed the effective distortion of hydrodynamic shape by sedimentation velocity analysis which allows one to calculate a frictional coefficient. The ratio, f/f_0, indicates how much the hydrated shape of the experimental protein through its dimensional asymmetry deviates from a compact, non-hydrated sphere. Upon α-neurotoxin binding to AChBP, no significant increase in f/f_0 is observed in contrast to what might be expected if the five toxin molecules were oriented in rigid radial positions shown in the crystal structure (Figure V.4D, E). These data

indicate that binding of α-neurotoxin has a minimal effect on the translational diffusion properties of AChBP beyond that predicted from a simple addition of the equivalent compact molecular mass. A parsimonious explanation for this stems from flexibility of the core of the toxin molecule that is likely imparted by joints in the toxin fingers permitting segmental motion of the core disulfide structure. Accordingly, we sought a comparison between motion in the binding protein and the bound toxin molecule.

3. Analysis of segmental motion by decay of fluorescence anisotropy

Since time-resolved fluorescence anisotropy decay analysis allows one to monitor torsional and segmental motion in proteins as well as their global rotational diffusion, we employed this technique not only to examine global rotation of AChBP and its complex, but more importantly to assess the flexibility of bound α-neurotoxin at four positions on the toxin molecule in relation to stationary reference positions on AChBP itself. We found that when the α-neurotoxin is bound to AChBP, the majority of the α-neurotoxin structure remains quite flexible relative to AChBP itself. The exception was at position Lys^{23}, which showed slower segmental motion of limited amplitude upon binding such that its backbone mobility was comparable to that of the F-loop of AChBP.

In light of the α-cobratoxin-AChBP crystal structure (*7*), a high degree of flexibility is not surprising at the Loop III position (Lys^{49}) or at the C-terminus (Lys^{69}) of the α-neurotoxin, as these regions do not appear to interact directly with the surface of AChBP. However, it is noteworthy that the α-carbon backbone region around Lys^{35} in the α-neurotoxin exhibits greater mobility than that around Lys^{23}. At first inspection, these results are somewhat surprising since Lys^{35} is closer to the tip of loop II and site of

interaction with the binding interface. This residue also appears sandwiched against the C-loop of AChBP. If the toxin were behaving as a relatively rigid entity with a fulcrum at the tip of loop II, one might expect movement over a greater segmental arc as one extends from the fulcrum point. However, closer examination of the crystal structure of the toxin reveals that Lys^{23} is structured in a β-pleated sheet, whereas Lys^{35} is in a loop that lacks secondary structure. One can consider the motion of the toxin region near Lys^{23} as being restricted by two factors, its surrounding secondary structure and the overall immobilization of the toxin via its interaction at the tip of loop II with AChBP. Therefore, the kinetic component with the dominant amplitude contributing to the decay of anisotropy from FITC-Lys^{23} approaches that of the global rotation rates of the entire complex. The immediate region surrounding Lys^{35} of the toxin, being less constrained by secondary structure, reveals additional segmental motion contributing to the decay of anisotropy from FITC labeled at this site. These data are in agreement with NMR experiments using α-cobratoxin bound to a short C-loop peptide cognate (*36*) wherein an overlay of 10 solution structures of the toxin reveals a single orientation for Lys^{23} whereas the side chain and α-carbon backbone of Lys^{35} undergo at least a 180° rotation even while bound to the short C-loop peptide mimic.

To impart a frame of reference for assessing segmental motion in α-neurotoxin, we examined time-resolved fluorescence anisotropy decay from two different sites of MTS-Fl conjugation in AChBP itself (D194C, N158C). Data from both sites that lie on opposing sides of the subunit interface indicate far less α-carbon backbone flexibility than we observed from the bound α-neurotoxin. Using MTS-EDANS, a longer lifetime

fluorescent probe, labeled at the D194C site in AChBP, enabled us to monitor the slow component of the anisotropy decay that corresponds to the global rotation rate of the macromolecule (Table V.4).

To compare our experimentally-determined rotational correlation times to a hypothetical value, from the Stokes-Einstein equation, we calculated theoretical rotational correlation times for apo and α-neurotoxin-bound AChBP. Using the molecular weights determined by mass spectrometry, this equation yields rotational correlation times of 64 ns for apo AChBP (from HEK 293 cells) and 81 ns for the α-neurotoxin-AChBP complex. These estimated values, which do not account for associated water, are much lower than the experimentally-determined values of 124 and 142 ns, respectively. The structured, retained water in the vestibule of AChBP and associated hydration of the oligosaccharide and other surface residues increase the effective mass and immobilized volume of the molecule. An increase of 26% in rotational correlation times calculated from apo and α-neurotoxin-bound AChBP is slightly greater than the 15% increase in the experimentally determined values. Consistent with the translational hydrodynamic analyses, the small increase in the experimentally-determined rotational correlation time indicates that the influence of the bound α-neurotoxin to rotational diffusion can be accounted for simply by the molecular weight addition and not an increase in dimensional asymmetry in the complex.

Comparison of the time-resolved fluorescence anisotropy decay curves of MTS-Fl and MTS-EDANS conjugated D194C in AChBP reveals differences in probe sensitivity to the segmental and whole-body motions. In preliminary studies, MTS-Fl conjugates of AChBP were consistently more sensitive to ligand-induced changes in fast segmental

motions, while MTS-EDANS more reliably reported on the whole body rotational diffusion (Hibbs, R.E. and Johnson, D.A., unpublished observations). The capacity of MTS-EDANS conjugates to measure this slow rotational decay component arises primarily from longer emission lifetimes ($<\tau> \sim 17$ ns) than MTS-fluorescein conjugates ($<\tau> \sim 3$ ns). The variation in capacity of MTS-EDANS conjugates to monitor segmental motions may be due to their longer tether arm (eight versus five atoms) and/or the amphipathic character of the reporter group.

Elapid α–neurotoxins exhibit a high degree of subtype selectivity for nAChRs. Their highest affinity is found for the muscle receptors from vertebrate species, yet certain residue substitutions and glycosylation can make certain animal species more resistant to the three-fingered α–neurotoxins than others (*37-39*). Many neuronal receptors are resistant to the α-neurotoxins, yet the homomeric neuronal species, typified by α7, show high affinities for the long neurotoxins. AChBP thus will serve as a structural template for the nicotinic receptor subtypes, and through mutagenesis, it should be possible to replicate the affinity changes and presumably ascertain the α-neurotoxin binding determinants of the various receptor subtypes. A suggestion that the nAChR and AChBP determinants are not identical comes from a comparison of the anisotropy decay data where the fluorescein conjugated at residue 69 in the nAChR-bound toxin shows a faster initial rate of decay than the other substituted lysines (*29*). In the case of AChBP, the fluorescein decay rate at position 69 is not distinguishable from that at residues 35 and 49 (Table V.3 and Figure V.6).

In summary, hydrodynamic measurements of translational diffusion and time-resolved fluorescence anisotropy decay analyses of rotational diffusion and intrinsic segmental motion yield a consistent picture of the dynamics of the AChBP-bound α-neurotoxin molecules. Internal motion of the α-neurotoxin molecule imparted by flexibility in the peptide chains in the α-neurotoxin fingers allows for the core of the molecule to move segmentally in a limited conical arc independent of the pentameric complex. This is demonstrated in lower resistance to rotational and translational diffusion than would be predicted from rigid α-neurotoxin molecules extended radially from the AChBP surface. Furthermore, time-resolved fluorescence anisotropy decay reveals additional degrees of segmental motion of the α-neurotoxin core not evident in the residues found on the binding interface of AChBP.

F. Acknowledgements

This chapter is material as it appears in: Ryan E Hibbs, David A Johnson, Jianxin Shi, Scott B Hansen, and Palmer Taylor "Structural dynamics of the α-neurotoxin-acetylcholine-binding protein complex: hydrodynamic and fluorescence anisotropy decay analyses," *Biochemistry* (2005) 44:16602-11. The dissertation author was the primary investigator in the development and execution of the study, and the principal author of this paper. This research was supported by a grant from the National Institutes of Health (R37-GM18360 to PT) and a pre-doctoral fellowship from the Pharmaceutical Research Manufacturers Association Foundation (REH).

I thank Dr. David Johnson for many hours of assistance with the anisotropy decay measurements, as well as patient discussion relating to the methodology. I thank Dr. Jian

Shi for providing mass spectrometry expertise, and Dr. Scott Hansen for providing GnTI$^-$ cell lines stably expressing AChBP from *Lymnaea*.

G. References

1. Karlin, A. (2002) Emerging structure of the nicotinic acetylcholine receptors, *Nat Rev Neurosci 3*, 102-114.

2. Nirthanan, S., and Gwee, M. C. (2004) Three-finger alpha-neurotoxins and the nicotinic acetylcholine receptor, forty years on, *J Pharmacol Sci 94*, 1-17.

3. Changeux, J. P., Kasai, M., and Lee, C. Y. (1970) Use of a snake venom toxin to characterize the cholinergic receptor protein, *Proc Natl Acad Sci U S A 67*, 1241-1247.

4. Taylor, P., Molles, B., Malany, S., and Osaka, H. (2002) in *Perspectives in Molecular Toxinology* (Menez, A., Ed.) pp 271-280, John Wiley & Sons, Chichester, England.

5. Brejc, K., van Dijk, W. J., Klaassen, R. V., Schuurmans, M., van Der Oost, J., Smit, A. B., and Sixma, T. K. (2001) Crystal structure of an ACh-binding protein reveals the ligand-binding domain of nicotinic receptors, *Nature 411*, 269-276.

6. Bouzat, C., Gumilar, F., Spitzmaul, G., Wang, H. L., Rayes, D., Hansen, S. B., Taylor, P., and Sine, S. M. (2004) Coupling of agonist binding to channel gating in an ACh-binding protein linked to an ion channel, *Nature 430*, 896-900.

7. Bourne, Y., Talley, T. T., Hansen, S. B., Taylor, P., and Marchot, P. (2005) Crystal structure of a Cbtx-AChBP complex reveals essential interactions between snake alpha-neurotoxins and nicotinic receptors, *Embo J 24*, 1512-1522.

8. Harel, M., Kasher, R., Nicolas, A., Guss, J. M., Balass, M., Fridkin, M., Smit, A. B., Brejc, K., Sixma, T. K., Katchalski-Katzir, E., Sussman, J. L., and Fuchs, S. (2001) The binding site of acetylcholine receptor as visualized in the X-Ray structure of a complex between alpha-bungarotoxin and a mimotope peptide, *Neuron 32*, 265-275.

9. Antil-Delbeke, S., Gaillard, C., Tamiya, T., Corringer, P. J., Changeux, J. P., Servent, D., and Menez, A. (2000) Molecular determinants by which a long chain toxin from snake venom interacts with the neuronal alpha 7-nicotinic acetylcholine receptor, *J Biol Chem 275*, 29594-29601.

10. Fruchart-Gaillard, C., Gilquin, B., Antil-Delbeke, S., Le Novere, N., Tamiya, T., Corringer, P. J., Changeux, J. P., Menez, A., and Servent, D. (2002) Experimentally based model of a complex between a snake toxin and the alpha 7 nicotinic receptor, *Proc Natl Acad Sci U S A 99*, 3216-3221.

11. Malany, S., Osaka, H., Sine, S. M., and Taylor, P. (2000) Orientation of alpha-neurotoxin at the subunit interfaces of the nicotinic acetylcholine receptor, *Biochemistry 39*, 15388-15398.

12. Osaka, H., Malany, S., Molles, B. E., Sine, S. M., and Taylor, P. (2000) Pairwise electrostatic interactions between alpha-neurotoxins and gamma, delta, and epsilon subunits of the nicotinic acetylcholine receptor, *J Biol Chem 275*, 5478-5484.

13. Reynolds, J. A., and Karlin, A. (1978) Molecular weight in detergent solution of acetylcholine receptor from *Torpedo californica*, *Biochemistry 17*, 2035-2038.

14. Karlsson, E., Arnberg, H., and Eaker, D. (1971) Isolation of the principal neurotoxins of two Naja naja subspecies, *Eur J Biochem 21*, 1-16.

15. Hansen, S. B., Radic, Z., Talley, T. T., Molles, B. E., Deerinck, T., Tsigelny, I., and Taylor, P. (2002) Tryptophan fluorescence reveals conformational changes in the acetylcholine binding protein, *J Biol Chem 277*, 41299-41302.

16. Hibbs, R. E., Talley, T. T., and Taylor, P. (2004) Acrylodan-conjugated cysteine side chains reveal conformational state and ligand site locations of the acetylcholine-binding protein, *J Biol Chem 279*, 28483-28491.

17. Reeves, P. J., Callewaert, N., Contreras, R., and Khorana, H. G. (2002) Structure and function in rhodopsin: high-level expression of rhodopsin with restricted and homogeneous N-glycosylation by a tetracycline-inducible N-acetylglucosaminyltransferase I-negative HEK293S stable mammalian cell line, *Proc Natl Acad Sci U S A 99*, 13419-13424.

18. Hansen, S. B., Sulzenbacher, G., Huxford, T., Marchot, P., Taylor, P., and Bourne, Y. (2005) Structures of Aplysia AChBP complexes with nicotinic agonists and antagonists reveal distinctive binding interfaces and conformations, *Embo J 24*, 3635-3646.

19. Johnson, D. A., and Cushman, R. (1988) Purification and characterization of four monofluorescein cobra alpha-toxin derivatives, *J Biol Chem 263*, 2802-2807.

20. Correia, J. J. (2000) Analysis of weight average sedimentation velocity data, *Methods Enzymol 321*, 81-100.

21. Laue, T. M., Shah, B. D., Ridgeway, T. M., and Pelletier, S. L. (1992) *Analytical Ultracentrifugation in Biochemistry and Polymer Science*, Royal Society of Chemistry, Cambridge.

22. Cantor, C. R., and Schimmel, P. R. (1980) in *Biophysical Chemistry* (Bartlett, A. C., Vapnek, P. C., and McCombs, L. W., Eds.) pp 539-641, W. H. Freeman and Company, San Francisco.

23. Birch, D. J. S., and Imhof, R. E. (1991) in *Topics in Fluorescence Spectroscopy: Techniques* (Lakowicz, J. R., Ed.), Plenum, New York.

24. Gangal, M., Cox, S., Lew, J., Clifford, T., Garrod, S. M., Aschbaher, M., Taylor, S. S., and Johnson, D. A. (1998) Backbone flexibility of five sites on the catalytic subunit of cAMP-dependent protein kinase in the open and closed conformations, *Biochemistry 37*, 13728-13735.

25. Li, F., Gangal, M., Jones, J. M., Deich, J., Lovett, K. E., Taylor, S. S., and Johnson, D. A. (2000) Consequences of cAMP and catalytic-subunit binding on the flexibility of the A-kinase regulatory subunit, *Biochemistry 39*, 15626-15632.

26. Boyd, A. E., Dunlop, C. S., Wong, L., Radic, Z., Taylor, P., and Johnson, D. A. (2004) Nanosecond dynamics of acetylcholinesterase near the active center gorge, *J Biol Chem 279*, 26612-26618.

27. Shi, J., Tai, K., McCammon, J. A., Taylor, P., and Johnson, D. A. (2003) Nanosecond dynamics of the mouse acetylcholinesterase cys69-cys96 omega loop, *J Biol Chem 278*, 30905-30911.

28. Cantor, C. R., and Schimmel, P. R. (1980) in *Biophysical Chemistry* (Bartlett, A. C., Vapnek, P. C., and McCombs, L. W., Eds.) pp 459-461, W. H. Freeman and Company, San Francisco.

29. Johnson, D. A. (2005) C-terminus of a long alpha-neurotoxin is highly mobile when bound to the nicotinic acetylcholine receptor: a time-resolved fluorescence anisotropy approach, *Biophys Chem 116*, 213-218.

30. Wilson, E. B., Decius, J. C., and Cross, P. C. (1955) in *Molecular Vibrations: The Theory of Infrared and Raman Vibrational Spectra* pp 77-101, McGraw-Hill Book Company, Inc., New York, Toronto, London.

31. Unwin, N. (1993) Nicotinic acetylcholine receptor at 9 A resolution, *J Mol Biol 229*, 1101-1124.

32. Cantor, C. R., and Schimmel, P. R. (1980) in *Biophysical Chemistry* (Bartlett, A. C., Vapnek, P. C., and McCombs, L. W., Eds.) pp 561, W. H. Freeman and Company, San Francisco.

33. Celie, P. H., Klaassen, R. V., van Rossum-Fikkert, S. E., van Elk, R., van Nierop, P., Smit, A. B., and Sixma, T. K. (2005) Crystal structure of acetylcholine-

binding protein from Bulinus truncatus reveals the conserved structural scaffold and sites of variation in nicotinic acetylcholine receptors, *J Biol Chem 280*, 26457-26466.

34. Hansen, S. B., Sulzenbacher, G., Huxford, T., Marchot, P., Taylor, P., and Bourne, Y. (2005) Structures of *Aplysia* AChBP complexes with agonists and antagonists reveal distinctive binding interfaces and conformations, *Submitted for publication*.

35. Hibbs, R. E., Hansen, S. B., Talley, T. T., Kem, W. R., and Taylor, P. (2005) Unpublished results (1.7 Angstroms).

36. Zeng, H., and Hawrot, E. (2002) NMR-based binding screen and structural analysis of the complex formed between alpha-cobratoxin and an 18-mer cognate peptide derived from the alpha 1 subunit of the nicotinic acetylcholine receptor from Torpedo californica, *J Biol Chem 277*, 37439-37445.

37. Kachalsky, S. G., Jensen, B. S., Barchan, D., and Fuchs, S. (1995) Two subsites in the binding domain of the acetylcholine receptor: an aromatic subsite and a proline subsite, *Proc Natl Acad Sci U S A 92*, 10801-10805.

38. Barchan, D., Kachalsky, S., Neumann, D., Vogel, Z., Ovadia, M., Kochva, E., and Fuchs, S. (1992) How the mongoose can fight the snake: the binding site of the mongoose acetylcholine receptor, *Proc Natl Acad Sci U S A 89*, 7717-7721.

39. Barchan, D., Ovadia, M., Kochva, E., and Fuchs, S. (1995) The binding site of the nicotinic acetylcholine receptor in animal species resistant to alpha-bungarotoxin, *Biochemistry 34*, 9172-9176.

40. Betzel, C., Lange, G., Pal, G. P., Wilson, K. S., Maelicke, A., and Saenger, W. (1991) The refined crystal structure of alpha-cobratoxin from Naja naja siamensis at 2.4-A resolution, *J Biol Chem 266*, 21530-21536.

41. Zeng, H., Moise, L., Grant, M. A., and Hawrot, E. (2001) The solution structure of the complex formed between alpha-bungarotoxin and an 18-mer cognate peptide derived from the alpha 1 subunit of the nicotinic acetylcholine receptor from Torpedo californica, *J Biol Chem 276*, 22930-22940.

Chapter VI

Influence of Agonists and Antagonists on the Segmental Motion of Residues Near the Agonist Binding Pocket of the Acetylcholine Binding Protein

A. Abstract

Using the *Lymnaea* acetylcholine binding protein as a surrogate of the extracellular domain of the nicotinic receptor, we combined site-directed labeling with fluorescence spectroscopy to assess possible linkages between ligand binding and conformational dynamics. Specifically, 2-[(5-fluoresceinyl)aminocarbonyl]ethyl methanethiosulfonate was conjugated to a free cysteine on loop C and to five substituted cysteines at strategic locations in the subunit sequence, and the backbone flexibility around each site of conjugation was measured with time-resolved fluorescence anisotropy. The sites examined were in loop C (C188 using a C187S mutant), in the β9 strand (T177C), in the β10 strand (D194C), in the β8-β9 loop (N158C and Y164C), and in the β7 strand (K139C). Conjugated fluorophores at these locations show distinctive anisotropy decay patterns indicating different degrees of segmental fluctuations near the agonist binding pocket. Ligand occupation and decay of anisotropy were assessed for one agonist (epibatidine) and two antagonists (α-bungarotoxin and *d*-tubocurarine). The Y164C and C188 conjugates were also investigated with additional agonists (nicotine and carbamylcholine), partial agonists (lobeline and 4-hydroxy, 2-methoxy-benzylidene anabaseine), and an antagonist (methyllycaconitine). With the exception of the T177C conjugate, both agonists and antagonists perturbed the backbone flexibility of each site; however, agonist-selective changes were only observed at Y164C in loop F where the

agonists and partial agonists increased the range and/or rate of the fast anisotropy decay processes. The results reveal that agonists and antagonists produced distinctive changes in the flexibility of a portion of loop F.

B. Introduction

The nicotinic acetylcholine receptor (nAChR[1]) represents a group of acetylcholine-gated cation channels that are prototypic of the Cys-loop superfamily of pentameric ligand-gated ion channels that includes the $GABA_A$, $GABA_C$, 5-HT_3 and glycine receptors. nAChRs are primarily responsible for fast neurotransmission in both the peripheral and central nervous systems, and nAChR isoforms are defined by their subunit composition that, in turn, determines their ligand selectivity, cation permeability, and channel gating kinetics (*1*).

Prior to the availability of an atomic-resolution model of the nAChR, the agonist/antagonist binding site was localized to subunit interfaces and mapped with reference to the primary subunit sequences by mutagenesis and chemical modification. Seven segments that appeared to form the agonist/antagonist binding pocket were identified and arbitrarily denoted alphabetically as segments A-C (in the so-called 'principal' subunit face that include the distinctive vicinal cysteines in loop C) D-F, (in the neighboring and so-called 'complementary' subunit) (2,3), and a final segment involved in binding peptidic toxins (4).

Great insight into the structure of the nAChR has come from analyses of X-ray crystallographic structures of the acetylcholine binding protein (AChBP) (5-9). AChBPs are soluble homopentameric proteins that are found in several salt and fresh water mollusks and share close structural identity with the extracellular domain of the *Torpedo*

nAChR. AChBP appears to be both a structural and functional surrogate for the extracellular domain of the nAChR. In fact, acetylcholine activates a channel of a chimera formed from a modified AChBP and the ion-channel domain of the 5-HT_3 receptor (10). This finding indicates that the molecular basis for ligand gating of ion channels is conserved across the entire pentameric ligand-gated ion channel superfamily. The most recent electron micrograph reconstruction of the receptor in *Torpedo* electroplax membranes has yielded a 4 Å-resolution model of the *Torpedo* nAChR, and by superimposing the AChBP structure on to the receptor, a detailed template of the entire receptor has been developed (11).

A fundamental question in receptor structure-function relationships now focuses on the molecular basis for agonist activation of these channels, since the residues that form the extracellular binding site lie some distance from the ion gate in the transmembrane domain. The most studied allosteric gating theory posits a series of intra-principal subunit rigid-body movements that starts with a twisting, inward movement of the β9-β10 hairpin (loop C) toward acetylcholine as it binds in a crevice formed by the β9-β10 hairpin and a portion of the β7-β8 loop (loop B) in the principal subunit and elements of the β5 and β6 strands in the complementary subunit (8,11-13). This movement is then thought to effect a displacement of the β1-β2 loop next to the transmembrane helix (M2) lining the ion channel in the same subunit as the β9-β10 hairpin, that in turn leads to channel opening. We reasoned that this intra-subunit mechanistic linkage or one involving the adjacent subunit would require agonist-specific changes in the α-carbonyl backbone mobility along an activation pathway that extends to the transmembrane ion gate.

To examine the potential role of regions near the ACh binding site in initiating conformational changes that may result in an activation signal, we measured the influence of nicotinic ligands on α-carbon backbone flexibility using AChBP as a receptor surrogate and a combination of site-directed labeling and fluorescence spectroscopy. Specifically, fluorescein was selectively conjugated to five substituted cysteines and a free cysteine in separate mutants of the *Lymnaea stagnalis* AChBP, and the backbone flexibility around each site of conjugation was assessed by monitoring the time-resolved fluorescence anisotropy decay of the reporter group. Of the six sites examined one was in the β9-β10 hairpin at the tip of loop C (C188 using a C187S mutant), one in the β9 strand (T177C), one in the β10 strand (D194C), two in the loop connecting the β8 and β9 strands (N158C and Y164C, loop F), and one in the β7 strand (K139C). In the absence of ligand, regional variation in α-carbon backbone mobility was observed, with loop C being the most ordered. Ligand-induced changes in loop C mobility did not correlate with agonist-antagonist behavior; however, the loop F site Y164C was found to undergo agonist-specific changes in mobility.

C. Experimental Procedures

1. Ligands and labeling reagents

(+)Epibatidine, α-bungarotoxin, nicotine, lobeline, and carbamylcholine were purchased from Sigma-Aldrich. *d*-Tubocurarine chloride was from ICN Pharmaceuticals, Inc. Methyllycaconitine citrate (MLA) was from Tocris (Ellisville, MO). 4-Hydroxy, 2-methoxy-benzylidene anabaseine (4-OH,2MeOBA) was obtained from Dr. William Kem at the University of Florida. 2-[(5-Fluoresceinyl)aminocarbonyl]ethyl methanethiosulfonate (MTS-Fl) was purchased from Toronto Research Chemicals, Inc

(Ontario, Canada). [^{125}I]-α-Bungarotoxin (specific activity: 130 Ci/mmol) and [^{3}H]-(+/-)-epibatidine (specific activity: 65 Ci/mmol) were products of PerkinElmer Life Sciences, Inc (Wellesley, MA). Tetramethylrhodamine-α-bungarotoxin (TMR-Bgt) was purchased from Invitrogen. All other chemicals were of the highest grade commercially available.

2. Expression, mutagenesis and purification of AChBP

Wild-type AChBP from *Lymnaea stagnalis* was expressed from a cDNA synthesized from oligonucleotides selected for mammalian codon usage, as previously described (14,15). Briefly, the cDNAs were inserted into a pFLAG-CMV-3 expression vector (Sigma) containing a preprotrypsin leader peptide followed by an NH_2-terminal 1×FLAG epitope. A COOH-terminal 6×histidine tag was attached to the protein for radioligand binding assays. Stable cell lines of single cysteine mutants of AChBP were generated as previously described (16). AChBPs, typically in amounts between 4-6 mg, were purified from tissue culture medium by adsorption onto an α-FLAG antibody column and elution with FLAG peptide as previously described (16). Purity and assembly of subunits as a pentamer were assessed by SDS-PAGE and fast protein liquid chromatography. We attempted to engineer single cysteines at sites in loop C other than those presented in this study, but our attempts (T184C, Y185C, S186C, P189C, E190C, Y192C, E193C) resulted in non or weak binding, presumably misfolded protein.

3. Radioligand binding assays

A scintillation proximity assay (SPA, Amersham Biosciences) was adapted for use in a soluble radioligand-binding assay as previously described (16). Briefly, AChBP (0.5 nM binding sites) was incubated with increasing concentrations of either [^{125}I]-labeled α-bungarotoxin or [^{3}H]-(+/-)-epibatidine in a solution of 0.1 mg/mL anti-His SPA

beads. In competition assays, [^{125}I]-labeled α-bungarotoxin was held constant at 20 nM and the competing ligand was added in variable concentrations. Radioactivity was measured on a Beckman LS 6500 liquid scintillation counter. Conversions from EC_{50} to K_D were made with the Prism 4 software package from GraphPad Software, Inc (San Diego, CA), using a sigmoidal dose-response plot with a variable slope fitting. All radioligand binding data are averages of at least three replicate experiments.

4. MTS-Fl labeling

For each mutant MTS-Fl and AChBP were dissolved in 100 μL of 50 mM Tris-HCl, 150 mM NaCl, 0.02% NaN_3, pH 7.4, to final concentrations of 100 μM and 20 μM of binding sites, respectively. After sixty minutes at room temperature and shielded from light, the reaction mixtures were eluted through G-25 Sephadex columns (20 cm x 1 cm; Amersham Biosciences) equilibrated with 0.1 M $NaPO_4$, pH 7.0, to remove unconjugated MTS-Fl.

Specific labeling was assessed by comparison of fluorophore emission, at equilibrium, from the labeled mutant with that of a sample of wt-AChBP that was labeled in parallel with the mutant, after standardization to protein concentration by UV absorbance. Steady-state emission spectra were measured at room temperature using a Jobin Yvon/Spex FluoroMax II spectrofluorometer (Instrument S.A., Inc., Edison, NJ) with the excitation and emission bandwidths set at 2 nm. In all cases, non-specific labeling was ≤5%. Stoichiometry of labeling for each preparation was estimated from a comparison of fluorophore concentration (absorbance at 496 nm for MTS-Fl, extinction coefficient 85,000 M^{-1} cm^{-1}) and protein concentration (by absorbance at 280 nm, extinction coefficient 268,000 M^{-1} cm^{-1}). Stoichiometries of labeling for each mutant

were as follows: K139C, 19%; N158C, 10%; Y164C, 32%; T177C, 19%; C187S, 22%; D194C, 37%.

5. Stopped-flow kinetic measurements

Stopped-flow experiments on ligand association and dissociation kinetics were conducted using an Applied Photophysics SX.18MV (Leatherhead, UK) stopped-flow spectrofluorometer. The Fl-C188 AChBP mutant was excited at 490 nm, and a 515-nm cuton filter was used to select the fluorescence signal. The second-order association rate constants for binding of α-bungarotoxin and epibatidine were determined from the slope of plots of the observed rate of fluorescence change versus ligand concentration. The first-order rate constant of α-bungarotoxin dissociation was determined by mixing the preformed AChBP:α-bungarotoxin complex with concentrations of epibatidine in large excess over its K_D, and measuring the rate of resulting change in fluorescence. As binding of epibatidine resulted in a smaller fluorescence enhancement than α-bungarotoxin, a decrease in fluorescein emission was observed. The first-order rate constant of epibatidine dissociation was measured by mixing the preformed AChBP:epibatidine complex with concentrations of gallamine (which alone gave no fluorescence enhancement) in large excess over its K_D, and observing the time course of the decrease in fluorescein emission. Equilibrium dissociation constants were determined as a ratio of the dissociation and association rate constants. Similar experiments were performed with Fl-D194C to monitor epibatidine binding, and Fl-Y164C to monitor α-bungarotoxin binding. In the case of Fl-D194C, the competing ligand used to determine

the dissociation rate was α-bungarotoxin, and for Fl-Y164C the competing ligand was epibatidine.

6. Estimation of ligand dissociation constants by fluorescein to tetramethylrhodamine fluorescence resonance energy transfer (FRET)

In cases where ligand binding yielded little change in fluorescein fluorescence, we employed tetramethylrhodamine (TMR) conjugated to α-bungarotoxin to measure ligand occupation. Proximity of the Fl-TMR pair yields donor (Fl) quenching and acceptor (TMR) fluorescence sensitization. Excitation and emission spectra of this fluorescent pair shows excellent donor-acceptor overlap free from interference from the native protein fluorescence (17). The titrations provide a direct estimate of the dissociation constant for the substituted toxin. Association of competing ligands were estimated by back titration and concomitant reversal of FRET.

7. Time-resolved fluorescence anisotropy

Emission anisotropy was determined as previously described (18). Unless stated otherwise, emission anisotropy decay was analyzed with the impulse reconvolution method implemented in the DAS6^{TM} software package from HORIBA Jobin Yvon IBH Ltd. (Glasgow, U.K.) described elsewhere (19). Briefly and simply, this approach splits the analysis into two steps − analysis of the total emission decay, S(t), followed by analysis of the vertical/perpendicular difference emission decay, D(t). S(t), free of anisotropy effects, is given by the expression

$$S(t) = I_{\parallel}(t) + G \bullet I_{\perp}(t) \qquad (1)$$

and was analyzed as a biexponential function. D(t*)*, which includes both fluorescence and anisotropy parameters, is given by the expression

$$D(t) = I_{\parallel}(t) - G \bullet I_{\perp}(t). \quad (2)$$

D(t) is deconvolved with the results from the *S(t)* analysis as a constraint yielding

$$r(t) = \beta_1 \exp(-t/\phi_1) + \beta_2 \exp(-t/\phi_2). \quad (3)$$

Here, β_1 and β_2 are the amplitudes of the anisotropy at time zero for the fast and slow anisotropy decay processes, respectively. ϕ_1 and ϕ_2 are the fast and slow rotational correlation times of the anisotropy decay, respectively. We define the fractional magnitude of the observable anisotropy decay associated with the 'fast' diffusional processes as *fxb*, which is equal to $\beta_1 / (\beta_1 + \beta_2)$, and the ratio fxb/ϕ_1, which is a complex function of the rate and range of 'fast' diffusional processes that are usually associated with segmental motion around each site of fluorophore conjugation (20). A nonassociative model was assumed, where the emission relaxation times are common to all the rotational correlation times. Goodness of fit was evaluated from the values of the reduced χ^2_r and by visual inspection of the weighted-residual plots.

D. Results

1. Production and characterization of cysteine mutants

Six single-residue substitution mutants of the AChBP from *Lymnaea* were engineered—five cysteine substitution mutants (K139C, N158C, Y164C, T177C, and

D194C) and a serine substitution mutant (C187S) (Figure VI.1A). The C187S mutant prevented the normal disulfide bond formation between C187 and C188 and, in turn, allowed for selective labeling of C188. Radioligand binding assays were used with a pair of reference ligands for each AChBP mutant to verify that mutagenesis had not affected the overall fold or structure of the binding site (Table VI.1). Direct saturation binding measurements were made with [^{125}I]-α-bungarotoxin, and in separate experiments the K_D for epibatidine (Figure VI.2) was determined by competition against the radiolabeled α-neurotoxin. All the mutants retained a high affinity for both ligands assayed. The largest deviations from wild-type affinity observed for the substituted cysteines was the D194C mutant which lost ~25-fold in binding affinity for α-bungarotoxin, and the C187S mutant which lost ~200-fold in binding affinity for epibatidine. Even in these most-extreme cases, the cysteine-substituted AChBP mutants bind the reference ligands with dissociation constants in the low to mid nanomolar range. Therefore, we conclude that the interaction determinants are maintained, but with lower interaction energy for the D194C substitution mutation and the C187S substitution. Losses in binding affinity at other mutation positions were judged to be small and non-significant when compared with the unmodified enzyme.

2. Determination of the ligand binding parameters of the fluorescently-labeled AChBPs

In the case of the C187S mutant devoid of the native vicinal disulfide bond, a significant loss of interaction energy occurred, and we were concerned that at this site in particular, conjugation of the cysteine with MTS-Fl could further reduce ligand binding. We observed, however, that binding of both α-bungarotoxin and epibatidine to the Fl-

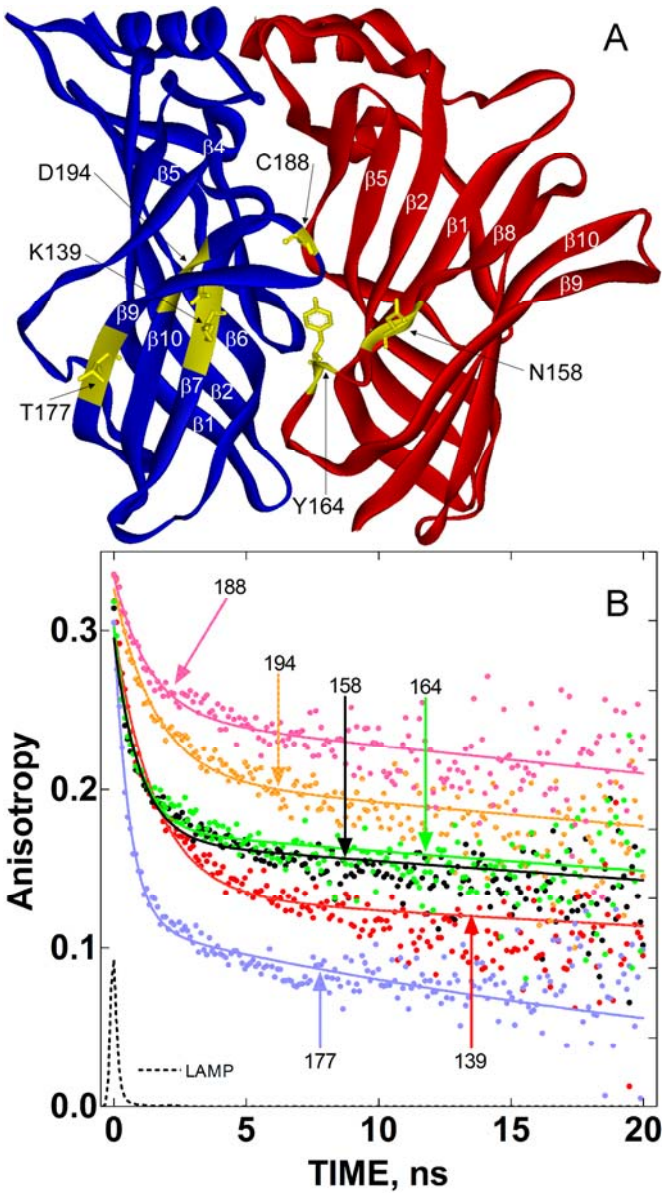

Figure VI.1: Positions of Fluorescein Labeling of the Acetylcholine Binding Protein (AChBP) and Time-Resolved Fluorescence Anisotropy Decay for Apo AChBP. Panel A: Ribbon diagram of the X-ray structure of two adjacent AChBP subunits from *Lymnaea* (PDB accession code 1I9B (5)), with the principal subunit in blue and complementary subunit in red. Five amino acid side chains were mutated to cysteine for subsequent fluorescein labeling (K139, N158, Y164, T177, D194), and one free cysteine was created (C188) by replacing its disulfide bonding partner (C187) with a serine residue. In the orientation presented in this figure, the top of AChBP corresponds to the apical portion of the nAChR, and the bottom is where the transmembrane α-helices of the nAChR would attach. Panel B: Time-resolved fluorescence anisotropy decays of fluorescein-conjugated AChBPs in the absence of ligand. The plot labeled 'Lamp' is the instrument response function.

Table VI.1

K_D Values for AChBP Mutants with Reference Ligands

AChBP Mutant	α-Bungarotoxin K_D (nM)	Epibatidine K_D (nM)
WT	1.8	0.16
K139C	16	0.22
N158C	1.6	0.16
Y164C	2.2	0.36
T177C	1.8	0.19
C187S	20	20
D194C	46	1.7

For direct saturation binding, [^{125}I]-α-bungarotoxin was incubated in increasing concentrations with AChBP from *Lymnaea* at 0.5 nM in binding sites. Bound ligand was measured by a scintillation proximity assay (16). For competition experiments, epibatidine was incubated in increasing concentrations with AChBP, 0.5 nM in binding sites and a constant concentration of [^{125}I]-α-bungarotoxin of 20 nM. Measurements were made in triplicate, and variance from the mean was less than 30%. Conversions from EC_{50} to K_D were made using Prism version 4 (GraphPad Software, Inc.), where $K_D = IC_{50}/(1+ [I]/K_I)$.

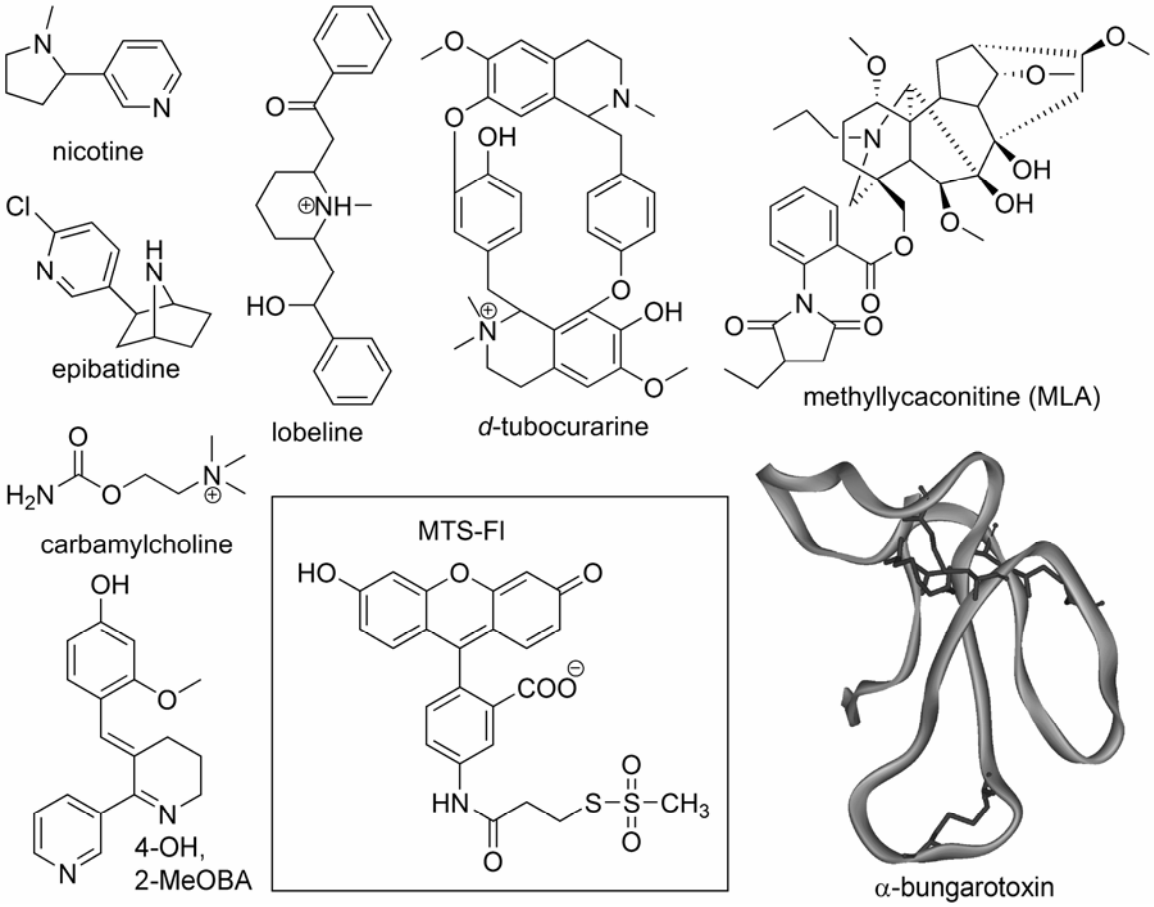

Figure VI.2: Structures of the Fluorescent Probe 2-[(5-Fluoresceinyl)aminocarbonyl]-ethyl methanethiosulfonate (MTS-Fl) and the Nicotinic Ligands Used in Anisotropy Decay Analyses. The pharmacologic activities of the majority of ligands used in these experiments have been well studied (21). Epibatidine, nicotine, and carbamylcholine are classical full agonists at muscle and neuronal nAChRs, while *d*-tubocurarine, α-bungarotoxin and MLA are competitive antagonists. Lobeline is reported as a mixed agonist/antagonist of nAChRs; in AChBP it induces conformations mimicking other agonists (8). 4-OH,2MeOBA is the primary active metabolite of DMXBA (also known as GTS-21), and shows partial agonism selective for α7 receptors (22).

labeled mutant resulted in a substantial enhancement of steady-state fluorescence. Accordingly, using stopped-flow measurements of ligand association and dissociation rates, we were able to determine the K_D from the ratio of kinetic constants for both α-bungarotoxin and epibatidine at the covalently-modified binding site. Although both α-bungarotoxin and epibatidine lost approximately two orders of magnitude in binding affinity to the Fl-C188 protein, they still bound to AChBP with appreciable affinities (K_D = 1.6 μM and 0.05 μM, respectively), strongly suggesting substantial retention of the configuration of the binding site (Table VI.2).

For the cysteine substitutions and conjugations that exhibited little or no change in fluorescence anisotropy upon ligand binding, it was necessary to demonstrate that the ligands studied are in fact bound to the Fl-labeled binding site at the concentrations used in the anisotropy experiments. To this end, steady-state emission spectra for Fl-T177C were measured at room temperature as described for the determination of non-specific labeling (See *Experimental Procedures*). Saturation binding of a tetramethylrhodamine (TMR) conjugate of α-bungarotoxin was monitored, upon excitation of fluorescein at 485 nm, by observing the quenching of fluorescein fluorescence emission at 515 nm; incremental increases in the concentration of the TMR-Bgt resulted in incremental decreases in Fl-T177C fluorescein emission due to FRET from fluorescein to TMR (Figure VI.3A, B). Since the minimum concentration of binding sites required for a fully quantitatable signal was ~100 nM, the dissociation constant determined in this manner for the fluorescein-labeled T177C mutant could only be estimated to be ≤ 45 nM (Table VI.2). By comparison, the dissociation constants for both WT and unlabeled T177C AChBPs were determined by radioligand binding competition experiments with [3H]-

Table VI.2

K_D Values for Representative AChBP-fluorescein Conjugates

AChBP Mutant	Epibatidine K_D (nM)	α-Bungarotoxin K_D (nM)	TMR-Bgt K_D (nM)
WT[&]	0.16	1.8	17
Fl-Y164C	*n.d.*	14[†]	≤ 120[‡]
Fl-T177C	≤ 3[‡]	≤ 4.7[§]	≤ 45[‡]
Fl-C188	47[†]	1600[†]	*n.d.*
Fl-D194C	16[†]	*n.d.*	≤ 116[‡]

[†]K_D of ligands for the labeled binding sites was estimated from direct measurements of association and dissociation rates of ligand binding by stopped-flow methods exciting the conjugated fluorescein at 490 nm and selecting the fluorescein emission signal with a 515 nm cutoff filter. $K_D = k_{-1}/k_1$ where k_{-1} and k_1 are the respective dissociation and association rate constants.

[‡]K_D was estimated by observing steady-state quenching of fluorescein emission due to FRET with added TMR-Bgt, or by subsequent back titration of this quenching with a competing ligand.

[§]Binding of α-bungarotoxin to Fl-T177C was monitored through fluorescein donor sensitization of TMR-Bgt emission at 580 nm with excitation at 490 nm. Competition with non-labeled α-bungarotoxin results in a loss of acceptor sensitization (17).

[&]K_D of ligands for WT AChBP was determined by radioligand binding assay as described in Table VI.1.

Measurements were made in triplicate, and variance from the mean was less than 30%. *n.d.*, not determined.

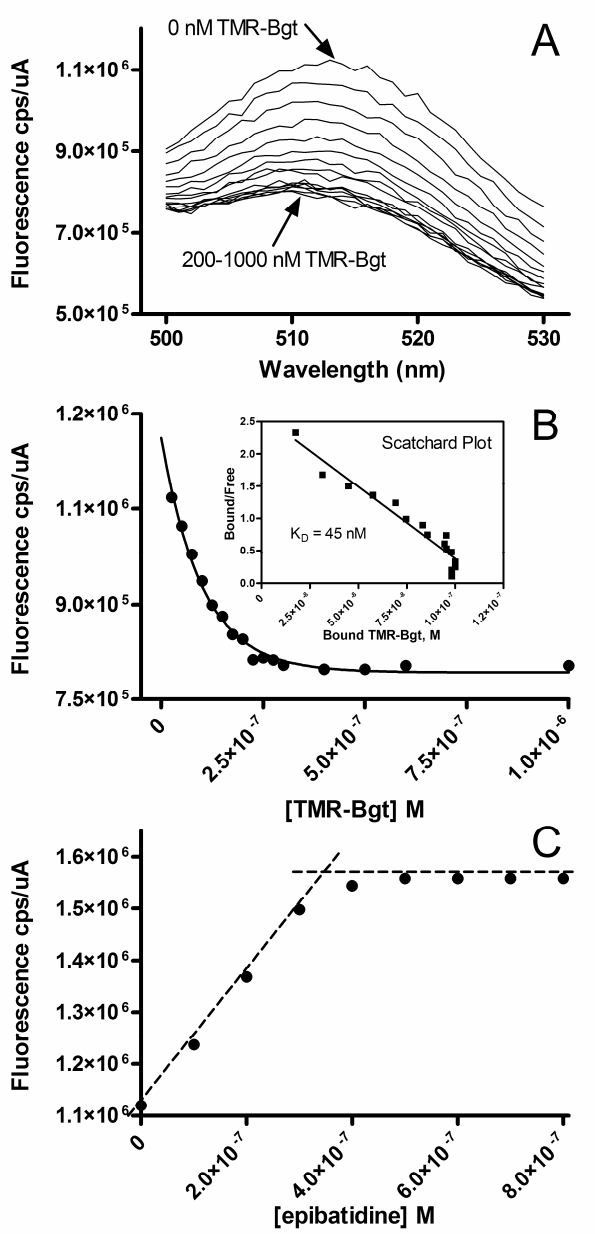

Figure VI.3: Determination of Ligand Binding to Fl-T177C. Panel A: Steady-state emission of fluorescein was monitored in the presence of TMR-Bgt until fluorescence energy transfer was maximal (200 nM). Total binding sites = 100 nM. Panel B: Binding of TMR-Bgt as determined by fluorescence quenching indicated in Panel A. K_D was determined from the negative inverse slope of the linear fit of the Scatchard Plot (Inset), where Bound = $1\times10^7(y_{max}-y_{[x]})/(y_{max}-y_{min})$, $y_{[x]}$ = fluorescence signal at concentration x, and Free = Total TMR-Bgt added minus Bound Fraction. Linearity in Scatchard plot reveals little or no difference in affinity between fluorescein-modified and unmodified sites. Panel C: Reversal of TMR-Bgt quenching of fluorescein, upon addition of 100 nM increasing concentrations of epibatidine. [Binding sites] = 200 nM.

epibatidine to be 17 nM. Hence, the TMR-labeled toxin has an affinity for AChBP comparable to the native toxin, and fluorescein labeling of the T177C mutant results in at most a 3-fold reduction in affinity for the labeled toxin. These data provide convincing evidence that the native toxin used in anisotropy decay should fully occupy the binding sites in the Fl-T177C conjugated AChBP at the μM concentrations used in those experiments.

To characterize further ligand binding to the Fl-T177 conjugate, epibatidine was added in incremental concentrations to compete with bound TMR-α-bungarotoxin and promote its dissociation (Figure VI.3C). Using 200 nM binding sites, at 500 nM epibatidine a complete reversal of the fluorescein quenching was observed. As the competing TMR-α-bungarotoxin, present at 700 nM was ~15-fold over its dissociation constant, half-maximal dissociation by epibatidine competition would require its concentration to be at least 15-fold over its dissociation constant. Nearly complete saturation of epibatidine would require an additional 10-fold concentration increase over its dissociation constant. From this titration epibatidine has a dissociation constant for the Fl-labeled interface of ≤ 3 nM (Table VI.2), again indicating that these ligands will saturate all sites in AChBP in anisotropy assays.

In two other combinations of mutants and ligands, Fl-D194C with epibatidine, and Fl-Y164C with α-bungarotoxin, no significant change in fluorescence anisotropy was observed. As with the Fl-C188 mutant, we were fortunate that in both of these cases binding of the ligand in question resulted in a large enhancement of steady-state fluorescence of the conjugated fluorescein. We again used stopped-flow measurements to determine rates of association and dissociation by monitoring changes in fluorescein

emission. Dissociation constants determined in this manner were 16 nM for epibatidine binding to Fl-D194C, and 14 nM for α-bungarotoxin binding to Fl-Y164C (Table VI.2). Hence, in anisotropy assays, the lack of observed change in backbone mobility is not explained by a lack of ligand occupation. To verify that the approximate K_D values obtained in the TMR-bgt experiments with Fl-T177C yielded equivalent results, we used the FRET method to examine the interaction of Fl-Y164C with the TMR-labeled toxin. In this experiment we are limited to a lower threshold of 100 nM binding sites, so while we were only able to determine with confidence that our K_D for TMR-Bgt was ≤ 120 nM, these findings are consistent with the stopped-flow data for the same conjugated mutant AChBP.

3. Time-resolved fluorescence anisotropy decay of apo AChBP

To map α-carbonyl backbone flexibility around the agonist/antagonist binding sites and monitor ligand-induced changes in this flexibility, the sulfhydryl-reactive fluorophore MTS-Fl was selectively conjugated to substituted cysteine residues and nondisulfide-bonded C188 in separate AChBP mutants. Time-resolved fluorescence anisotropy decay of each conjugate was monitored in the absence and presence of nicotinic agonists and antagonists. This approach typically distinguishes up to three types of rotational-diffusion processes in proteins: 'very fast' and irresolvable anisotropic fluctuations associated with the fluorophore undergoing torsional movement about its linker arm and amino acid side chain (<1 ns); 'fast' anisotropic motions that largely correspond to local fluctuations in the α-carbon backbone around the site of conjugation (ϕ_1, ~1-10 ns); and slower, isotropic global rotational diffusion of the entire biomolecule (ϕ_2) (18,20,23-26). The determination of the rotational correlation times (ϕ_1 and ϕ_2) and

their amplitudes (β_1 and β_2) associated with these diffusional processes is inherently challenging particularly when the emission lifetime of the reporter group is many times faster than the rotational correlation time of the biomolecule studied as is the case here with MTS-Fl (τ ~3-4 ns) and AChBP (φ_r ~ 120 ns). To reduce the uncertainty in the fitting analysis results, the ϕ_2 parameter was allowed to either float or be constrained to the ϕ_2 values that had been previously determined with a longer-lifetime fluorescent probe (124 ns for apo and small ligand-bound AChBP or 142 ns for α-bungarotoxin-bound AChBP) (18). With the exception of the T177C mutant results, constraining or floating ϕ_2 yielded comparable χ^2_r values and no systematic variation of the residual plots. Reasoning that constraining ϕ_2 to the previous experimentally determined values would produce better estimates of the fast anisotropy decay parameters, only the results from the constrained fits are reported here for all the samples except the T177C mutant. Because of its complex and extensive mobility, the T177C data were best fit when all the anisotropy parameters were unconstrained.

4. Comparative residue analysis of segmental motion in AChBP

The results from the fitting analysis described in *Experimental Procedures* are summarized in Table VI.3 and Figure VI.1B. The ratios of the fractional amplitude to fast rotational correlation time (fxb/ϕ_1), which generally reflect the rate and/or range of segmental motions around each site of conjugation, strongly suggest a rank order of α-carbon backbone mobility of Fl-T177C > Fl-K139C > Fl-N158C > Fl-Y164C > Fl-D194C > Fl-C188. Fl-C188 in the β9-β10 hairpin loop (loop C) and Fl-D194C in the

Table VI.3: Time-resolved Fluorescence Anisotropy Decay Parameters for Fl-AChBP Conjugates[a]

AChBP Conjugation Site	Ligand	β_1	β_2	ϕ_1 (ns)	Ψ^2_r	fxb/ϕ_1	$<\tau>$ (ns)
Fl-K139C[b]	Apo	0.116 ± 0.003	0.125 ± 0.009	2.3 ± 0.1	1.9 ± 0.1	0.209 ± 0.020	3.2 ± 0.0
	Epibatidine	0.108 ± 0.001	0.130 ± 0.007	2.3 ± 0.1	1.8 ± 0.3	0.195 ± 0.001	3.1 ± 0.0
	α-Bungarotoxin	0.090 ± 0.002	0.160 ± 0.012	2.7 ± 0.2	1.4 ± 0.3	0.135 ± 0.017	3.0 ± 0.0
	d-Tubocurarine	0.095 ± 0.002	0.154 ± 0.005	2.5 ± 0.1	1.7 ± 0.3	0.154 ± 0.008	3.3 ± 0.0
Fl-N158C[b]	Apo	0.078 ± 0.002	0.153 ± 0.005	1.8 ± 0.1	1.7 ± 0.3	0.187 ± 0.017	4.0 ± 0.0
	Epibatidine	0.092 ± 0.003	0.143 ± 0.006	1.3 ± 0.1	1.8 ± 0.3	0.296 ± 0.015	4.1 ± 0.0
	α-Bungarotoxin	0.040 ± 0.004	0.241 ± 0.004	2.9 ± 0.7	1.3 ± 0.1	0.052 ± 0.013	4.2 ± 0.0
	d-Tubocurarine	0.079 ± 0.003	0.156 ± 0.005	1.3 ± 0.1	1.5 ± 0.3	0.258 ± 0.017	4.1 ± 0.0
Fl-Y164C[b]	Apo	0.064 ± 0.002	0.162 ± 0.004	1.8 ± 0.1	1.4 ± 0.3	0.161 ± 0.004	3.1 ± 0.0
	Epibatidine	0.095 ± 0.001	0.135 ± 0.008	1.4 ± 0.1	1.7 ± 0.1	0.293 ± 0.006	3.3 ± 0.0
	Carbachol	0.075 ± 0.001	0.151 ± 0.004	1.5 ± 0.1	1.4 ± 0.1	0.221 ± 0.019	3.3 ± 0.0
	Nicotine	0.080 ± 0.003	0.152 ± 0.004	1.5 ± 0.1	1.5 ± 0.3	0.225 ± 0.004	3.2 ± 0.0
	Lobeline	0.064 ± 0.001	0.158 ± 0.004	1.4 ± 0.1	1.8 ± 0.1	0.209 ± 0.021	2.8 ± 0.1
	4-OH,2MeOBA	0.090 ± 0.002	0.134 ± 0.003	1.8 ± 0.1	3.0 ± 0.7	0.222 ± 0.002	3.2 ± 0.0
	α-Bungarotoxin	0.065 ± 0.002	0.163 ± 0.002	1.9 ± 0.1	1.5 ± 0.1	0.148 ± 0.008	3.2 ± 0.0
	d-Tubocurarine	0.054 ± 0.002	0.182 ± 0.004	2.2 ± 0.3	1.7 ± 0.1	0.104 ± 0.011	3.1 ± 0.0
	MLA	0.047 ± 0.004	0.195 ± 0.004	1.9 ± 0.2	1.4 ± 0.2	0.105 ± 0.021	3.5 ± 0.0
Fl-T177C[c]	Apo	0.111 ± 0.004	0.106 ± 0.004	0.7 ± 0.0	2.0 ± 0.3	0.703 ± 0.023	3.6 ± 0.0
	Epibatidine	0.112 ± 0.004	0.114 ± 0.003	0.7 ± 0.1	2.2 ± 0.2	0.753 ± 0.150	3.6 ± 0.0
	α-Bungarotoxin	0.110 ± 0.001	0.110 ± 0.002	0.7 ± 0.1	1.9 ± 0.1	0.709 ± 0.054	3.6 ± 0.0
	d-Tubocurarine	0.121 ± 0.007	0.111 ± 0.000	0.7 ± 0.0	1.8 ± 0.3	0.780 ± 0.035	3.6 ± 0.0
Fl-C188[b]	Apo	0.048 ± 0.005	0.220 ± 0.008	5.6 ± 1.6	1.9 ± 0.6	0.035 ± 0.014	3.1 ± 0.1
	Epibatidine	0.058 ± 0.004	0.211 ± 0.007	3.9 ± 1.1	1.6 ± 0.1	0.057 ± 0.012	3.5 ± 0.0
	Carbachol	0.056 ± 0.001	0.208 ± 0.001	5.3 ± 0.5	1.7 ± 0.1	0.041 ± 0.003	3.2 ± 0.0
	Nicotine	0.063 ± 0.003	0.199 ± 0.003	2.8 ± 0.3	1.6 ± 0.1	0.087 ± 0.007	3.5 ± 0.0
	Lobeline	0.030 ± 0.001	0.250 ± 0.007	5.4 ± 1.0	1.6 ± 0.1	0.020 ± 0.004	3.7 ± 0.0
	4-OH,2MeOBA	0.079 ± 0.004	0.168 ± 0.007	2.9 ± 0.2	1.7 ± 0.2	0.110 ± 0.009	3.5 ± 0.0
	α-Bungarotoxin	0.050 ± 0.004	0.247 ± 0.005	6.5 ± 0.8	2.1 ± 0.1	0.026 ± 0.001	3.6 ± 0.0
	d-Tubocurarine	0.047 ± 0.002	0.227 ± 0.001	3.3 ± 0.3	1.6 ± 0.0	0.052 ± 0.005	3.7 ± 0.0
	MLA	0.085 ± 0.003	0.165 ± 0.005	1.8 ± 0.1	1.6 ± 0.1	0.187 ± 0.002	3.7 ± 0.0
Fl-D194C[b]	Apo	0.077 ± 0.006	0.197 ± 0.003	2.4 ± 0.5	1.6 ± 0.4	0.121 ± 0.026	3.0 ± 0.0
	Epi	0.092 ± 0.003	0.188 ± 0.009	2.5 ± 0.5	1.7 ± 0.2	0.136 ± 0.023	3.3 ± 0.0
	α-Bungarotoxin	0.061 ± 0.003	0.191 ± 0.009	5.3 ± 1.7	2.4 ± 0.4	0.052 ± 0.024	2.9 ± 0.1
	d-Tubocurarine	0.083 ± 0.002	0.176 ± 0.004	1.6 ± 0.2	1.6 ± 0.0	0.206 ± 0.024	3.0 ± 0.0

[a]Multi-exponential anisotropy decay profiles from fluorescein-labeled AChBP mutants were fit to eq. 3, where β_1 and β_2 are the magnitudes of the anisotropy decay associated with the 'fast' and 'slow' diffusion processes, respectively, ϕ_1 is the rate of anisotropy decay associated with the 'fast' process, Ψ^2_r is the reduced χ^2 of the fitting analyses, and $<\tau>$ is the amplitude-weighted average fluorescence lifetime. fxb/ϕ_1 is a complex function of the rate and range of motion associated with the 'fast' diffusional process, where larger values correspond to increased flexibility. [b]For all positions of fluorophore conjugation except T177C, β_2 was fixed at values previously determined (124 ns for apo or small molecule complex, 142 ns for α-bungarotoxin complex). [c]In the case of Fl-T177C, the best fit of the anisotropy decay profiles was achieved by allowing all variables to float. Anisotropy decay measurements of Fl-AChBP mutants were performed with 0.5-2 μM in binding site concentrations, diluted in 0.1 M NaPO4, pH 7.0. Ligands were added to achieve a minimum 3-fold excess over binding site concentration and always kept at least 5-fold over their dissociation constant. All data are the average of at least three replicate experiments ± standard deviation.

β10 strand, a residue in contact with the protein core based on the crystal structures (5,9,27), were associated with the lowest segmental mobility of the sites examined. In contrast, Fl-T177C in the β9 strand, which is part of a β sandwich that is primarily stabilized by its interaction with the β10 strand, was associated with the greatest segmental motion. The characteristics of the rotational diffusion of the reporter group at T177C are more complex than the other sites examined, because constraining its ϕ_2 to the previously determined values yielded unacceptable fits and suggests fast, large amplitude excursions of its transition moment that are more complex than with the other conjugates. Accordingly, the complexity of the diffusion and the relatively rapid depolarization of the emission from the T177C conjugate is consistent with a highly mobile segment. Sites in the β8-β9 loop (Fl-Y164C and Fl-N158C, loop F), a region poorly resolved in several crystal structures, displayed comparable and intermediate segmental flexibilities. Fl-K139C in the β7 strand appeared to be associated with considerable segmental flexibility.

5. Effects of ligand binding on anisotropy decay parameters

Initially, all the Fl-conjugates were screened with one agonist, epibatidine, and two antagonists: *d*-tubocurarine, an alkaloid, and α-bungarotoxin, an 8-kD peptidic α-neurotoxin (Figure VI.2). Fl-K139C, located in the β7 strand on the membrane side of the binding pocket on the principal side of the subunit interface, was stabilized by binding of the two antagonists, but not significantly affected by the agonist epibatidine. This is most easily seen in the anisotropy decay profiles (Figure VI.4A) and in the fxb/ϕ_1 values (Table VI.3) where *d*-tubocurarine and α-bungarotoxin decreased fxb/ϕ_1 from 0.21 to 0.15 and 0.14, respectively.

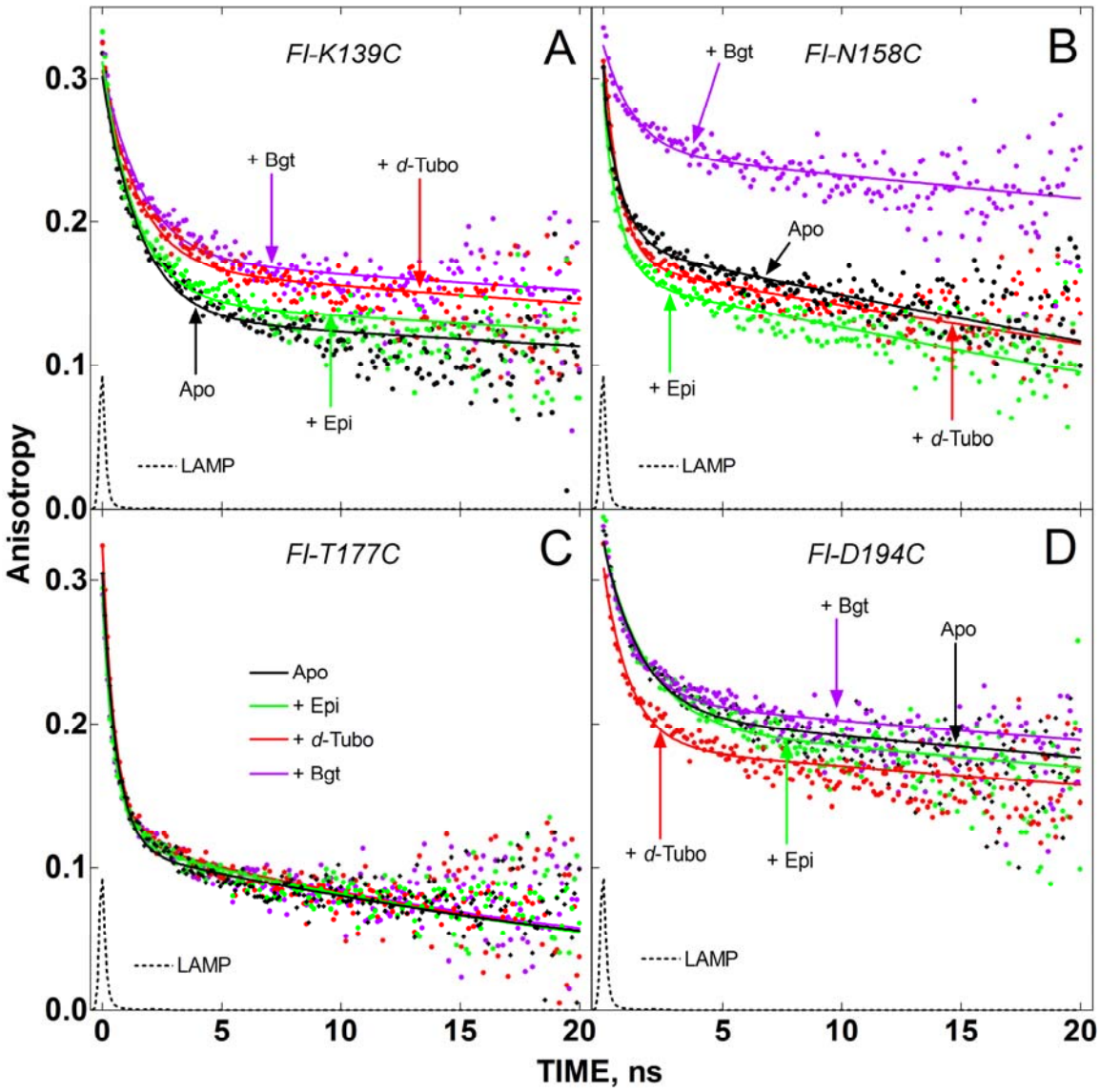

Figure VI.4: Time-Resolved Fluorescence Anisotropy Decay for the Fluorescein-conjugated AChBP Mutants. Panel A: Fl-K139C (0.5 μM); Panel B: Fl-N158C (2 μM); Panel C: Fl-T177C (1 μM); Panel D: Fl-D194C (1.4 μM). Experiments were run either in the absence of ligand (apo), or in the presence of epi (epibatidine, 3.3 μM for Fl-K139C and Fl-T177C, 6.7 μM for Fl-N158C, and 15 μM for Fl-D194C), *d*-tubo (*d*-tubocurarine, 33 μM for Fl-K139C and Fl-T177C, 67 μM for Fl-N158C, and 100 μM for Fl-D194C), or bgt (α-bungarotoxin, 3.3 μM for Fl-K139C and Fl-T177C, 6.7 μM for Fl-N158C, and 13 μM for Fl-D194C).

Fl-N158C, located in the apical portion of the F-loop on the complementary side of the subunit interface, was significantly stabilized by α-bungarotoxin binding, but was mobilized by both epibatidine and *d*-tubocurarine (Figure VI.4B). α-Bungarotoxin decreased fxb/ϕ_1 from 0.19 to 0.05, while epibatidine and *d*-tubocurarine increased fxb/ϕ_1 from 0.19 to 0.30 and 0.26, respectively (Table VI.3). The dramatic stabilization of Fl-N158C by α-neurotoxin is consistent with the crystal structure of α-cobratoxin bound to AChBP that shows loop II of the α-neurotoxin interacting with this segment of loop F (9). The lack of stabilization by the relatively large alkaloid *d*-tubocurarine suggests that it does not interact directly with this more apical portion of loop F. Fl-T177C, located in the β9 strand, was highly flexible as discussed above and its mobility was unaffected by any of the ligands assayed (Figure VI.4C and Table VI.3). For Fl-D194C on the β10 strand, epibatidine binding had no significant effect on the fast mobility of the reporter while *d*-tubocurarine binding increased fxb/ϕ_1 from 0.12 to 0.21 and α-bungarotoxin decreased fxb/ϕ_1 from 0.12 to 0.05 (Figure VI.4D and Table VI.3).

The site on loop C was of particular interest since agonists induced a closing movement of loop C toward the core of the protein (8), and this conformational change may be associated with propagation of the agonist binding event to the ion channel gate in the transmembrane domain (3). Consequently, we examined Fl-C188, positioned at the tip of loop C, with several ligands, but differences in the decay of anisotropy did not correlate with the behavior of the respective compounds as agonists and antagonists (Figure VI.5A). In the absence of any ligand the value of the fxb/ϕ_1 parameter was 0.04.

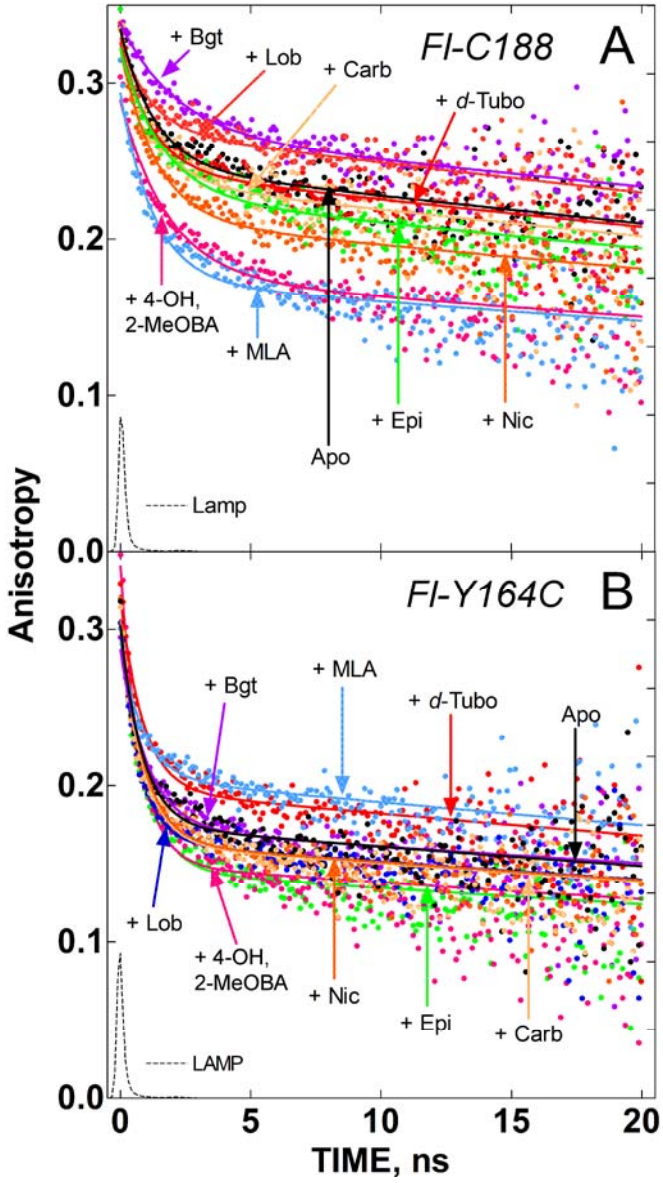

Figure VI.5: Time-Resolved Fluorescence Anisotropy Decay for the Fluorescein-conjugated AChBP Mutants. Panel A: Fl-C188 (1.2 μM); Panel B: Fl-Y164C (1.5 μM). Experiments were run either in the absence of ligand (apo), or in the presence of epi (epibatidine, 14 μM), *d*-tubo (*d*-tubocurarine, 28 μM for Fl-Y164C and 14 μM for Fl-C188), bgt (α-bungarotoxin, 14 μM for Fl-Y164C and 36 μM for Fl-C188), carb (carbamylcholine, 28 μM for Fl-Y164C and 140 μM for Fl-C188), nic (nicotine, 14 μM), lob (lobeline, 14 μM), MLA (methyllycaconitine, 14 μM), or 4-OH,2MeOBA (4-OH,2-MeO-benzylidene-anabaseine, 28 μM for Fl-Y164C and 2.4 μM for Fl-C188).

The addition of three agonists, epibatidine (0.06), nicotine (0.09) and 4-OH,2MeOBA (0.11), and one antagonist, MLA (0.19), increased segmental flexibility, while the addition of another agonist, lobeline (0.02), decreased mobility as measured by the fxb/ϕ_l parameter (Table VI.3). Carbamylcholine, an agonist and α-bungarotoxin (0.03) were without significant effect (Table VI.3). Accordingly, mobility parameters of loop C when modified by removal of one of the two vicinal cysteines for fluorophore conjugation were not correlated with the pharmacologic actions of the ligands.

Initial screening of Fl-Y164C, located in the C-terminal portion of loop F approaching the membrane, suggested a possible distinct agonist response with epibatidine, an agonist, increasing flexibility dramatically (fxb/ϕ_l increased from 0.16 to 0.29), and the antagonist, *d*-tubocurarine, decreasing the flexibility (fxb/ϕ_l decreased from 0.16 to 0.10) while the larger peptide antagonist, α-bungarotoxin, produced no significant effect on mobility (fxb/ϕ_l = 0.15)(Figure VI.5B, Table VI.3). Four additional agonists were assayed; nicotine, carbamylcholine, lobeline, and 4-OH,2MeOBA (an α7-selective partial agonist) all increased α-carbon backbone mobility in this loop F region with their fxb/ϕ_l values increasing from 0.16 to 0.23, 0.22, 0.21, and 0.22, respectively (Table VI.3). MLA, an antagonist, behaved like *d*-tubocurarine and decreased mobility; the fxb/ϕ_l value decreased from 0.16 to 0.11 (Table VI.3) confirming that agonists increase and antagonists either have no effect or decrease segmental mobility of the segment of loop F proximal to the membrane.

Assuming the difference between the fundamental anisotropy for fluorescein (0.35) and the sum of the observed decay amplitudes ($\beta_1 + \beta_2$; Table VI.3) represents the

maximum angular excursions of the very rapid linker-arm (or tether-arm) motions, then ligands only significantly affected the maximum angular excursions of fluorescein attached to the N158C and C188 AChBP mutants. For both of these conjugates α-bungarotoxin uniquely produced very significant decreases in the amplitudes of the very rapid excursions. In the case of the N158C conjugate, the very rapid decay amplitude decreased from 0.119 to 0.069 and for the C188 conjugate it decreased from 0.82 to 0.053. These results are consistent with either a direct 'interaction' of the bound-toxin with the reporter group or a toxin-induced conformational state that is associated with restrictions of very fast torsional motions of conjugated fluorescein. In the case of the C187S mutant, the 80-fold decrease in α-bungarotoxin affinity for the Fl-C188 conjugate over the unlabeled mutant makes the case for a direct interaction more probable.

E. Discussion

Using *Lymnaea* AChBP as a surrogate of the extracellular domain of the nAChR, we combined site-directed labeling with time-resolved fluorescence anisotropy to measure the effects of agonists and competitive antagonists on the α-carbon backbone flexibility at six sites near the agonist binding pocket. Control experiments demonstrated that the conjugated fluorescent probes did not block ligand occupation under the conditions of the anisotropy measurements. Specifically, we monitored anisotropy decay from fluorescein conjugated to three sites in the β9-β10 sandwich, as well as a site in the β7 strand on the membrane side of the binding pocket in the principal subunit face, and two sites in the loop connecting the β8 and β9 strands across from the binding pocket in the complementary subunit face (Figure VI.1). With the exception of the highly flexible site in the β9 strand, both agonists and antagonists perturbed the backbone flexibility of

each site examined; however, agonist-selective changes were only observed in the complementary subunit in a segment of the β8-β9 loop at Y164C (in loop F). More precisely, agonists and partial agonists increased the range and/or rate of the fast anisotropy decay processes that are usually associated with the α-carbon backbone fluctuations. This agonist-selective change in conformational dynamics probably occurs across fresh water and marine species in the animal kingdom, because we observe comparable agonist-specific differences in anisotropy decay for the homologous site (S167C) in loop F of AChBP from *Aplysia californica* (data not shown).

Although X-ray crystallographic studies have not revealed ligand-dependent changes in the conformation of loop F, solution-based studies have suggested structural and/or functional links between ligand binding and loop F. With AChBP, hydrogen-deuterium exchange analysis (28) and steady-state spectrofluorometric measurements using acrylodan conjugates (16) have identified ligand-specific changes in the solvent accessibility of loop F. Accessibility studies with cysteine-substituted mutant $GABA_A$ receptors (29) and site-directed mutagenesis with the $5\text{-}HT_3$ receptor (30) also indicate state-dependent changes in the solvent exposure of loop F. Additionally, hydrophobic photolabeling of the nAChR loop F occurs in the open state of the receptor, but not during the closed or desensitized states (31), indicating that this region likely moves during channel gating. Also, labeling of the portion of loop F proximal to the membrane occurs only when agonist is bound (32), again indicating a potential agonist-specific movement in a portion of loop F some distance from the binding pocket. Furthermore, mutation of a single residue in the β8-β9 loop of the mammalian α4β2 nAChR (αE180Q), homologous to R170 in AChBP) abolishes Ca^{2+} potentiation of the ACh

response (33). Taken together the above observations show loop F to be a dynamic entity that most likely adopts conformations not evident from crystallographic structures. Our data with the Fl-Y164C conjugate support the notion that an agonist activation signal is transmitted to a portion of loop F. Within the limitations of our soluble surrogate protein as a model, we can only demonstrate that loop F responds with a change in conformational dynamics when agonists bind at their recognition site. Establishing the involvement of loop F in the direct transmission of a signal to the ion gate requires confirmation with intact receptors.

The observed, localized agonist-selective increase in backbone flexibility surrounding Fl-Y164C is most likely propagated across the principal-complementary subunit interface rather than within the β9-β10 sandwich from the principal-subunit β9-β10 hairpin (loop C). The reasons for this conclusion are first that no agonist-selective changes in the anisotropy decay rates of the reporter groups on either the β9-β10 hairpin or the β9 strand were observed. Indeed, the segment around T177C in the β9 strand is so flexible that no ligand examined produced measurable changes in the anisotropy decay, and it seems unlikely that conformational signals can be carried by highly dynamic, unconstrained structural elements. Additionally, the relative proximity of Y164C to the binding pocket across the nearby subunit interface compared to the relative long distance to loop C in the principal subunit make trans-subunit signal propagation a more reasonable alternative.

How agonist binding increases the rate and/or range of backbone motions of part of the β8-β9 loop is unclear. One way to enhance flexibility of a surface element would be through a reduction in the element's interaction with neighboring structural elements.

The nearest structural elements to the β8-β9 loop are an antiparallel β sheet and the β9-β10 hairpin. The antiparallel β sheet is formed by β5, β6, β2, and β1 strands with the β1 strand running almost parallel to most of the β8-β9 loop. Overlaying the X-ray structures of nicotine- and buffer-bound crystal structures (PDB access codes 1I9B and 1UW6) reveals little or no agonist (nicotine) specific perturbation of this β sheet suggesting that conformational changes in the β sheet probably do not cause changes in the flexibility of loop F. Additionally, while the β9-β10 hairpin moves inward toward the protein core with agonist binding, there does not appear to be any hydrogen or other non-covalent bonding with any part of the β8-β9 loop with or without nicotine. That said, examination of the B factors shows nicotine binding is associated with lower B factors in the β9-β10 hairpin upon binding and, interestingly, increased B factors and less secondary structure along most of the β8-β9 loop. While this is largely consistent with the present results, it does not explain the physical basis of the nicotine-elicited differences in the β8-β9 loop conformation.

In addition to elucidating ligand-induced changes in conformational dynamics, the results provide insight into the solution backbone dynamics of AChBP that is unobtainable from crystallographic B factors. B factors provide a measure of dispersion of each atom at rest without any time reference and, therefore, do not resolve static from dynamic disorder let alone reveal the time domain in which atomic fluctuations occur. Site-directed labeling combined with time-resolved fluorescence anisotropy, while modifying the native protein, on the other hand, provides information on the solution dynamics of reporter groups attached to areas of interest in the picosecond-nanosecond time domain. Here, of course, one assumes that the conjugated cysteine-substitution

mutant displays largely the same conformational dynamics as the wild-type molecule. With this caveat in mind, the present results reveal the β9-β10 sandwich to be dynamically heterogeneous with the β10 strand relatively anchored and undergoing limited and slow fluctuations in the picosecond-nanosecond time domain while the β9 strand is highly dynamic in this time domain. This is a reasonable conclusion because the β10 strand is extensively hydrogen bonded to the protein core while the β9 strand is not. Furthermore, assuming that the β9-β10 sandwich remains intact in the solution state, the apparent dynamic character of the β9 strand (as revealed in the anisotropy decay of Fl-T177C) probably reflects the unique characteristics of the motion of a reporter group attached to one strand of a β sandwich. These strands are primarily linked to the protein core through antiparallel hydrogen bonds to its partner (β10) that is extensively bonded (non-covalently) to the protein core. In such a situation the minimally constrained β strand (β9) should be able to undergo fast butterfly-like motions that allow very large and rapid angular excursions of the reporter group producing rapid, large-amplitude depolarization.

While our data are not consistent with the activation signal being propagated down the β9-β10 sandwich, the β9-β10 hairpin (loop C) plays a critical role in agonist binding. Similar to prior findings on the nAChR, we observe a large loss in binding affinity for both epibatidine and α-bungarotoxin upon reduction or removal of the loop C vicinal disulfide. Nevertheless, even with the loss in affinity, reduction and labeling of the vicinal cysteines resulted in functional channels (34,35). Thus, an intact loop C structure appears to play an important role in ligand binding energetics, but may still allow appreciable activation when disrupted. That other Cys-loop family members do

not have vicinal cysteines in the loop C tip, but likely have a conserved activation mechanism, supports the notion that loop C may provide binding affinity for cholinergic ligands but not be strictly essential for channel gating. Hence, the anisotropy decay results from Fl-C188 may be explained by thinking of stabilization that comes from binding of a given ligand as being due to an affinity of that ligand for loop C. Lobeline, for example, stabilizes loop C, consistent with the crystal structure showing loop C packed down tightly around the ligand (8). MLA, in contrast, results in the greatest increase in loop C mobility; the crystal structure of this complex displays loop C in varying degrees of closure around the binding pocket, which supports limited interaction of the ligand with the loop. Stabilization by MLA likely occurs elsewhere in the binding site. Epibatidine is intermediate in its effects on flexibility at this site, indicating it derives moderate affinity through interactions with loop C.

Our results with the Fl-C188 conjugate should be viewed cautiously. First, 2D-TROSY ^{15}N-^{1}H HSQC spectroscopy of ^{15}N-cysteine substituted AChBP indicate conformational heterogeneity of loop C cysteines (13). Time-resolved fluorescence anisotropy reveals a cumulative signal from all five subunits. Second, the elimination of the loop C disulfide bond with the C187S mutation undoubtedly changes the structure of loop C. Finally, the Fl-C188 fast anisotropy decay parameters indicated less backbone mobility than the reporter groups in the β9 (Fl-T177C) and β10 (Fl-D194C) sheets that form loop C (β9-β10 hairpin); this low segmental mobility may result in part from the conjugated fluorescein may forming a surface interaction between loop C and the core of the protein. Our attempts to label engineered cysteines at positions in loop C that would

not require breaking the vicinal disulfide resulted in lack of expression, likely due to misfolding and possibly a disulfide rearrangement.

With regard to the other sites examined, the anisotropy decays associated with the Fl-N158C and Fl-Y164C conjugates show the β8-β9 loop to be in a significantly more dynamic state than the constrained β10 strand (as reflected in the anisotropy decay of Fl-D194C). Similarly, the β7 strand in the absence of any ligand appears to be flexible and exhibits greater amplitudes for the fast phase of decay. The significance of the mobility of these sites is unclear, but flexible binding surfaces can increase the rate of ligand binding, broaden substrate specificity, and enhance free energy of binding by optimizing non-covalent interactions between protein and ligand thereby increasing enthalpy. Moreover, binding-induced increases in flexibility may minimize the entropy loss associated with binding and thus also increase the free energy of binding.

Various allosteric mechanisms and structural linkages have been proposed for agonist activation of the channel gate. Structural work from electron micrographs of the full-length nAChR led to the hypothesis of an agonist-induced 10-15° rotation of the core of the extracellular β-sandwich of only the principal subunits about an axis normal to the plasma membrane (11,36). More recently, Auerbach and colleagues tested this hypothesis with a combination of electrophysiology and mutagenesis and found no evidence to support a synchronous rigid body movement in the extracellular domain of the receptor (37-39). This mutagenesis work was consistent with agonist-induced movements in both the β1-β2 linker and the β6-β7 linker (known as the Cys-loop), proximal to the membrane interface, following a movement in the β4-β5 linker that constitutes a portion of the agonist binding site (Y89). Our time-resolved fluorescence

results reveal regional variations in mobility that are consistent with this hypothetical sequential mechanism of activation, but do not offer evidence for the synchronous rigid body rotation hypothesis. As the anisotropy decay does not measure events slower than global rotation of the pentameric protein, we cannot exclude ligand-elicited rigid body motions. Nevertheless, the changes in conformation reflected in segmental motion distal to the agonist binding site reveal segmental mobility and communication across the subunit interfaces as being potentially critical for the activation process.

In addition to generating evidence for a functional role of loop F conformational dynamics in ligand activation and a potential trans-subunit propagation of the agonist binding signal across the principal/complementary subunit interface, our results show AChBP, and presumably the nAChR extracellular domain, to be a dynamic entity. AChBP exhibits a wide range of segmental fluctuations between discrete regions in the α-carbon backbone. Structurally and pharmacologically-distinctive ligands exert disparate effects on the stability of different domains of AChBP well removed from the binding site. This information on backbone flexibility expands our understanding of the solution behavior of the existing model of nAChR extracellular domain structure and should be applicable in drug design. The crystal structures provide a critical starting template for study; decay of fluorescence anisotropy enables one to examine the dynamic dimensions of structure in solution within the picosecond-nanosecond time frame. Additionally, the apparent principal-complementary transmission of the activation signal to part of the β8-β9 loop (loop F) is consistent with concerted models of nAChR activation, which require inter-subunit communication.

F. Acknowledgements

This chapter is material as it appears in: Ryan E Hibbs, Zoran Radic, Palmer Taylor, and David A Johnson "Influence of agonists and antagonists on the segmental motion of residues near the agonist binding pocket of the acetylcholine binding protein," *Journal of Biological Chemistry* (2006) in press. The dissertation author was the primary investigator in the development and execution of the study, and the principal author of this paper. This research was supported by a grant from the National Institutes of Health (R37-GM18360 to PT) and a pre-doctoral fellowship from the Pharmaceutical Research Manufacturers Association Foundation (REH).

G. References

1. Karlin, A. (2002) *Nat Rev Neurosci* **3**, 102-114

2. Changeux, J. P., and Edelstein, S. J. (2005) *Nicotinic Acetylcholine Receptors: From Molecular Biology to Cognition*, Editions Odile Jacob/Johns Hopkins University Press

3. Sine, S. M., and Engel, A. G. (2006) *Nature* **440**, 448-455

4. Sine, S. M., Kreienkamp, H. J., Bren, N., Maeda, R., and Taylor, P. (1995) *Neuron* **15**, 205-211

5. Brejc, K., van Dijk, W. J., Klaassen, R. V., Schuurmans, M., van Der Oost, J., Smit, A. B., and Sixma, T. K. (2001) *Nature* **411**, 269-276

6. Celie, P. H., Kasheverov, I. E., Mordvintsev, D. Y., Hogg, R. C., van Nierop, P., van Elk, R., van Rossum-Fikkert, S. E., Zhmak, M. N., Bertrand, D., Tsetlin, V., Sixma, T. K., and Smit, A. B. (2005) *Nat Struct Mol Biol* **12**, 582-588

7. Celie, P. H., Klaassen, R. V., van Rossum-Fikkert, S. E., van Elk, R., van Nierop, P., Smit, A. B., and Sixma, T. K. (2005) *J Biol Chem* **280**, 26457-26466

8. Hansen, S. B., Sulzenbacher, G., Huxford, T., Marchot, P., Taylor, P., and Bourne, Y. (2005) *Embo J* **24**, 3635-3646

9. Bourne, Y., Talley, T. T., Hansen, S. B., Taylor, P., and Marchot, P. (2005) *Embo J* **24**, 1512-1522

10. Bouzat, C., Gumilar, F., Spitzmaul, G., Wang, H. L., Rayes, D., Hansen, S. B., Taylor, P., and Sine, S. M. (2004) *Nature* **430**, 896-900

11. Unwin, N. (2005) *J Mol Biol* **346**, 967-989

12. Henchman, R. H., Wang, H. L., Sine, S. M., Taylor, P., and McCammon, J. A. (2005) *Biophys J* **88**, 2564-2576

13. Gao, F., Mer, G., Tonelli, M., Hansen, S. B., Burghardt, T. P., Taylor, P., and Sine, S. M. (2006) *Mol Pharmacol* **70**, 1230-1235

14. Hansen, S. B., Radic, Z., Talley, T. T., Molles, B. E., Deerinck, T., Tsigelny, I., and Taylor, P. (2002) *J Biol Chem* **277**, 41299-41302

15. Hansen, S. B., Talley, T. T., Radic, Z., and Taylor, P. (2004) *J Biol Chem* **279**, 24197-24202

16. Hibbs, R. E., Talley, T. T., and Taylor, P. (2004) *J Biol Chem* **279**, 28483-28491

17. Johnson, D. A., Voet, J. G., and Taylor, P. (1984) *J Biol Chem* **259**, 5717-5725

18. Hibbs, R. E., Johnson, D. A., Shi, J., Hansen, S. B., and Taylor, P. (2005) *Biochemistry* **44**, 16602-16611

19. Birch, D. J. S., and Imhof, R. E. (1991) in *Topics in Fluorescence Spectroscopy: Techniques* (Lakowicz, J. R., ed) Vol. 1, Plenum, New York

20. Shi, J., Tai, K., McCammon, J. A., Taylor, P., and Johnson, D. A. (2003) *J Biol Chem* **278**, 30905-30911

21. Daly, J. W. (2005) *Cell Mol Neurobiol* **25**, 513-552

22. Meyer, E. M., Kuryatov, A., Gerzanich, V., Lindstrom, J., and Papke, R. L. (1998) *J Pharmacol Exp Ther* **287**, 918-925

23. Gangal, M., Cox, S., Lew, J., Clifford, T., Garrod, S. M., Aschbaher, M., Taylor, S. S., and Johnson, D. A. (1998) *Biochemistry* **37**, 13728-13735

24. Li, F., Gangal, M., Jones, J. M., Deich, J., Lovett, K. E., Taylor, S. S., and Johnson, D. A. (2000) *Biochemistry* **39**, 15626-15632

25. Boyd, A. E., Dunlop, C. S., Wong, L., Radic, Z., Taylor, P., and Johnson, D. A. (2004) *J Biol Chem* **279**, 26612-26618

26. Schroder, G. F., Alexiev, U., and Grubmuller, H. (2005) *Biophys J* **89**, 3757-3770

27. Celie, P. H., van Rossum-Fikkert, S. E., van Dijk, W. J., Brejc, K., Smit, A. B., and Sixma, T. K. (2004) *Neuron* **41**, 907-914

28. Shi, J., Koeppe, J. R., Komives, E. A., and Taylor, P. (2006) *J Biol Chem* **281**, 12170-12177

29. Newell, J. G., and Czajkowski, C. (2003) *J Biol Chem* **278**, 13166-13172

30. Thompson, A. J., Padgett, C. L., and Lummis, S. C. (2006) *J Biol Chem* **281**, 16576-16582

31. Leite, J. F., Blanton, M. P., Shahgholi, M., Dougherty, D. A., and Lester, H. A. (2003) *Proc Natl Acad Sci U S A* **100**, 13054-13059

32. Lyford, L. K., Sproul, A. D., Eddins, D., McLaughlin, J. T., and Rosenberg, R. L. (2003) *Mol Pharmacol* **64**, 650-658

33. Rodrigues-Pinguet, N., Jia, L., Li, M., Figl, A., Klaassen, A., Truong, A., Lester, H. A., and Cohen, B. N. (2003) *J Physiol* **550**, 11-26

34. Bartels, E., Deal, W., Karlin, A., and Mautner, H. G. (1970) *Biochim Biophys Acta* **203**, 568-571

35. Damle, V. N., and Karlin, A. (1980) *Biochemistry* **19**, 3924-3932

36. Unwin, N., Miyazawa, A., Li, J., and Fujiyoshi, Y. (2002) *J Mol Biol* **319**, 1165-1176

37. Chakrapani, S., Bailey, T. D., and Auerbach, A. (2004) *J Gen Physiol* **123**, 341-356

38. Chakrapani, S., Bailey, T. D., and Auerbach, A. (2003) *J Gen Physiol* **122**, 521-539

39. Mitra, A., Cymes, G. D., and Auerbach, A. (2005) *Proc Natl Acad Sci U S A* **102**, 15069-15074

Chapter VII

Closing Remarks

My dissertation research focused on exploring the solution dynamics of the nAChR extracellular domain, using AChBP as a soluble protein surrogate. The X-ray crystal structure of AChBP provided an essential starting point for these studies. However, as the crystal of AChBP provides one static picture of the arrangement of atoms, and biological molecules do not carry out their functions in a crystalline lattice, there is great interest in building off of the atomic-resolution information in a crystal structure with dynamic studies in solution. To this end, I generated single cysteine mutants of AChBP which allowed me to label selectively positions on the molecule with fluorescent reporter groups. Using different spectroscopic techniques, these engineered reporter groups allowed me to examine ligand-induced changes in solvent exposure over the surface of AChBP (Chapter IV), interaction of an α-neurotoxin with AChBP (Chapter V), regional variations in AChBP backbone flexibility, and ligand induced changes in this segmental mobility (Chapter VI). While fluorescence was the main technique I used to study protein dynamics, the information gained from the fluorescent studies was bolstered by more traditional biochemical, hydrodynamic and pharmacological binding assays. Taken together, this research reveals AChBP do be a highly dynamic molecule with conformational states not evident in the static crystal structure.

A. Summary and Implications

1. Acrylodan labeling and steady-state fluorescence spectroscopy

Nine single cysteine mutants in AChBP were characterized in terms of their ability to bind nicotinic ligands, their reactivity with acrylodan, and ligand-induced changes in acrylodan fluorescence emission (1). Acrylodan fluorescence emission is highly sensitive to its local environment when bound to protein, and exhibits changes in both emission wavelength and intensity that reflect the effective dielectric constant of the environment around the fluorophore. Changes in steady-state acrylodan emission were used to assess the effects of ligand binding on solvent exposure at the nine positions of conjugation around the agonist binding site at the subunit interface.

All ligands studied, including agonists, alkaloid and peptide antagonists, occluded solvent from the positions of labeling in the competitive binding pocket as predicted from the HEPES-bound AChBP structure (2). α-Bungarotoxin binding occluded solvent from the membrane side of the C-loop that folds over the binding pocket, and increased solvent exposure slightly in the apical portion of the binding pocket, from which we concluded that the peptide toxin likely binds at the competitive interface from the membrane side of the C-loop. These conclusions were later supported by a crystal structure of a complex of AChBP and α-cobratoxin (3).

Two positions of labeling, in particular, revealed changes in solvent exposure upon ligand binding not predictable from the X-ray crystal structure. Binding of small molecules, both agonists and antagonists, to the Q178C conjugate, resulted in an increase in solvent exposure at this position on the linker between the β9 strand and the C-loop (Figure VII.1). α-Bungarotoxin binding caused a decrease in solvent exposure at this position. We proposed two possible explanations of these results, first that an agonist-induced rotation of subunits as described by Nigel Unwin and co-workers (4,5) could

cause the side chain of Q178C-acrylodan to become more or less solvent exposed, or second, that Q178 is at a hinge position about which the C-loop moves as a rigid flap to accommodate larger or smaller ligands. In this latter model, which is most consistent with recent structural data (6-8), the C-loop would pack down around small molecules and in the process its side chain which is buried in the original structure would move into the solvent; in contrast, upon binding of the large peptide toxin, the C-loop would twist outward and the Q178 side chain would become more buried in the hydrophobic protein core. This model of toxin binding that would require an open C-loop conformation to be selected out from the array of fluctuating conformations present at a given time in solution is consistent with observed slow association and dissociation rates of α-neurotoxins with both the nAChR and AChBP.

At the E157C acrylodan conjugate, all ligands studied caused a shift in the emission maximum to shorter wavelength, consistent with a decrease in solvent exposure, upon binding. This mutant is positioned on the β8-β9 linker, or F-loop, in the more apical portion of the protein, and based on the crystal structure would not predictably interact directly with small ligands (Figure VII.1). It is again possible to explain this change in solvent exposure with a rotation of subunits wherein the exposed complementary face would become more buried, however existing data are more consistent with local structural re-arrangements. First, thermal (B) factors from an accumulating body of AChBP structures consistently reveal more mobility in the F-loop region of the protein than elsewhere. Second, this region has been labeled by agonist-based photo-affinity and chemical labeling probes in several experiments. Lastly,

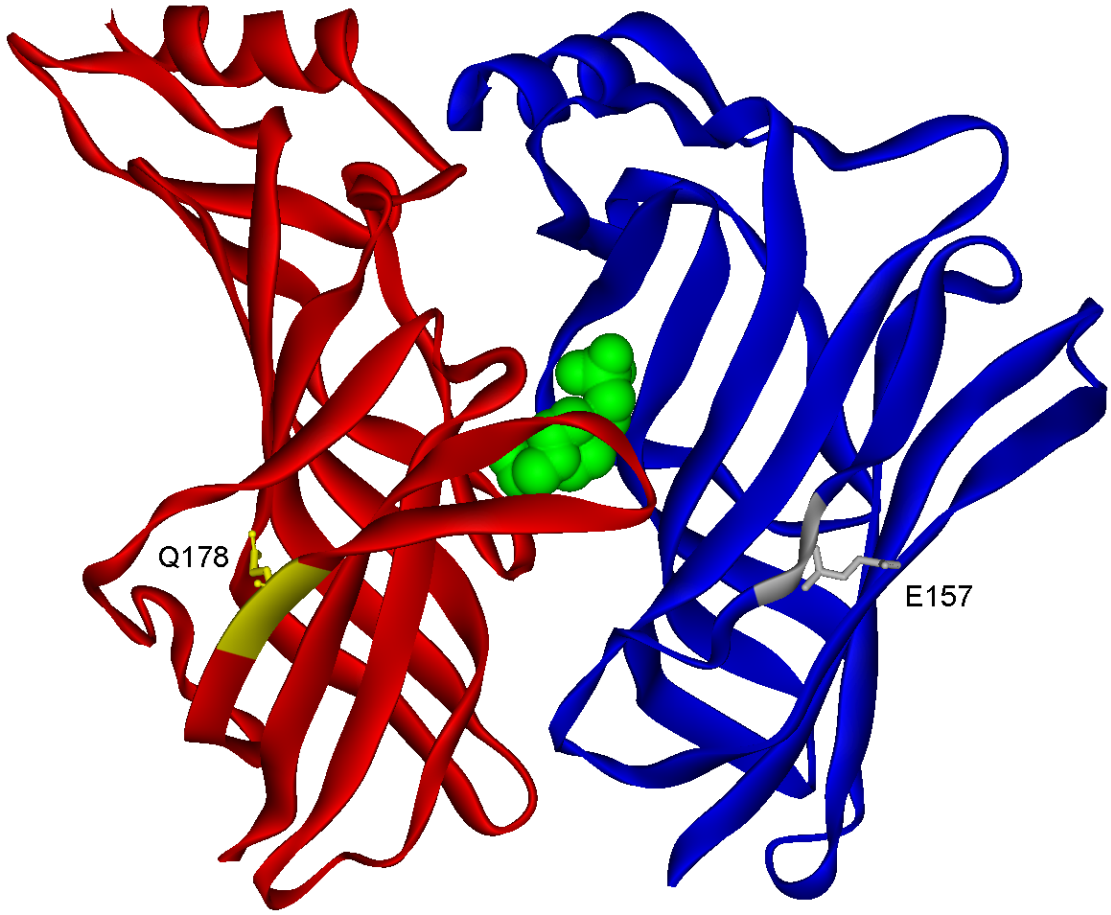

Figure VII.1: AChBP Subunit Interface. Positions of cysteine mutagenesis and acrylodan labeling that resulted in particularly distinctive ligand-induced changes in solvent exposure were Q178 (yellow) and E157 (grey). Hepes buffer molecule as a reference for the agonist binding site is shown in green.

decay of anisotropy experiments (Chapter VI) reveal that the flexibility of the F-loop is affected by binding of small molecule agonists and antagonists. The simplest explanation consistent with all of the data is that the F-loop, at least its apical portion, is highly dynamic and interacts directly with small molecule ligands.

The acrylodan labeling experiments revealed no changes in solvent exposure that distinguished agonists from antagonists. These results may not be surprising as AChBP is thought to resemble the desensitized state of the receptor (2). Alternatively, we may not have found the distinguishing site(s). While AChBP is an excellent structural surrogate for nAChR study, and is capable of functional ion gating when fused to the 5-HT_3 receptor ion channel (9), it is also possible that it is not capable of mimicking the functional conformational changes of the receptor when the transmembrane α-helices are not attached. This last possibility is supported by the observed lack of cooperativity of binding in AChBP, which contrasts with considerable cooperativity in the nAChR. Regardless, the local structural rearrangements determined through the acrylodan labeling experiments reveal conformations not evident from the crystal structure, that are consistent with the chemical labeling studies of the full-length receptor, and hence provide relevant new information about the receptor structure and ligand interaction that should prove useful in therapeutic design.

2. Hydrodynamic and fluorescence anisotropy decay studies of α-neurotoxin binding

In early 2005 the crystal structure of a complex of AChBP and α-cobratoxin was solved thereby lending insight into 40 years of research on the interaction of this family of toxins with nAChRs (3). As the crystal structure shows 5 molecules of α-cobratoxin

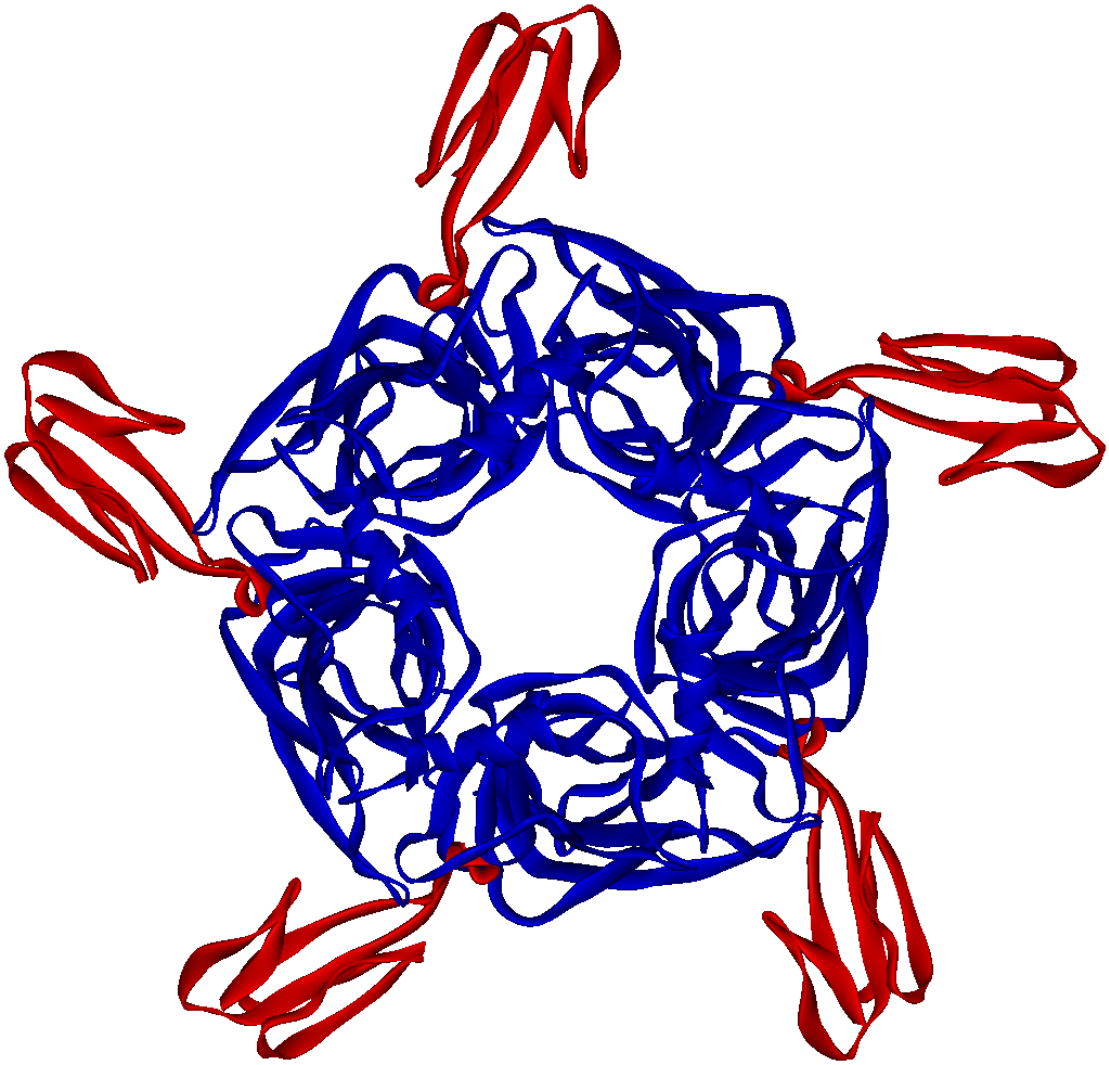

Figure VII.2: AChBP-α-Cobratoxin Complex (3). AChBP subunits are shown in blue, α-cobratoxin molecules are shown in red.

bound one at each of the 5 subunit interfaces, oriented radially like blades on a propeller, we reasoned that binding of α-neurotoxin should affect the hydrodynamic properties of AChBP in solution (Figure VII.2). To advance our understanding of this interaction, we examined the flexibility of bound α-neurotoxin with a combination of hydrodynamic and time-resolved fluorescence techniques (10).

Hydrodynamic experiments with both α-cobratoxin and α-bungarotoxin revealed no increase in translational friction of AChBP upon toxin binding beyond what would be predicted from the simple expansion of a non-hydrated compact molecular mass. These results support the model of a flexible α-neurotoxin molecule. To study the flexibility of the bound toxin more precisely, we examined the decay of fluorescence anisotropy from four different FITC-labeled α-cobratoxins free in solution and bound to AChBP. When free in solution, regional variations in segmental mobility of the α-cobratoxins were indistinguishable due to a fast global rotation rate that overlaps with the rate of peptide backbone fluctuation. However when bound to AChBP, regional variations in backbone flexibility were distinguishable. The results indicated that the bound toxin structure is quite flexible (see Figure VII.3), more flexible than the surrounding AChBP itself, and that the least flexible region surrounds Lys^{23} which is constrained by a high degree of secondary structure.

The interest in the nAChR field with three-fingered α-neurotoxins rests in their receptor-subtype selectivity. If one were able to mimic the selectivity generated by evolution in the family of α-neurotoxins with small-molecule therapeutic agents,

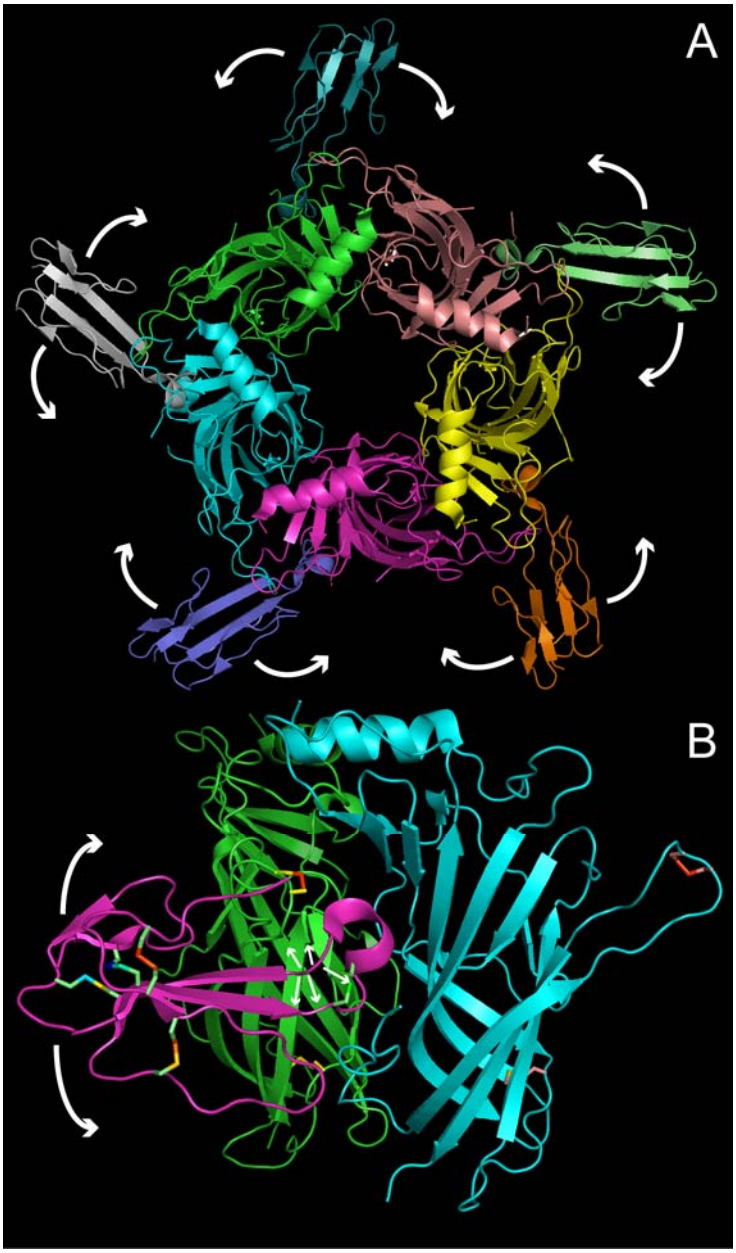

Figure VII.3: Conformational Dynamics of AChBP-α-Cobratoxin Complex. Top View (A) and Side View (B). Large amplitude rigid body motions of toxin are indicated by large arrows, and fast segmental motions that may give rise to flexibility around Lys^{35} are shown with small arrows in B.

undesirable side effects of therapeutics that result from a lack of specificity in target binding could be minimized. Mutational studies reported in the literature have demonstrated many of the individual amino acid residues that contribute to the selectivity of one toxin for a given receptor subtype (11). Those studies, combined with the 3-dimensional structural information from crystal structures and describing the dynamics of the interaction in solution, advance the goal of defining the molecular bases of high affinity and exquisite nAChR subtype selectivity of three-fingered α-neurotoxins. Such an approach can be extended to smaller pharmaceutical agents with different drug disposition profiles.

3. Ligand effects on segmental mobility

Several hypothetical allosteric gating mechanisms have been proposed over the course of study of the nAChR. When comparing different crystal structures, the C-loop of AChBP undergoes the largest conformational changes of any region (6). Complexes with nicotine and epibatidine, established agonists for the receptor, and lobeline, reported as a mixed agonist-antagonist, reveal C-loops that pack down tightly around the bound ligand. Antagonist-bound structures, such as the complexes with methyllycaconitine, two α-conotoxins, and the α-cobratoxin, and those with only polyethylene glycol in the binding pocket, display C-loops that in an open conformation; the difference in C-loop radial extension between closed and open is on the order of 5-10 angstroms. Hence, most of the current gating mechanism hypotheses are initiated by the C-loop packing in around the bound agonists; to my knowledge, this distinction as the first step in the activation pathway was first proposed by Arthur Karlin in 1969 (12). The C-loop then acts on the transmembrane α-helices that constitute the ion gate either by breaking and forming new

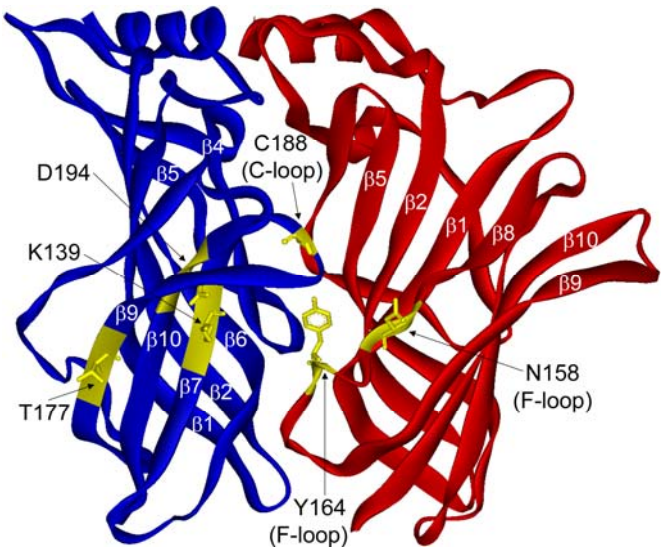

Figure VII.4: Sites of Cysteine Mutagenesis and Fluorophore Conjugation for Anisotropy Decay Studies.

salt bridges near the membrane interface (13), through a proline isomerization (14), through propagation of an activation wave (15), through a rigid body rotation of the subunit core (5), or a combination of these conformational events. We reasoned that regardless of the specific pathway, any of these hypotheses regarding the path of an activation signal would result in a change in the α-carbon backbone flexibility along the activation path. Hence, we used cysteine mutagenesis and fluorophore labeling in combination with measurements of time-resolved decay of fluorescence anisotropy to examine the regional variations in AChBP backbone mobility and changes induced by bound ligand (Figure VII.4). Due to the necessity for a relatively large signal in the measurement of decay of anisotropy, acrylodan was not useful; however, the methanethiosulfonate derivative of fluorescein met our requirements in terms of its reactivity, labeling specificity, and emission intensity.

In the absence of ligands, anisotropy decay measurements from six positions of fluorophore conjugation revealed a high degree of regional variation in the α-carbon backbone flexibility of AChBP. Overall, the C-loop exhibited the least amount of mobility in the picosecond-nanosecond time domain. These results may seem somewhat surprising as this is the region of the protein that shows the most conformational distortion in the available crystal structures. However, our results support the model of the C-loop moving “slowly” as a rigid flap rather than undergoing rapid internal segmental fluctuations in structure; these ideas are consistent with both the crystal structures and the slower binding kinetics for ligands of dimensions sufficient to require the C-loop to open to a more extended conformation. The most flexible region overall was the β9 strand that links to the C-loop. This strand is the outermost in the sheet

making up the extracellular domain of the receptor, and as such is the least constrained by interactions with neighboring protein structure.

In our effort to examine possible activation pathways, we studied the effects of ligand binding on segmental flexibility from the C-loop and the β-strands that extend from it toward the membrane. We also studied two sites on the F-loop on the complementary side of the binding interface that has been implicated in both direct and indirect ligand interactions, but that does not obviously interact with ligands based on the crystal structure (discussed in section VII.A.1).

Neither the C-loop nor the β-strands that extend from the C-loop toward the membrane show conformational characteristics upon ligand binding that correlate with the pharmacological action of the ligand. In order to label the tip of the C-loop, I replaced one of the vicinal cysteines with a serine, and in the process removed the disulfide bond that presumably tethers the loop tip with a constraining kink; hence, interpretation of the data from the loop tip is muddied by the modifying residue itself. However, ligands were still able to bind to the mutated and labeled interface with moderate affinity, indicating that the overall structure of the binding pocket and interactions were maintained. Another recent study reported similar proper assembly and ligand binding with a similar loss in affinity upon mutation of both vicinal cysteines (16).

Anisotropy decay data from the two F-loop sites revealed a highly dynamic structure that is exquisitely sensitive to ligand binding, consistent with what was observed in the acrylodan labeling studies. The Y164C site of fluorophore labeling on the section of the F-loop extending toward the membrane responded distinctively to agonists and antagonists: all agonists tested made this region more flexible, while

alkaloid antagonists made it less flexible, and the peptide antagonist α-bungarotoxin had no effect on flexibility. Larger antagonists like methyllycaconitine may interact directly with this portion of the F-loop proximal to the membrane and thus stabilize it, however the cause of the agonist-induced increase in flexibility is less clear.

Similar to the conclusions from the acrylodan experiments, I hypothesize that the effects on F-loop flexibility are through a direct interaction that one would not predict from the crystal structure, that the F-loop is a flexible flap that moves into or out of the binding interface to form part of the binding site. This is the simplest explanation and is consistent with affinity labeling of the F-loop by agonists. It is also possible, and has been predicted by others (as described in detail in Chapter VI) that the F-loop is a mediator of the activation signal relaying to the ion gate. Cooperativity in binding and channel activation are observed with the nAChR, and for this reason channel activation is largely regarded as a concerted process wherein the conformation of more than one subunit is affected by agonist binding. Transmission of the activation signal across the subunit interface to the F-loop in the complementary subunit would be consistent with this type of concerted activation mechanism.

The recently published set of crystal structures of agonist and antagonist-bound AChBP complexes shows the C-loop packing down tightly around epibatidine and lobeline, both described as agonists, and moving out to accommodate the bulkier antagonists (6). As such, these structures provide good support for the mechanistic hypothesis that initiates with the C-loop movement. The anisotropy data that did not show pharmacologically-correlated changes in C-loop backbone mobility do not provide evidence directly contradictory to this hypothesis, but do suggest an alternative in the F-

loop. I offer the possibility that the C-loop, with its unique and evolutionarily-conserved vicinal cysteines at its tip, provides specific affinity for acetylcholine and nicotinic agonists, while its flexibility allows for larger antagonists to bind competitively, but that it is not strictly required for functional agonist-induced receptor gating. That the AChBP-5HT_3 chimera is functional implies a common allosteric gating mechanism conserved between Cys-loop receptor family members. Other members in this family, such as the 5-HT_3, GABA and glycine ligand-gated ion channels, do not contain vicinal cysteines at the C-loop tip, do not bind acetylcholine or nicotine, but are obviously quite functional with regards to their respective endogenous ligands.

The explanation of C-loop position being related to affinity for some nicotinic ligands is supported by examination of conserved hydrogen bond interactions amongst the ligands that have been crystallized in complex with AChBP: all small molecules contain a basic, protonated amine that hydrogen bonds to the backbone carbonyl oxygen of W143 (W147 in *Aplysia*) and a second amine that hydrogen bonds to structural water in the apical region of the binding pocket that is coordinated by multiple residues in the interface core. Recent unpublished structures of AChBP (complexes with cocaine, galanthamine, imidacloprid, thiacloprid, anabaseine, 4-OH, 2-MeO-benzylidene anabaseine, and 2,4-dimethoxy-benzylidene anabaseine), reveal the C-loop adopting multiple conformations irrespective of ligand position. These crystallographic results are consistent with some nicotinic ligands deriving their binding free energy in most part or exclusively from interactions with the core of the interface, while others, such as epibatidine, lobeline, and nicotine, require the electron-dense disulfide that the intact C-loop tip provides for their high affinity.

Taken together, these solution-based structural studies reveal AChBP to be a highly dynamic protein with conformational states not evident in the static crystal structures. The fluorescence labeling techniques are laborious and have significant limitations; it takes months to generate mutant protein and characterize the labeled species, and structural resolution and hence certainty in the conclusions are limited by the uncertainty of the position of the fluorophore, as well as by the effects of mutagenesis and adding a bulky side chain. However, the techniques complement and improve on the information from rigid, high resolution X-ray crystal structures by providing relevant steady-state or real time measurements of ligand-induced conformational changes. AChBP offers an excellent soluble surrogate for nAChR study, however there are limitations within it as a model system that lacks a functioning ion channel. It is very likely that native receptor extracellular domains will be solubilized in coming years, and these techniques will be readily applicable to and useful for the new soluble systems. An ongoing project in the laboratory involves making AChBP more like the different nAChR subtypes, which may prove more immediately successful than solubilizing a native receptor subunit. Also of great interest will be defining the non-competitive or allosteric modulator binding site(s) and structural fluctuations involved in binding of this class of ligands, either via crystallographic or fluorescence, or other biophysical approaches.

B. References

1. Hibbs, R. E., Talley, T. T., and Taylor, P. (2004) *J Biol Chem* **279**, 28483-28491

2. Brejc, K., van Dijk, W. J., Klaassen, R. V., Schuurmans, M., van Der Oost, J., Smit, A. B., and Sixma, T. K. (2001) *Nature* **411**, 269-276

3. Bourne, Y., Talley, T. T., Hansen, S. B., Taylor, P., and Marchot, P. (2005) *Embo J* **24**, 1512-1522

4. Unwin, N., Miyazawa, A., Li, J., and Fujiyoshi, Y. (2002) *J Mol Biol* **319**, 1165-1176

5. Unwin, N. (2005) *J Mol Biol* **346**, 967-989

6. Hansen, S. B., Sulzenbacher, G., Huxford, T., Marchot, P., Taylor, P., and Bourne, Y. (2005) *Embo J* **24**, 3635-3646

7. Celie, P. H., van Rossum-Fikkert, S. E., van Dijk, W. J., Brejc, K., Smit, A. B., and Sixma, T. K. (2004) *Neuron* **41**, 907-914

8. Celie, P. H., Kasheverov, I. E., Mordvintsev, D. Y., Hogg, R. C., van Nierop, P., van Elk, R., van Rossum-Fikkert, S. E., Zhmak, M. N., Bertrand, D., Tsetlin, V., Sixma, T. K., and Smit, A. B. (2005) *Nat Struct Mol Biol* **12**, 582-588

9. Bouzat, C., Gumilar, F., Spitzmaul, G., Wang, H. L., Rayes, D., Hansen, S. B., Taylor, P., and Sine, S. M. (2004) *Nature* **430**, 896-900

10. Hibbs, R. E., Johnson, D. A., Shi, J., Hansen, S. B., and Taylor, P. (2005) *Biochemistry* **44**, 16602-16611

11. Nirthanan, S., and Gwee, M. C. (2004) *J Pharmacol Sci* **94**, 1-17

12. Karlin, A. (1969) *J Gen Physiol* **54**, 245-264

13. Lee, W. Y., and Sine, S. M. (2005) *Nature* **438**, 243-247

14. Lummis, S. C., Beene, D. L., Lee, L. W., Lester, H. A., Broadhurst, R. W., and Dougherty, D. A. (2005) *Nature* **438**, 248-252

15. Chakrapani, S., Bailey, T. D., and Auerbach, A. (2004) *J Gen Physiol* **123**, 341-356

16. Gao, F., Mer, G., Tonelli, M., Hansen, S. B., Burghardt, T. P., Taylor, P., and Sine, S. M. (2006) *Mol Pharmacol* **70**, 1230-1235